INSTITUTE OF NUCLEAR PHYSICS, ASTRONOMICAL
INSTITUTE OF THE ACADEMY OF SCIENCES
OF THE REPUBLIC OF UZBEKISTAN

A manuscript
UDC: 530.12:531.51

ATAMUROTOV FARRUH SHUHRATOVICH

OPTICAL AND ENERGETIC PROCESSES IN VICINITY OF ROTATING RELATIVISTIC COMPACT OBJECTS

01.03.01- Astronomy

DISSERTATION
written to get the Doctor of Philosophy degree of physical and mathematical sciences

Supervisor: Ahmedov Bobomurat Juraevich
doctor of sciences in physics and mathematics, professor

Tashkent – 2018

Contents

Introduction

Topicality and relevance of the theme of the dissertation.

Nowadays, great attention is paid to solving the important problems of astrophysics through study of optical and energetic processes around relativistic compact objects. Although a black hole is not visible, one can observe it nonetheless - it casts a shadow if it is in front of a bright background from far source. The International Event Horizon Telescope (EHT) and Black Hole Cam (BHC) projects, which are planning to detect for the first time image of the black hole candidate at the center of M87 and our Milky Way galaxies. The main goal is to obtain a shadow of M87 and Sagitarius A* the supermassive black holes in the centers of the galaxies through series of presently ongoing observations. The topicality of theoretical investigation of the shadow of the black hole is related to use the shape of the silhouette to test the corresponding theory of gravity in the strong field regime.

During these years of independence of our country, the science has been developed by providing theoretical and experimental investigations on relativistic astrophysics to solve fundamental problems, and as a results valuable progress have been achieved. Theoretical and observational studies of the gravitational lensing systems, particularly black hole shadow and spacetime structure through the application of fundamental investigations in the area of relativistic astrophysics of compact objects has significant value in the Strategy of Actions on

Further Development of Uzbekistan.

The investigation of the optical properties and the spacetime structure of the black hole and construction of new tests of general relativity and other gravity theories are now one of the most important tasks in modern relativistic astrophysics. Theoretical study of the shadow of the black hole in the various gravity theories and study the gravitational lensing contribute an important tool to build the tests of the gravity models using the information events on the central object in our galaxy and M87 within the Black Hole Cam (BHC) and Event Horizon Telescope (EHT) International projects and understand the fundamental properties of the gravity. These objectives justify the topicality of the global level of scientific research.

This research corresponds to the tasks stipulated in governmental regulatory documents and Decree of the President of the Republic of Uzbekistan No.PD-4512 "On works of further development of alternative energy sources" of 1 March 2013, Resolution No.PR-2789 "On measures of further improvement of the activities of the Academy of Sciences, organization, management and financing of scientific research works" of 17 February 2017, and Decree No.PD-4947 "On the Strategy of Actions on Further Development of the Republic of Uzbekistan" of 7 February 2017 and others

Relevance of the research to the priority areas of science and technology development of the Republic Uzbekistan. The dissertation research was carried out in accordance with the priority areas of science and technology development of the Republic of Uzbekistan: II. ?Power, energy and resource saving?.

Degree of study of the problem

Number of scientists of the world, for example German scientisits (C. Laem-

merzahl, J. Kuntz, E. Hackmann, A. Grezenbach, V. Perlick), Indian scientists (N. Dadhich, S. Ghosh, P. Joshi, M. Patil), Italian scientists (C. Bambi, L. Rezzolla, L. Modesto, D. Malafarina, O. Zanotti), Russian scientists (O. Tsupko, G. Bisnovatyi-Kogan, A. Zakharov, D. Galtsov), Czech scientists (Z. Stuchlik, M. Kolos, J. Schee, J. Kovar, V. Karas), Uzbek scientists (B. Ahmdeov, A. Abdujabbarov and V. Morozova) and others have done huge number of theoretical and observational investigations to study the optical and energetic processes around rotating black hole.

Uzbek scientists (B. Ahmedov, A. Abdujabbarov, V. Morozova and others) worked on developing a new formalism of black hole shadows description and method to derive analytical solutions of the Maxwell equations in curved spacetime.

Earlier research works on gravitational lensing where consentrated only on weak lensing effects around spherical symmetric compact objects. However, in the strong gravitational field limit one may consider strong gravitational lensing or retrolensing. These effects may be used as an useful tool to test the gravity in the strong field regime.

The concept of the black hole shadow was known since 70s of the 20th century but the idea to image it in the black hole in the center of our Milky Way was first presented in a paper by Falcke in early 2000. The shape and the size of the shadow of black hole strongly depend on the main two parameters of the black hole: its mass and spin. The dependence of the black hole?s shadow shape on electric charge, brane parameter and angle of inclination of the axis of rotation of the black hole have been widely studied in the literature.

However, the effects due to the parameters of alternative theories of gravity have been remained unstudied. The shadows of the deformed, Born-Infeld, NUT

black holes and 5D Myers-Perry black hole have not been investigated.

Connection of the topic of dissertation with the scientific researches of the higher educational institutions, where the dissertation was conducted.

The PhD dissertation was carried out in the framework of the scientific projects of the Institute of Nuclear Physics and Astronomical Institute: F2-FA-F113 "Gravitational and Electromagnetic Processes in Relativistic Astrophysics and Cosmology" (2012-2016); EF2-FA-0-12477 "Motion of particles with spin and propagation of electromagnetic waves in the vicinity of compact gravitational objects" (2014-2015); VA-FA-F2-008 "Astrophysical Processes in Stationary and Dynamic Relativistic Gravitation Objects" (2017-2020).

The aim of the research is the development and astrophysics application of a theoretical method of description of radius and distortion of the black hole shadow and thermal radiation from the rotating black holes

The tasks of the research:

- to study deflection angle of the light ray around black hole and its images, brightness of the compact objects using gravitational lensing effect;
- to estimate the emission energy from the black hole through the thermal radiation;
- to consider the collision of particles near the black hole;
- to determine the influence of different parameters of the rotating black hole in the different gravity models;
- to analyze the effects of the black hole parameters on event horizon structure of the rotating black hole in different gravity models;

- to study the energy extraction mechanism and estimate the maximal value of the extractable energy from the rotating black hole;
- to obtain and analyze a shadow of a black hole and to find the dependence of the radius and distortion parameter of the shadow from the different parameters of the gravity models;
- to compare silhouette of the black hole shadow in four dimensional and higher dimensional gravity theories.

The objects of the research are relativistic compact objects, the black holes.

The subjects of the research are optical properties of the black hole, energy emission and energy extraction from the rotating black holes.

The methods of the research. The research methods are mathematical apparatus of general relativity and metric affine differential geometry, analytical and numerical methods for solving differential equations of motion for particles and field.

The scientific novelty of the research is the follows: is the follows:

The exact analytical expressions for the deflection angle of the light rays due to the effect of weak gravitational lensing around black hole in braneworld have been obtained and dimensionless brane parameter as $W^2/R^2 = 0.96 \times 10^{-7}$ has been estimated.

It was shown that the increase of the black hole brane tidal charge causes the increase of the energy release process and it was shown that with the increase of the rotation parameter the efficiency of the energy emission decreases in spacetime of five dimensional black hole.

It was shown, that the increase of the gravitomagnetic charge causes the increase of the event horizon of the Kerr-Taub-NUT black hole and the upper limit

for the dimensionless gravitomagnetic charge as $l/M < 0.85$ and deformation parameter as $|\epsilon| < 80$ have been estimated.

It was obtained that with increasing either rotation parameter or electric charge of black hole particle is moving closer to the central object in Einstein-Born-Infeld model.

Practical results of the research are as follows: are as follows:

Results of the research of astrophysical processes in the vicinity of deformed rotating black holes can be used to develop new tests of alternative theory of gravity in the strong field regime.

Processing the X-ray source data leads to more accurate evaluation of different parameters of black holes, including deformation parameter. The limiting values of the parameters can be used in astrophysical description of the structure of spacetime and energetic processes in the vicinity of compact objects.

Obtained shapes and parameters of black hole shadows in various theories of gravity can be used in comparative analysis of observational data and theoretical results in order to test alternative theories of gravity.

The reliability of the research results is provided by the followings: modern methods of general relativity and the theoretical physics and highly effective numerical methods and algorithms are used; careful check of a consistence of the received theoretical results with observational data and results of other authors is performed; conclusions are well consistent with the main provisions of the field theory of gravitational compact objects.

Scientific and practical significance of the research results. The scientific significance of the research results is determined by the ability of the developed description of black hole shadow to test the different theories of the gravity using the comaparative analysis of the future observations of shadow of supermas-

sive black holes at the galactic centers and obtain constraints on the parameters of the black hole in different gravity models.

The practical significance of the results of research lies in the fact that the comparison of the results of this dissertation and the observational data on gravitational lensing can be used to estimate or get the constraints on the parameters of the black hole in alternative theories of gravity. The results can be also used to understand the fundamental aspects of the gravitational interaction in Nature.

Implementation of the research results

The obtained results on shadows of the rotating black hole with the gravitomagnetic charge and dependence of observable parameters from the gravitomagnetic charge was used by international journals (Physical Review D 2017, Astrophysical Space Sciences 2017, European Physical Journal C 2017, Monthly Notices of Royal Astronomical Society 2015) to compare the results with shadows of black hole in other gravity models and numerical simulations. Application of the scientific results is that obtained results on black hole shadow have been used to get the constraints on different gravity models.

Energetic and optical properties of four and higher dimensional spacetimes in modified theories of gravity have been used in international scientific journals (Physical Review D, 2017; Astrophysical Space Sciences, 2017; European Physical Journal C, 2017; Monthly Notices of Royal Astronomical Society, 2015) to develop fundamental theories of gravitational interactions using the comparison of the black hole shadow in different gravity models.

Testing of the research results. The research results were reported and tested at 8 international and local scientific conferences.

Publication of the research results. On the theme of dissertation 20 scientific works were published, including 9 scientific papers scientific papers in

international scientific journals recommended by the Supreme Attestation Commission of the Republic of Uzbekistan for publishing basic scientific results of PhD dissertations.

Volume and structure of the dissertation. The PhD dissertation consists of an introduction, four chapters, conclusion and a bibliography. The size of the dissertation is 119 pages.

Throughout the dissertation, we use a space-like signature $(-,+,+,+)$ and a system of units in which $G = 1 = c$. Greek indices are taken to run from 0 to 3 and Latin indices from 1 to 3.

Chapter I

Gravitational lensing and retrolensing

1.1 Introduction

Deflection angle for relativistic object using gravitational effect has been observed by big number of telescopes. One of the example is the Sun, deflection angle of which is $(1.75 \pm 0.05)''$ [1]. This gives us good motivation to find the deflection angle for compact objects in alternative theories of gravity. One can easily estimate the parameters of the black hole using deflection angle by comparing theoretical and observational results.

The strong gravitational field surrounding the compact objects causes the deflection of the light called the effect of gravitational lens. The gravitational lens differs from the optical one since the deflection due to gravitational lens makes a maximum deflection of light passing closest to central object and a minimum deflection of light passing far from center. Studying the gravitational lens systems gives us the opportunity to study the source image of which will be created by gravitational lensing object and parameters of the compact object which is playing the role of gravitational lens. The light deflection is decreasing when it comes closer to the light sphere of the compact object and one can observe so-called retrolensing.

The study of the retrolensing by charged rotating black hole has been considered in [2]. The retrolensing of light ray caused by wormhole has been considerd in [3]. Different aspects of the weak and strong lensing, as well as light rays motion in vacuum and plasma environment have been studied in Refs. [4, 5, 6, 7, 8, 9, 10].

A huge number of works have been dedicated to the study of microlensing during the last decades. Starting the pioneer work on microlensing [11, 12, 13] strong gravitational lensing in the Schwarzschild metric has been considered in [9]. The reference [10] reviews the gravitational lensing effect around compact gravitating objects in general relativity. The angular sizes and magnification factors for relativistic rings formed by the light ray which undergo one or several turns around the black hole have been considered in [9]. The influence of plasma on gravitational lensing has been considered in [8, 6, 7, 14]. In [15] the general-relativistic radiative transfer theory in refractive and dispersive media has been considered.

In the recent work [16] the gravitational lensing by regular black holes surrounded by plasma has been considered. Gravitational lensing and ghost images in the regular Bardeen no-horizon spacetimes has been studied in [17]. Extreme gravitational lensing in vicinity of Schwarzschild-de Sitter black holes has been stusied in [18]. Optical properties of spacetime surrounded different types of the black hole [19, 20, 21, 22] as well as shadow of the compact gravitational compact objects in different models [23, 24, 25, 26, 27, 28, 29, 30, 31, 32, 33, 34] have been studied by various authors.

In the weak field approximation the expressions for deflection of light have the same character for both the regular black hole and no-horizon spacetimes that were extensively studied in the strong field situations in [35, 17].

1.2 Deflection of light by a Braneworld lensing object in the presence of the plasma

Consider the spacetime metric around the static and spherically symmetric black hole in braneworld, which has the following form [36, 37]:

$$ds^2 = -f(r)dt^2 + \frac{1}{f(r)}dr^2 + r^2(d\theta^2 + \sin^2\theta d\phi^2), \tag{1.1}$$

where the function $f(r)$ has the following form

$$f(r) = 1 - \frac{2M}{r} - \frac{W^2}{r^2}, \tag{1.2}$$

and W is brane tidal charge. The spacetime metric (1.1) mathematically has the form similar to Reissner-Nordström solution's and the difference is that values of W are negative. When the brane tidal charge W vanishes the spacetime metric (1.1) coincides with the Schwarzschild metric.

Weak field approximation is useful tool to study the gravitational effect and within this approximation one can express the spacetime metric tensor components in the form:

$$g_{\alpha\beta} = \eta_{\alpha\beta} + h_{\alpha\beta} \ , \tag{1.3}$$

with the notations

$$\begin{aligned} &\eta_{\alpha\beta} = \text{diag}(-1, 1, 1, 1), \\ &h_{\alpha\beta} \ll 1, \quad h_{\alpha\beta} \to 0 \quad \text{under} \quad x^i \to \infty \\ &g^{\alpha\beta} = \eta^{\alpha\beta} - h^{\alpha\beta}, \quad h^{\alpha\beta} = h_{\alpha\beta} \end{aligned} \tag{1.4}$$

To study and describe the light ray trajectory in a medium we will use the Hamiltonian approach and using the variational principle as

$$\delta\left(\int p_\alpha dx^\alpha\right) = 0 \tag{1.5}$$

one can easily obtain the equations of motion for light ray in a medium in the following form

$$\frac{dx^\alpha}{d\lambda} = \frac{\partial H}{\partial p_\alpha}, \quad \frac{dp_\alpha}{d\lambda} = -\frac{\partial H}{\partial x^\alpha} \ , \tag{1.6}$$

where we have used the restriction condition for the Hamiltonian [38] in the form of

$$H(x^\alpha, p^\alpha) = \frac{1}{2}\left[g^{\alpha\beta}p_\alpha p_\beta - (n^2-1)(p_\alpha V^\alpha)^2\right] = 0 \ . \tag{1.7}$$

In the Eq. (1.7) p^α is the light rays momentum, V^α is the four velocity of the observer, n is the refractive index of the medium surrounding the central object, and λ is the affine parameter along the trajectory of the light ray.

We will rewrite the Eq. (1.7) in the form

$$H = \frac{1}{2}\left[g^{00}p_0 p_0 + g^{ik}p_i p_k - (n^2-1)\frac{\hbar^2\omega^2(x^i)}{c^2}\right], \tag{1.8}$$

where $\hbar$ is the Planck constant, $\omega(x^i)$ is the light ray frequency, which depends on coordinates x^i due to gravitational redshift effects, and c is the speed of light propagation in vacuum and

$$p_\alpha V^\alpha = -\frac{\hbar\omega(x^i)}{c}, \tag{1.9}$$

The refractive index of plasma depends on the frequency $\omega(x^i)$ in the following way

$$n^2 = 1 - \frac{\omega_e^2}{\omega^2(x^i)}, \quad \omega_e^2 = \frac{4\pi e^2 N}{m} = K_e N, \tag{1.10}$$

where $N = N(x^i)$ is the electron density in plasma, e and m are the electric charge and mass of the electron, respectively. For the simplicity we will use the

notations:

$$\omega = \omega(x^i \to \infty)$$
$$\omega_0 = \omega_e(x^i \to \infty)$$
$$n_0 = n(x^i \to \infty) \tag{1.11}$$

The equations (1.8) and (1.10) allow us to find the equation of motion in the following:

$$\frac{dx^i}{d\lambda} = g^{ik}p_k = p^i \tag{1.12}$$
$$\frac{dp_i}{d\lambda} = -\frac{1}{2}g^{kl}_{,i}p_k p_l - \frac{1}{2}g^{00}_{,i}p_0^2 - \frac{1}{2}\frac{\hbar^2 K_e N_{,i}}{c^2} \tag{1.13}$$

Taking into account the weak field approximation and weak plasma the components of the momentum of the light ray propagating along z direction can be chosen in the following form:

$$p^\alpha = \left(\frac{\hbar\omega}{c}, 0, 0, \frac{n_0\hbar\omega}{c}\right), \quad p_\alpha = \left(-\frac{\hbar\omega}{c}, 0, 0, \frac{n_0\hbar\omega}{c}\right) \tag{1.14}$$

By the definition the deflection angle of the light ray in the plane orthogonal to the z axis is expressed in the form:

$$\hat{\alpha}_k = [p_k(\infty) - p_k(-\infty)]/p$$
$$p = \sqrt{p_1^2 + p_2^2 + p_3^2} = |p_3| = \frac{n_0\hbar\omega}{c}, \quad k = 1, 2\ . \tag{1.15}$$

Using the equation of motion obtained earlier, one can easily find the relation

$$\hat{\alpha}_k = \frac{1}{2}\int_{-\infty}^{\infty}\left(h_{33} + \frac{h_{00}\omega^2 - K_e N}{\omega^2 - \omega_0^2}\right)_{,k} dz\ . \tag{1.16}$$

Note, that negative values of $\hat{\alpha}_b$ correspond to the bending the light ray towards the central object and vice versa.

At the large distances from the central object, the static and asymptotically flat spacetime of the braneworld geometry can be expressed as [36]

$$ds^2 = ds_0^2 + \left(\frac{2M}{r} - \frac{W^2}{r^2}\right) dt^2 + \left(\frac{2M}{r} - \frac{W^2}{r^2}\right) dr^2, \tag{1.17}$$

where the part of the flat spacetime metric is $ds_0^2 = -dt^2 + dr^2 + r^2(d\theta^2 + \sin^2\theta d\phi^2)$.

In the Cartesian coordinates the components $h_{\alpha\beta}$ can be written as

$$\begin{aligned} h_{00} &= \left(\frac{R_s}{r} - \frac{W^2}{r^2}\right), \\ h_{ik} &= \left(\frac{R_s}{r} - \frac{W^2}{r^2}\right) n_i n_k, \\ h_{33} &= \left(\frac{R_s}{r} - \frac{W^2}{r^2}\right) \cos^2\chi \ , \end{aligned} \tag{1.18}$$

where for the simplicity we used the notation $R_s = 2M$.

Applying the formulae (1.16) one can calculate the light deflection angle using the components $h_{\alpha\beta}$ in the bagckground geometry of braneworld space-time in the presence of the plasma as [6, 9]

$$\begin{aligned} \hat{\alpha}_b &= \int_0^\infty \frac{\partial}{\partial b}\Bigg[\left(\frac{R_s}{\sqrt{b^2+z^2}} - \frac{W^2}{r^2}\right)\frac{z^2}{b^2+z^2} \\ &\quad + \frac{1}{1-\omega_0^2/\omega^2}\left(\frac{R_s}{\sqrt{b^2+z^2}} - \frac{W^2}{r^2}\right)\Bigg] dz \end{aligned} \tag{1.19}$$

where we have introduced the impact parameter $b^2 = x_1^2 + x_2^2$, and x_1 and x_2 are the coordinates on the plane orthogonal to the z axis and for the parameters of the plasma we use

$$\omega_0^2 = \frac{4\pi e^2 N(r)}{m}, \quad \omega^2 = \frac{\omega_\infty^2}{f(r)} \tag{1.20}$$

where ω_0 and ω are the plasma and light ray frequency, respectively, and ω_∞ is the asymptotic value of light ray frequency. Considering the power-law plasma density function as

$$N(r) = N_0 \frac{r_0}{r}$$

with the density number N_0 at the radial position of the inner edge of plasma environment r_0. For the small values of the brane tidal charge and large distances the expression (1.20) can be approximated in the following form:

$$n^2 = \left(1 - \frac{\omega_0^2}{\omega^2}\right)^{-1} \simeq 1 - \frac{4\pi e^2 N_0 r_0}{m\omega_\infty^2 r} + \frac{4\pi e^2 N_0 r_0 R_s}{m\omega_\infty^2 r^2} \ . \tag{1.21}$$

Using this approximation one can easily find the deflection angle $\hat{\alpha}_b$ of the light around compact object in the braneworld in the presence of plasma

$$\begin{aligned} \hat{\alpha}_b \ = \ & \frac{2R_s}{b}\left(1 + \frac{\pi^2 e^2 N_0 r_0}{m\omega_\infty^2 b} - \frac{4\pi e^2 N_0 r_0 R_s}{m\omega_\infty^2 b^2}\right) \\ & -\frac{W^2}{4b^2}\left(3\pi + \frac{4\pi e^2 N_0 r_0}{m\omega_\infty^2 b}\left(8 - \frac{3\pi R_s}{b}\right)\right) \end{aligned} \tag{1.22}$$

In the expression (1.22) expressions in the first bracket corresponds to the the deflection angle of the light ray in the field of the Schwarzschild black hole immersed into plasma, while the ones in the second bracket represents the contribution from the braneworld parameter. In the limiting case when plasma parameter $4\pi e^2 N_0 r_0/m\omega_\infty^2 = 0$ and brane parameter $W = 0$ vanish, deflection angle $\hat{\alpha}_b = 2R_s/b$ coincides with the value of the angle in the Schwarzschild spacetime [39, 11].

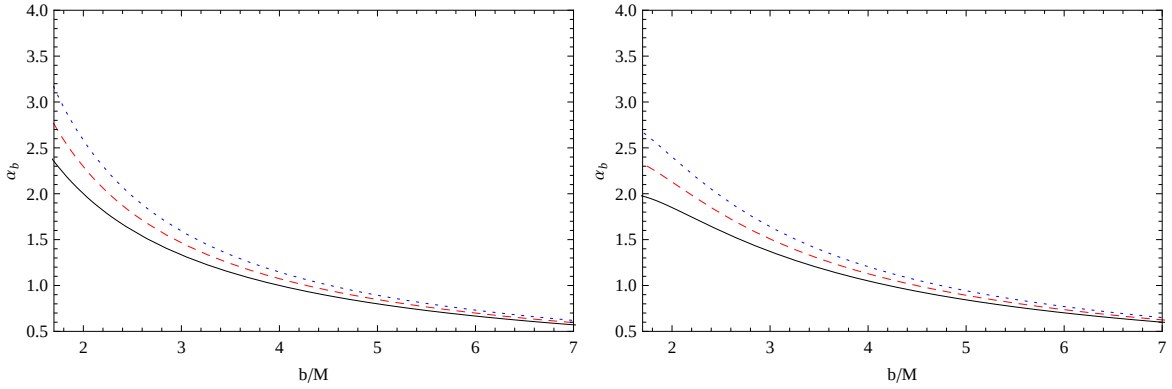

Figure 1.1: Deflection angle α_b as a function of the impact parameter b for different brane parameters W: $W^2 = 0$ is black-solid line, $W^2 = 0.5$ is red-dashed line and $W^2 = 0.99$ is blue-dotted line. Left panel is vacuum case and right panel is plasma case($4\pi e^2 N_0 r_0/m\omega_\infty^2 M = 0.7$).

Using expression (1.22) one can easily plot $\hat{\alpha}_b$ depends on b impact parameter. In Fig. 1.1 the dependence of the deflection angle on impact parameter b has been shown for the different values of brane tidal charge W^2. One can see from Fig. 1.1 that the deflection angle of the light ray from the braneworld black hole increases with increasing the value of the brane parameter. This is direct consequence of the fact that the braneworld parameter makes the black hole stronger, and increases the radii of event horizon and unstable null geodesic sphere.

1.3 Brightness of the image source

In this section we will study the image source magnification using the expression for the deflection angle in the presence of plasma.

Consider the gravitational lens equation in the following form [39]

$$\theta D_s = \beta D_s + \alpha D_{ls} \ , \tag{1.23}$$

where β is the angle of the real source from the observer-lens axis, θ is the angle of apparent image of the source due to lensing with the deflection angle α, D_s and D_{ls} are the distances from the observer to the lens and from the lens to the source, respectively. Since impact parameter is $b = D_l\theta$, where D_l is the distance from the observer to the lens, we obtain the relation in the form [6, 7]

$$\beta = \theta - \frac{D_{ls}}{D_s}\frac{F(\theta)}{D_l}\frac{1}{\theta} \tag{1.24}$$

with the new introduced quantity $F(\theta) = |\alpha_b|b = |\alpha_b(\theta)|D_l\theta$. Solutions of the eq. (1.24) give us the positions θ_k of the images of the object due to the lensing.

The special solution of the Eq. (1.24) is called Einstein angle θ_0 and corresponds to the case when the object, lens, and observer are on a straight line. Corresponding radius of the Einstein ring is $R_0 = D_l\theta_0$, where θ_0 is the solution of the (1.24) when $\beta = 0$. Usually the Einstein angle is very small in order to

be resolved by modern telescopes. However, the lensing by some astrophysical objects like a star or stellar black hole can be detectable because it changes the apparent brightness of the source (magnification of the image brightness). The magnification of image brightness can be calculated using the formula

$$\mu_{\Sigma} = \frac{I_{\rm tot}}{I_*} = \sum_k \left| \left(\frac{\theta_k}{\beta}\right) \left(\frac{d\theta_k}{d\beta}\right) \right| \ , \quad k = 1, 2, ..., s \ , \tag{1.25}$$

where s is the total number of images, $I_{\rm tot}$ is the total brightness of the images and I_* is the unlensed brightness of the source and k refers to the number of images.

Using the expression of the Einstein angle θ_0 in the Shwarzschild spacetime

$$\theta_0 = \sqrt{2R_s \frac{D_{ds}}{D_s D_d}} \tag{1.26}$$

we will consider the generalised expressionf for the Einstein ring $(\theta_0^{pl})_{brane}$ for the braneworld lensing in presence of a plasma using (1.22) and (1.24) as [40]

$$\begin{aligned} (\theta_0^{pl})_{brane} &= \theta_0 \Bigg[1 + \frac{\pi^2 e^2 N_0 r_0}{m\omega_\infty^2 b} - \frac{W^2}{8bR_s} \frac{4\pi e^2 N_0 r_0 R_s}{m\omega_\infty^2 b^2} \\ &\quad \times \left(3\pi + \frac{4\pi e^2 N_0 r_0}{m\omega_\infty^2 b} \left(8 - \frac{3\pi R_s}{b} \right) \right) \Bigg]^{1/2} \end{aligned} \tag{1.27}$$

Using (1.25) one can write magnification of the image source for the braneworld spacetime case:

$$\mu_{tot}^{pl} = \mu_+^{pl} + \mu_-^{pl} = \frac{x^2 + 2}{x\sqrt{x^2 + 4}} \tag{1.28}$$

where dimensionless parameter x is

$$\begin{aligned} x &= \frac{\beta}{(\theta_0^{pl})_{brane}} = x_0 \Bigg[1 + \frac{\pi^2 e^2 N_0 r_0}{m\omega_\infty^2 b} - \frac{4\pi e^2 N_0 r_0 R_s}{m\omega_\infty^2 b^2} \\ &\quad - \frac{W^2}{8bR_s} \left(3\pi + \frac{4\pi e^2 N_0 r_0}{m\omega_\infty^2 b} \left(8 - \frac{3\pi R_s}{b} \right) \right) \Bigg]^{-1/2} \end{aligned} \tag{1.29}$$

where we have used the notation $x_0 = \beta/\theta_0$

The magnification of the image source expressed as

$$\mu_+^{pl} = \frac{1}{4}\Big(\frac{x}{\sqrt{x^2+4}} + \frac{\sqrt{x^2+4}}{x} + 2\Big) \tag{1.30}$$

$$\mu_-^{pl} = \frac{1}{4}\Big(\frac{x}{\sqrt{x^2+4}} + \frac{\sqrt{x^2+4}}{x} - 2\Big) \tag{1.31}$$

In Fig. 1.2 the dependence of the magnification parameter on x_0 has been shown for the different values of brane charge. The presence of the brane charge causes the increase of the magnification parameter of the image source.

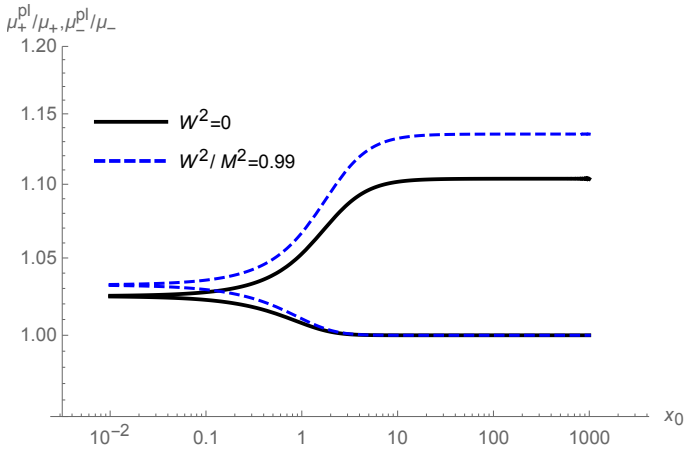

Figure 1.2: μ_+^{pl}/μ_+ and μ_-^{pl}/μ_- of the magnifications of the images in the plasma to the same value in vacuum for different value of brane parameter W^2. Plasma parameter is equal $4\pi e^2 N_0 r_0/m\omega_\infty^2 = 0.7$
[40].

1.4 Retrolensing in the braneworld spacetime

In this section we consider the deflection angle α_b in a strong gravity limit in the braneworld geometry in the absence of plasma. According to the work of [2]

we may look the solution for the deflection angle in the form of:

$$\alpha_b = -\bar{a}\ln\left(\frac{b}{b_{cr}} - 1\right) + \bar{b} + \mathcal{O}((b - b_{cr})\log(b - b_{cr})), \tag{1.32}$$

where b_{cr} is the critical value of the impact parameter and $\bar{a}$ and $\bar{b}$ are the functions of W^2/M^2. The first term in the right hand side of the Eq. (1.32) is due to impact parameter of the light ray (energy and angular momentum of the light rays), second term is due to changes of the spacetime structure in the presence of brane charge and third term is the error term in the deflection angle in strong deflection limit [2].

The light rays sphere radius $r_{\rm ph}$ around the black hole described in braneworld model and spacetime metric (1.1) is

$$r_{\rm ph} = \frac{3M + \sqrt{9M^2 - 8W^2}}{2}. \tag{1.33}$$

The critical value of the impact parameter for the light ray in braneworld spacetime geometry can be found using the condition [2, 3]

$$b_{cr}(r_{\rm ph}) = \lim_{r_0 \to r_{\rm ph}} b(r_0) = \lim_{r_0 \to r_{\rm ph}} \frac{r_0^2}{\sqrt{\Delta_W(r_0)}} \tag{1.34}$$

where $\Delta_W(r_0) = r_0^2 - 2Mr_0 + W^2$.

Near the light rays sphere the radial velocity vanishes and we will have

$$\left(\frac{dr}{d\phi}\right) = r^4\left(\frac{1}{b^2} - \frac{\Delta_W}{r^4}\right), \tag{1.35}$$

where we have used the relation $b = L/E$. The deflection angle of the light coming through light rays sphere are of black hole in braneworld model can be found using the expression:

$$\alpha_b = \lim_{r_0 \to r_{\rm ph}} 2\int_{r_0}^{\infty} \frac{dr}{r^2\sqrt{\frac{1}{b^2} - \frac{\Delta_W}{r^4}}} - \pi \tag{1.36}$$

Using the technique described in [2] one can easily obtain the analytic expressions of the functions $\bar{a}$ and $\bar{b}$ in the following form:

$$\bar{b} = \bar{a}\ln\left[\frac{8(3Mr_{\rm ph}-4W^2)^3}{M^2r_{\rm ph}^2(Mr_{\rm ph}-W^2)^2}\times \left(2\sqrt{Mr_{\rm ph}-W^2}-\sqrt{3Mr_{\rm ph}-4W^2}\right)^2\right]-\pi, \tag{1.37}$$

$$\bar{a} = \frac{r_{\rm ph}\sqrt{Mr_{\rm ph}-W^2}}{\sqrt{M(6M-r_{\rm ph})r_{\rm ph}^2+9r_{\rm ph}MW^2-4W^2}}. \tag{1.38}$$

The expression b_{cr}, b, $\bar{a}$ and $\bar{b}$ are obtained analytically. In the limiting case when brane tidal charge vanished the values of the $\bar{a}$ and $\bar{b}$ are the followings: $\bar{a}=1$ and $\bar{b}\simeq -2.92841$. Thus the physically meanings of the quantities $\bar{a}$ and $\bar{b}$ can be interpreted as deviation of the deflection angle due to modification of the spacetime metric. The dependences of these parameters are shown in Fig 1.3. In this plot we presented b_{cr}, b, $\bar{a}$ and $\bar{b}$ depending on brane parameter and other hand one can compare with parameter of Reissner-Nordström. It is clear that they have opposite properties braneworld with Reissner-Nordström gravity. The dependence of the double image of the source in the Braneworld spacetime on the brane charge W^2/M^2 has been shown in Fig 1.4.

In Fig. 1.5 the deflection angle of the light curve depending on the impact parameter of light rays motion has been shown for different values of brane parameter. One can easily notice from Fig. 1.5 that an increase in the value of brane parameter increases the impact parameter of the light curve and at the same time increases the deflection angle of it.

1.5 Conclusion

In this chapter we have presented the description of the equation of light propagation around black hole in braneworld in order to describe the gravitational

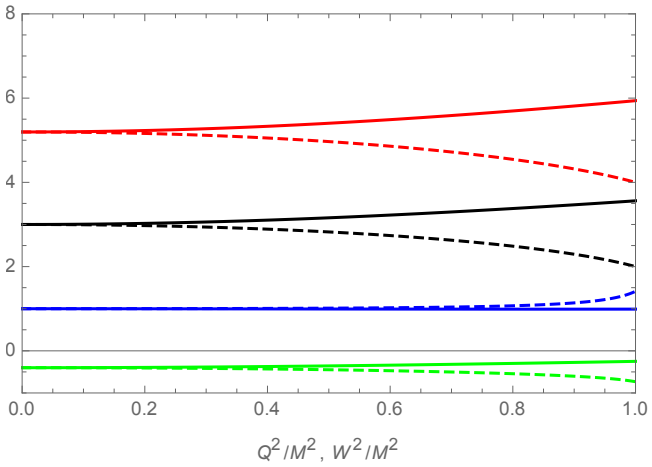

Figure 1.3: b_c/M(red line), r_{pc}/M(black line), $\bar{a}$(blue line), and $\bar{b}$(green line) in the Branewolrd spacetime(solid line) as the functions of W^2/M^2 comparing with Reissner-Nordström spacetime(dashed line).

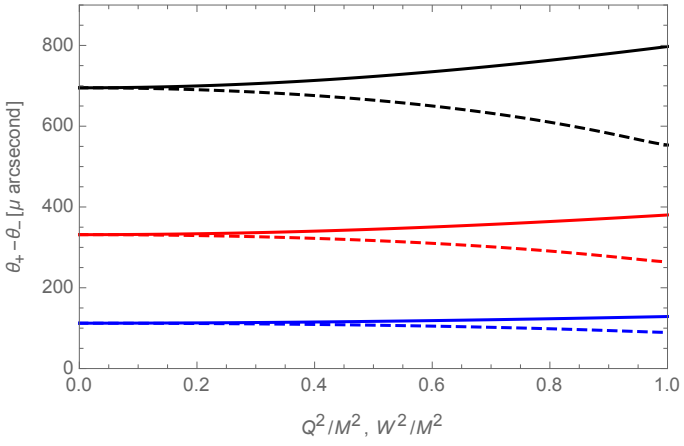

Figure 1.4: Double image in the Braneworld spacetime(solid line) as the functions of W^2/M^2 comparing with Reissner-Nordström spacetime(dashed line) for the different masses of the black hole: $M = 10M_o$ (the black line, $M = 30M_o$ (the red line), $M = 60M_o$ (the blue line).

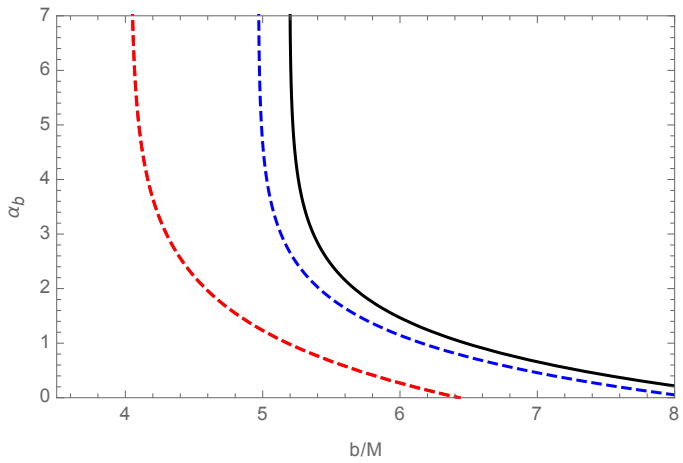

Figure 1.5: Deflection angle of light curve in branewolrd space-time for different value of brane parameter W as: $W^2 = 0(Black, solid)$, $W^2 = 0.5(Blue, dashed)$, $W^2 = 0.99(red, dashed)$ [40].

lensing effect due to bending the light beams. Considering nonvanishing brane tidal charge of the black hole we have obtained the exact expressions for the deflection angle of the light ray due to the effect of weak gravitational lensing. For Sun deflection angle has the value of $(1.75 \pm 0.05)''$ [1], using this observational result one can estimate for the dimensionless brane parameter as $W^2/R^2 = 0.96 \cdot 10^{-7}$.

The magnification of the image source brightness in the background spacetimes of black hole in braneworld have been also considered. It was shown, that the increase of the module of brane tidal charge of the black hole causes the increase the magnification of the size image.

In this chapter the retrolensing effect around black hole in braneworld has been also investigated. The analysis of the retrolensing effetct due to brane tidal charge shows that in the presence of the negative brane charge one can observe the sufficiently increase the image source magnification and larger bending angle with compare to black hole with electric charge.

Chapter II

Horizon structure of rotating black hole and energy extraction from it

2.1 Introduction

In Maxwell's electromagnetic field theory, the field of a point-like charge is singular at the charge position and hence it has infinite self-energy. To overcome this problem in classical electrodynamics, the non-linear electromagnetic field has been proposed by Born and Infeld [41], with main motivation, to resolve self-energy problem by imposing a maximum strength of the electromagnetic field. In this theory the electric field of a point charge is regular at the origin and this non-linear theory for the electromagnetic field was able to tone down the infinite self energy of the point-like charged particle. Later, Hoffmann [42] coupled general relativity with Born-Infeld electrodynamics to obtain a spherically symmetric solution for the gravitational field of an electrically charged object. Remarkably, after a long dormancy period, the Born-Infeld theory made a come back to the stage in the context of more modern developments, which is mainly due to the interest in non-linear electrodynamics in the context of low energy string theory, in which Born-Infeld type actions appeared [43]. Indeed, the low energy effective action in an open superstring in loop calculations lead to Born-Infeld type actions

[43]. These important features of the Born-Infeld theory, together with its corrective properties concerning singularities, further motivate to search for gravitational analogues of this theory in the past [44], and also interesting measures have been taken to get the spherically symmetric solutions [45]. The thermodynamic properties and causal structure of the Einstein-Born-Infeld black holes drastically differ from that of the classical Reissner-Nordstrom black holes. Indeed, it turns out that the Einstein-Born-Infeld black hole singularity is weaker than that of Reissner-Nordstrom black hole. Further properties of these black holes, including motion of the test particles has been also addressed [46]. It is worthwhile to mention that Kerr [47] and Kerr-Newman metrics [48] are undoubtedly the most significant exact solutions in the general relativity, which represent rotating black hole that can arise as the final fate of gravitational collapse. The generalization of the spherically symmetric Einstein-Born-Infeld black hole in the rotating case, Kerr-Newman like solution, was studied by Lombardo [49]. In particular, it is demonstrated [41] that the rotating Einstein-Born-Infeld solutions can be derived starting from the corresponding exact spherically symmetric solutions [42] by a complex coordinate transformation previously developed by Newman and Janis [50]. The rotating Einstein-Born-Infeld black hole metrics are axisymmetric, asymptotically flat and depend on the mass, charge and spin of the black hole as well as on a Born-Infeld parameter (β) that measure potential deviations from the Kerr metric Kerr-Newman metrics. The rotating Einstein-Born-Infeld metric includes the Kerr-Newman metric as the special case if this deviation parameter diverges ($\beta \to \infty$) as well as the Kerr metric when this parameter vanishes ($\beta = 0$). In this paper, we carry out detailed analysis of the horizon structure of rotating Einstein-Born-Infeld black hole and explicitly manifest the effect β has. Recently, horizon structure has been studied for various space-time geometris, see,

e.g., [51].

Black holes are very interesting gravitational as well as geometrical objects to study in four dimensions and may exist in higher dimensional space-time. In recent years, black hole solutions in more than four space-time dimensions, especially in five-dimensions (5D), have been the subject of intensive research, motivated by ideas in brane-world cosmology, string theory and gauge/gravity duality. Several interesting and surprising results have been found [52]. In dimensions higher than four, the uniqueness theorems do not hold due to the fact that there are more degrees of freedom. The discovery of black-ring solutions in five dimensions shows that non-trivial topologies are allowed in higher dimensions [53]. The Myers-Perry [54] black hole spacetime is higher dimensional generalization of the four-dimensional Kerr black hole spacetime.

2.2 Horizon of rotating Einstein-Born-Infeld black hole

The action for the gravitational field coupled to a nonlinear Born-Infeld electrodynamics (or a Einstein-Born-Infeld action) in (3+1) dimensions reads [41, 42]

$$S = \int d^4x\sqrt{-g}\left[\frac{R}{16\pi G} + \mathcal{L}(\mathcal{F})\right] , \tag{2.1}$$

where R is scalar curvature, $g \equiv \det|g_{\mu\nu}|$ and $\mathcal{L}(\mathcal{F})$ is given by

$$\mathcal{L}(\mathcal{F}) = \frac{\beta^2}{4\pi G}\left(1 - \sqrt{1 + \frac{2\mathcal{F}}{\beta^2}}\right) , \tag{2.2}$$

with $\mathcal{F} = \frac{1}{4}F_{\mu\nu}F^{\mu\nu}$, $F_{\mu\nu}$ denotes the electromagnetic field tensor. Here β^2 is the Born-Infeld parameter being equal to the maximum value of electromagnetic field intensity and has a dimension of $[length]^{-2}$. Eq. (2.1) leads to the Einstein field equations

$$R_{\mu\nu} - \frac{1}{2}g_{\mu\nu}R = \kappa T_{\mu\nu} , \tag{2.3}$$

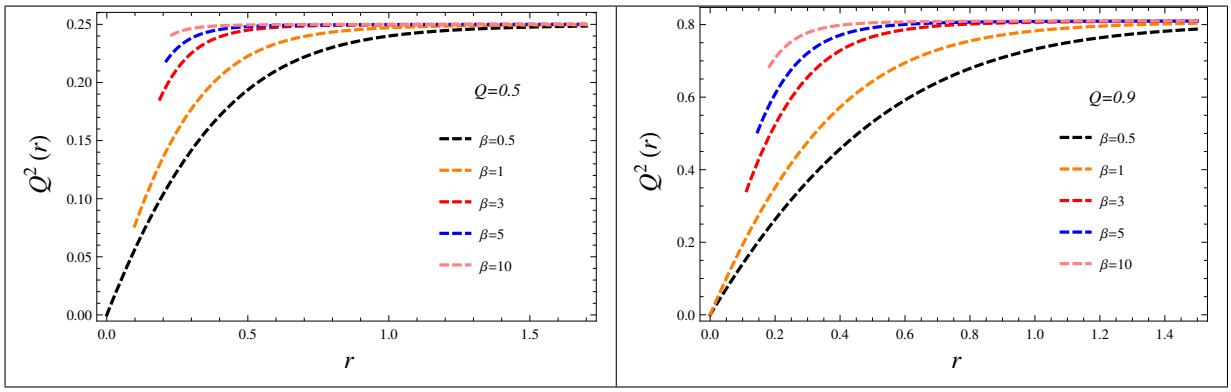

Figure 2.1: Plots showing the dependence of the square of the electric charge $Q^2(r)$ from the radial coordinate r for different values of Born-Infeld parameter β. Left panel is for $Q = 0.5$ and right panel is for $Q = 0.9$ in asymptotics.

and electromagnetic field equation

$$\nabla_\mu(F^{\mu\nu}\mathcal{L}_{,\mathcal{F}}) = 0 \ . \tag{2.4}$$

The energy momentum tensor is

$$T_{\mu\nu} = \mathcal{L}g_{\mu\nu} - F_{\mu\sigma}F^{\sigma}_{\nu} \ , \tag{2.5}$$

where $\mathcal{L}_{,\mathcal{F}}$ denotes partial derivative of $\mathcal{L}$ with respect to F.

The gravitational field of a static and spherically symmetric compact object with mass M and a non-linear electromagnetic source in the Einstein-Born-Infeld theory has first been investigated by Hoffmann [42] and the space-time metric is [42]

$$\begin{aligned} ds^2 = &-\left[1 - \frac{2GM}{r} + \frac{Q^2(r)}{r^2}\right] dt^2 \\ &+ \left[1 - \frac{2GM}{r} + \frac{Q^2(r)}{r^2}\right]^{-1} dr^2 + r^2\left(d\theta^2 + \sin^2\theta\, d\varphi^2\right) \ , \end{aligned} \tag{2.6}$$

with the square of electric charge

$$Q^2(r) \quad = \frac{2\beta^2 r^4}{3}\left(1 - \sqrt{1+\zeta^2(r)}\right) + \frac{4Q^2}{3}F\left(\frac{1}{4}, \frac{1}{2}, \frac{5}{4}, -\zeta^2(r)\right) \ , \tag{2.7}$$

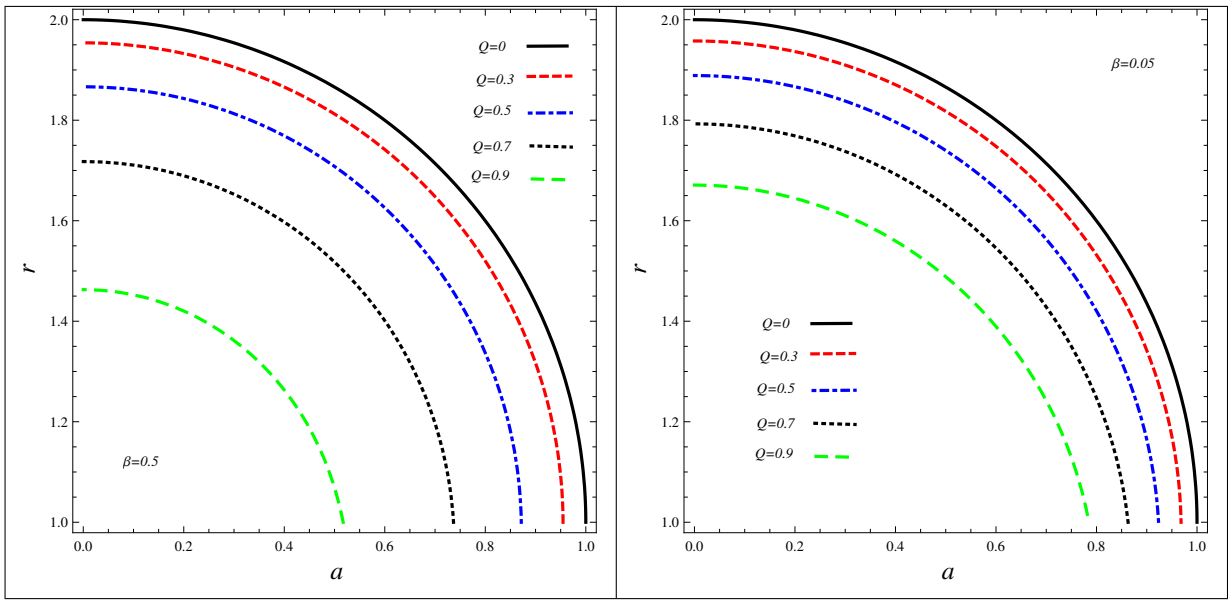

Figure 2.2: The rotation parameter a dependence of the radial coordinate r for the different value of electric charge Q and Born-Infeld parameter β. The lines separate the region of black holes with naked singularity ones. The left panel is for Born-Infeld parameter $\beta = 0.5$ and the right panel is for Born-Infeld parameter $\beta = 0.05$.

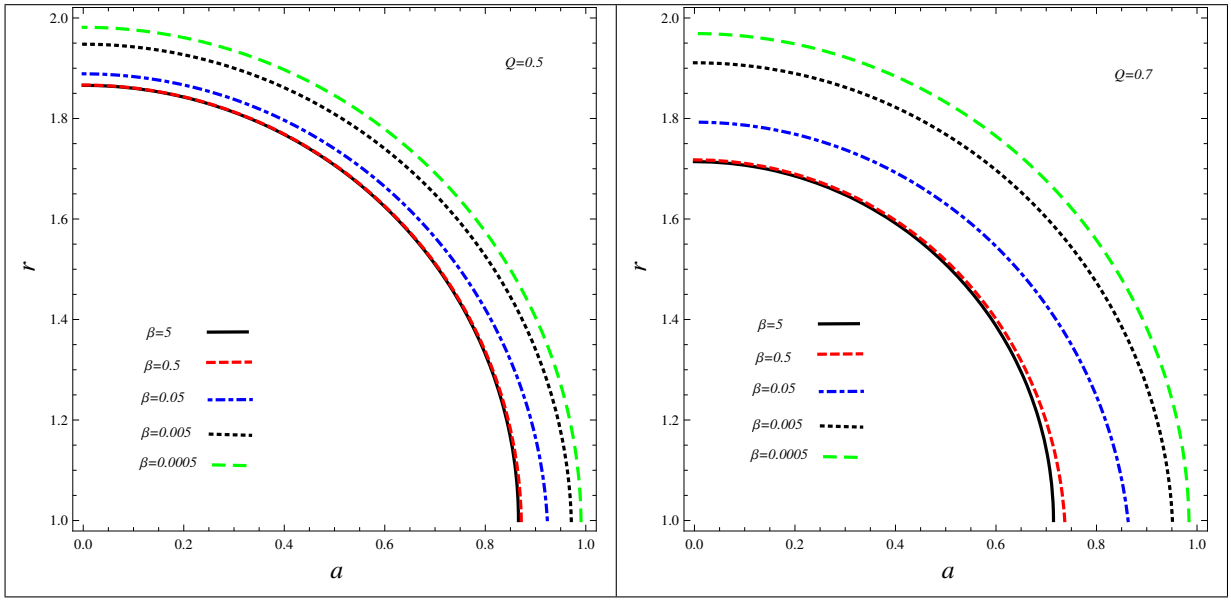

Figure 2.3: The rotation parameter a dependence of the radial coordinate r for the different value of electric charge Q and Born-Infeld parameter β. The lines separate the region of black holes with naked singularity ones. The left panel is for electric charge $Q = 0.5$ and the right panel is for electric charge $Q = 0.7$. [55]

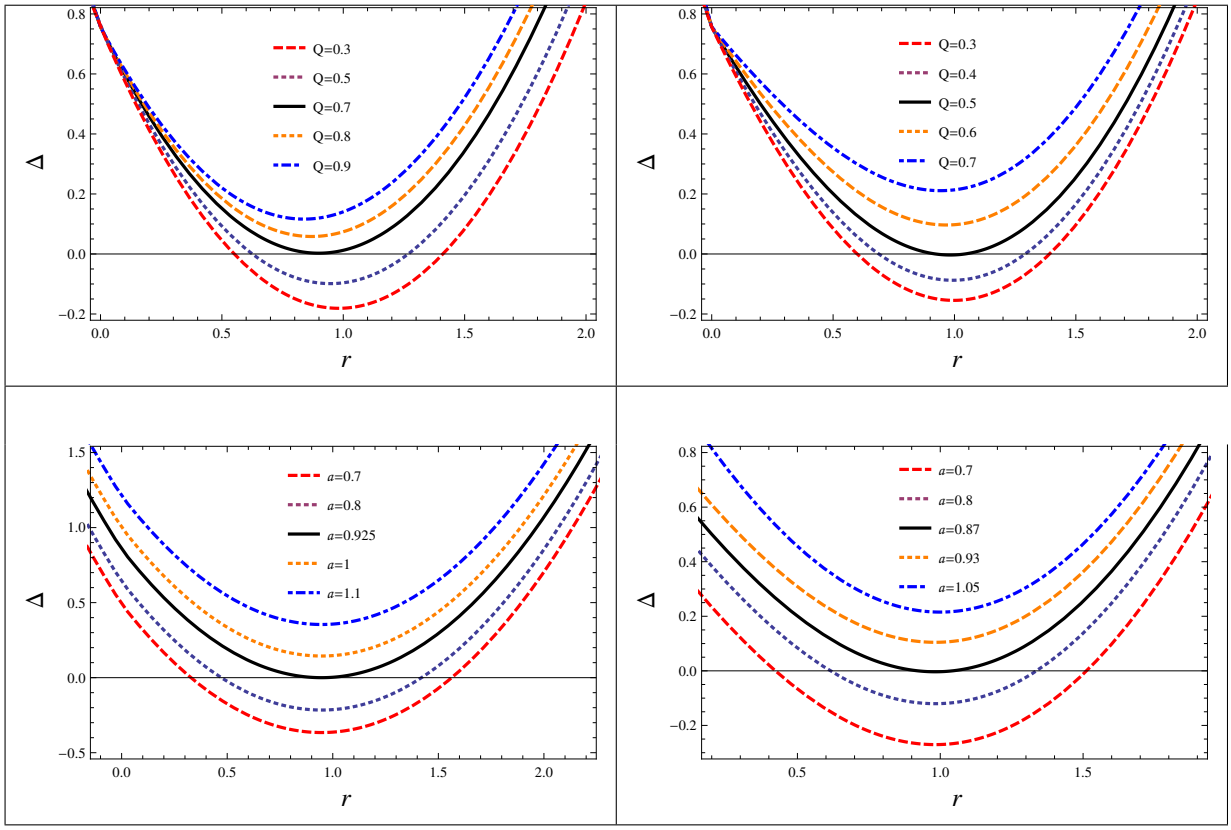

Figure 2.4: Plots showing the radial dependence of Δ for the different values of Born-Infeld parameter β, electric charge Q and rotation parameter a (with $M = 1$). Top, left panel is for $a = 0.87$ and $\beta = 0.05$. Top, right panel is for $a = 0.87$ and $\beta = 0.5$. Bottom, left panel is for $Q = 0.5$ and $\beta = 0.05$. Bottom, right panel is for $Q = 0.5$ and $\beta = 0.5$.

where F is a Gauss hypergeometric function [56] and new notation $\zeta^2(r) = Q^2/(\beta^2 r^4)$ is introduced. From the radial dependence of $Q^2(r)$ plotted in Fig.2.1 one can see its strong dependence from β parameter near to the center of the black hole. The rotating counterpart of the Einstein-Born-Infeld black hole has been obtained in [49]. The gravitational field of rotating Einstein-Born-Infeld black hole spacetime is described by the metric which in the Boyer-Lindquist coordinates is given by [49]

$$\begin{aligned} ds^2 &= \frac{\Delta - a^2\sin^2\theta}{\rho^2}dt^2 - \frac{\rho^2}{\Delta}\,dr^2 \\ &\quad +2a\sin^2\theta\left(1 - \frac{\Delta - a^2\sin^2\theta}{\rho^2}\right)dt\,d\phi - \rho^2\,d\theta^2 \\ &\quad - \sin^2\theta\left[\rho^2 + a^2\sin^2\theta\left(2 - \frac{\Delta - a^2\sin^2\theta}{\rho^2}\right)\right]d\phi^2\ , \end{aligned} \tag{2.8}$$

with

$$\Delta = r^2 - 2GMr + Q^2\,(r) + a^2, \text{and } \rho^2 = r^2 + a^2\cos^2\theta. \tag{2.9}$$

The parameters a, M, Q and β are, respectively correspond to rotation, mass, the electric charge and the Born-Infeld parameter. We let the parameters Q and β to be positive. In the limit $\beta \to \infty$ (or $Q(r) = Q$) and $Q \neq 0$, one obtains the corresponding solution for Kerr-Newman black hole, while one has Kerr black hole [47] when $\beta \to 0$. The metric (2.8) is a rotating charged black hole which generalizes the standard Kerr-Newman black hole and we call it as the rotating Einstein-Born-Infeld black hole. The non-rotating case, $a = 0$, corresponds to the metric of the static Einstein-Born-Infeld black hole obtained by Hoffmann in [42]. The metric (2.8) has curvature singularity at the set of points, where $\rho = 0$ and $M = Q \neq 0$. For $a \neq 0$, it corresponds to a ring with radius a, in the equatorial plane $\theta = \pi/2$ and hence termed as a ring singularity. The properties of the rotating Einstein-Born-Infeld metric (2.8) are similar to that of the general

relativity counterpart Kerr-Newman black hole. We first show that, it is possible to get certain range of values of a, M and Q, the metric (2.8) is a black hole. The metric (2.8), like the Kerr-Newman one, is singular at $\Delta = 0$ and it admits two horizons like surfaces, viz., the static limit surface and the event horizon. Here, we shall look for these two surfaces for the rotating Einstein-Born-Infeld metric (2.8) and discuss the effect of the nonlinear parameter β. The horizons of the Einstein-Born-Infeld black hole (2.8) are dependent on parameters M, a, Q and β, and are calculated by equating the g^{rr} component of the metric (2.8) to zero, i.e.,

$$\Delta = r^2 - 2GMr + Q^2(r) + a^2 = 0, \tag{2.10}$$

which depends on $Q(r)$ a function of r, and is different from the Kerr-Newman black hole, where Q is just a constant. The solution Eq. (2.10) can have either no roots (naked singularity), two roots (horizons) depending on the values of these parameters. It is difficult to solve the Eq. (2.10) analytically and hence we seek numerical solutions. It is seen that Eq. (2.10) admits two horizons r^-_{EH} and r^+_{EH} for suitable choice of parameters, which corresponds to two positive roots of Eq. (2.10), with r^+_{EH} determines the event horizons and r^-_{EH} the Cauchy horizon. Further, it is worthwhile to mention that one can set parameters when r^-_{EH} and r^+_{EH} are equal and we have an extremal black hole. We have plotted the event horizons in Fig. 2.2-2.3 for different values of mass M, charge Q, parameter β and spinning parameter a. Like, the Kerr-Newman black hole, the rotating spacetime (2.8) has two horizons, viz., the Cauchy horizon and the event horizon. The figures reveal that there exists set of values of parameters for which we have two horizons, i.e., a black hole with both inner and outer horizons. One can also find values of parameters for which one gets an extremal black hole where the two horizons coincide. The region between the static limit surface and the event

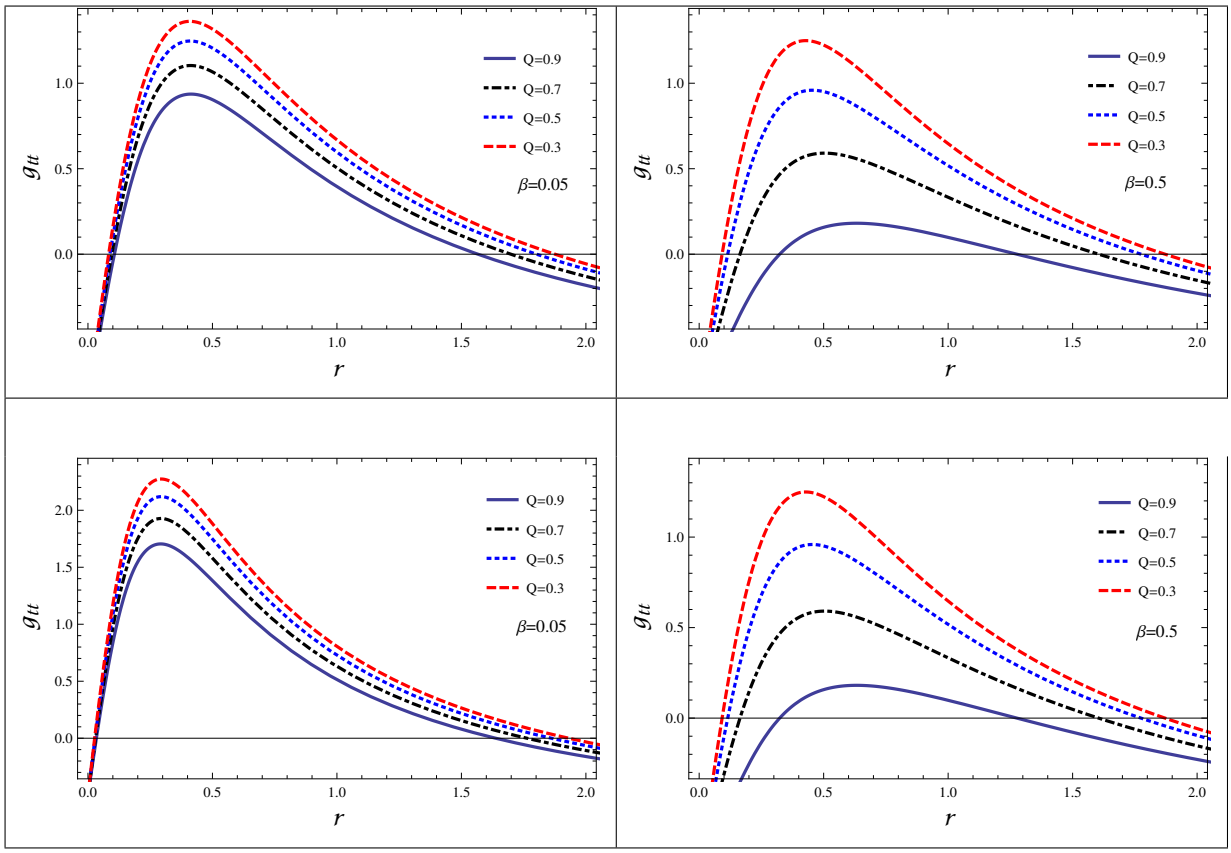

Figure 2.5: Plots showing the radial dependence of g_{tt} component of metric tensor for the different values of Born-Infeld parameter β and electric charge Q (with $M = 1$). Top, left panel is for $\beta = 0.05$, $a = 0.45$ and $\alpha = \pi/6$. Top, right panel is for $\beta = 0.5$, $a = 0.45$ and $\alpha = \pi/6$. Bottom, left panel is for $\beta = 0.05$, $a = 0.45$ and $\alpha = \pi/3$. Bottom, right panel is for $\beta = 0.5$, $a = 0.45$ and $\alpha = \pi/3$.

horizon is termed as quantum ergosphere, where it is possible to enter and leave again, and the object moves in the direction of the spin of black hole. We have numerically studied the horizon properties for nonzero values of a, β and Q (cf. Fig. 2.4) by solving Eq. (2.10). It turns out that the Born-Infeld parameter β makes a profound influence on the horizon structure when compared with the Kerr black hole. We find that for a given values of parameters β, Q, there exist extremal value of $a = a_E$ and $r = r_H^E$ such that for $a < a_E$, Eq. (2.10) admits two positive roots , which corresponds to respectively, a black hole has two horizons or black hole with both Cauchy and event horizons. We found no root at $a > a_E$ 'naked singularity', see Fig. 2.4, i.e., existence of a naked singularity. Further, one

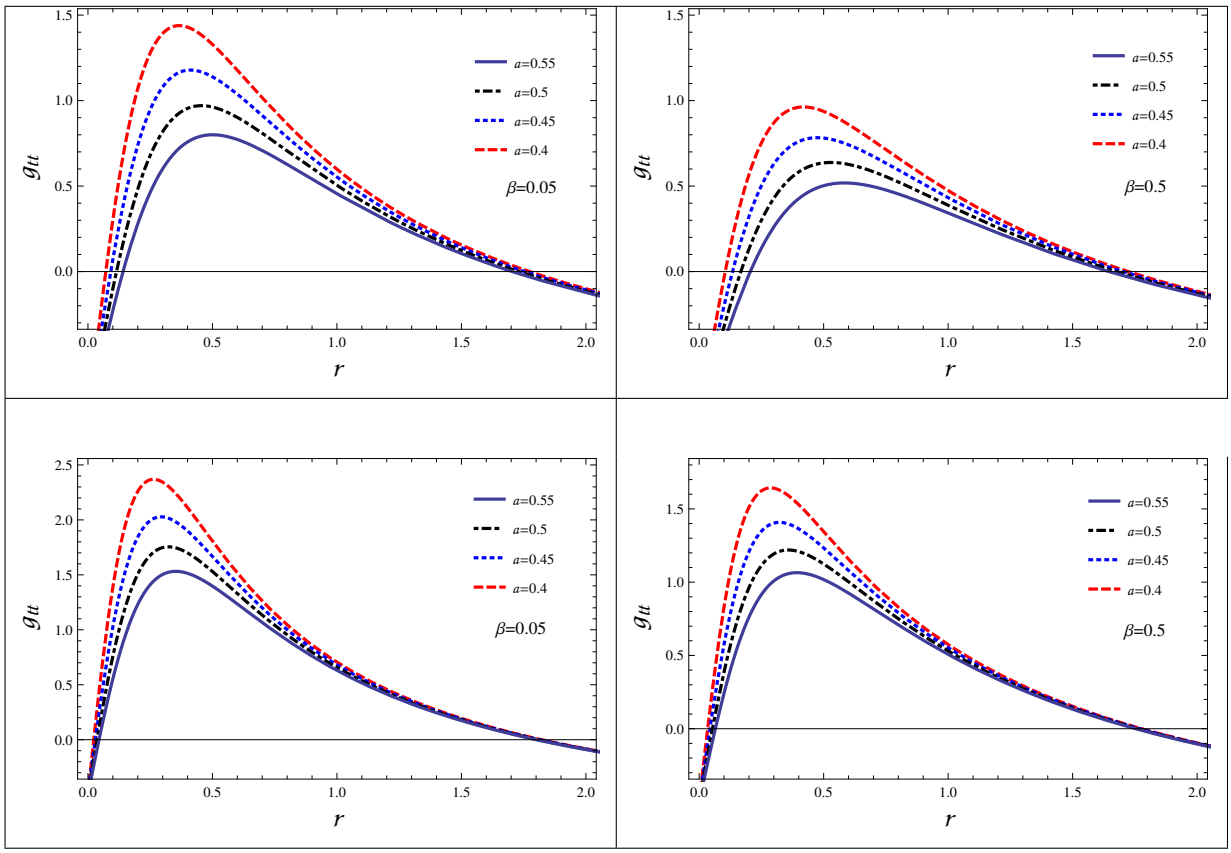

Figure 2.6: Plots showing the radial dependence of g_{tt} component of metric tensor for the different values of parameter β and rotation parameter a (with $M = 1$). Top, left panel is for $\beta = 0.05$, $Q = 0.6$ and $\alpha = \pi/6$. Top, right panel is for $\beta = 0.5$, $Q = 0.6$ and $\alpha = \pi/6$. Bottom, left panel is for $\beta = 0.05$, $Q = 0.6$ and $\alpha = \pi/3$. Bottom, right panel is for $\beta = 0.5$, $Q = 0.6$ and $\alpha = \pi/3$.[55]

can find values of parameters for which these two horizons coincide and we get extremal black holes. Similarly, we have shown that for given values of parameters a, β, we get an extremal value of $Q = Q_E$, for which two horizons coincide and we get extremal black holes as shown in Fig. 2.4. Interestingly, the value of Q_E decreases with increase in β.

Infinite red-shift surface or static limit surface. While in rotatig black hole, in general, the horizon is also the surface where g_{tt} changes sign, in rotating Einstein-Born-Infeld, like Kerr-Newman, these surfaces do not coincide. The location of infinite redshift surface or static limit surface requires the coefficient of dt^2 to vanish, i.e., it must satisfy

$$r^2 - 2GMr + Q^2(r) + a^2\cos^2(\theta) = 0. \tag{2.11}$$

Eq. (2.11) is solved numerically for the behavior of the static limit surface which is shown in Figs. 2.5 and 2.6. The Einstein-Born-Infeld metric (2.8) admits two static limit surfaces r^-_{SLS} and r^+_{SLS} corresponding to two positive roots of Eq. (2.11) when the parameters M, Q, a, and β are chosen suitably (cf. Figs. 2.5 and 2.6). Interestingly the radius of the static limit surface decreases with increase in the value of parameter β. The static limit surface has similar extremal behavior which is depicted in the Figs. 2.5 and 2.6). Like any other rotating black hole, there is a region outside the outer horizon where $g_{tt} > 0$. The region, i.e. $r^+_{SLS} < r < r^+_{EH}$ is called ergoregion, and its outer boundary $r = r^+_{SLS}$ is called the quantum ergosphere.

2.3 Horizon of Five-Dimensional Myers-Perry black hole

The metric of a 5D rotating Myers-Perry black hole in the Boyer-Lindquist coordinates reads [57]

$$\begin{aligned} ds^2 &= \frac{\rho^2}{4\Delta}dx^2 + \rho^2 d\theta^2 - dt^2 + (x+a^2)\sin^2\theta d\phi^2 \\ &\quad + (x+b^2)\cos^2\theta d\psi^2 + \frac{r_0^2}{\rho^2}\Big[dt + a\sin^2\theta d\phi + b\cos^2\theta d\psi\Big]^2, \end{aligned} \tag{2.12}$$

with ρ^2 and Δ are given by

$$\rho^2 = x + a^2\cos^2\theta + b^2\sin^2\theta, \quad \Delta_{5D} = (x+a^2)(x+b^2) - r_0^2 x.$$

It may be noted that the metric (2.12) is singular when $\Delta_{5D} = g_{rr} = 0$ and $\rho^2 = 0$. Here a and b are two spin parameters, and $0 \leq \phi \leq 2\pi$ and $0 \leq \psi \leq \pi/2$ are two angles. Following [58] instead of the radius r we use the coordinate $x = r^2$ to simplify the calculations. The ADM mass of black hole is $2M = r_0^2$. Also note that the metric (2.12) reduces to 5D Tangherlini solution [59] for $a = b = 0$.

The black hole horizon is determined by taking roots of the equation $\Delta_{5D} = 0$, which admit solutions

$$x_\pm = \frac{1}{2}\left[r_0^2 - (a^2+b^2) \pm \sqrt{[r_0^2 - (a^2+b^2)]^2 - 4a^2b^2}\right].$$

Here, x_+ denotes outer horizon and x_- the inner horizon. It is clear that the metric (2.12) describes non-extremal black hole for $x_+ > x_-$ and when $x_+ = x_-$, one obtains an extremal black hole. The horizon exists when $a^2 + b^2 < r_0^2$ and $[r_0^2 - (a^2+b^2)]^2 \geq 4a^2b^2$. This defines a region in the (a, b) where metric represents black hole and not a naked singularity.

Eq. (3.2), when $a = b$, yields

$$x_\pm = \frac{1}{2}(r_0^2 - 2a^2 \pm \sqrt{r_0^4 - 4a^2 r_0^2}). \tag{2.13}$$

The extremal black hole occurs when $r_0^2 = 4a^2$ horizon merges. On the other hand for $r_0^2 < 4a^2$ we have a naked singularity and black hole occurs when $r_0^2 > 4a^2$. It

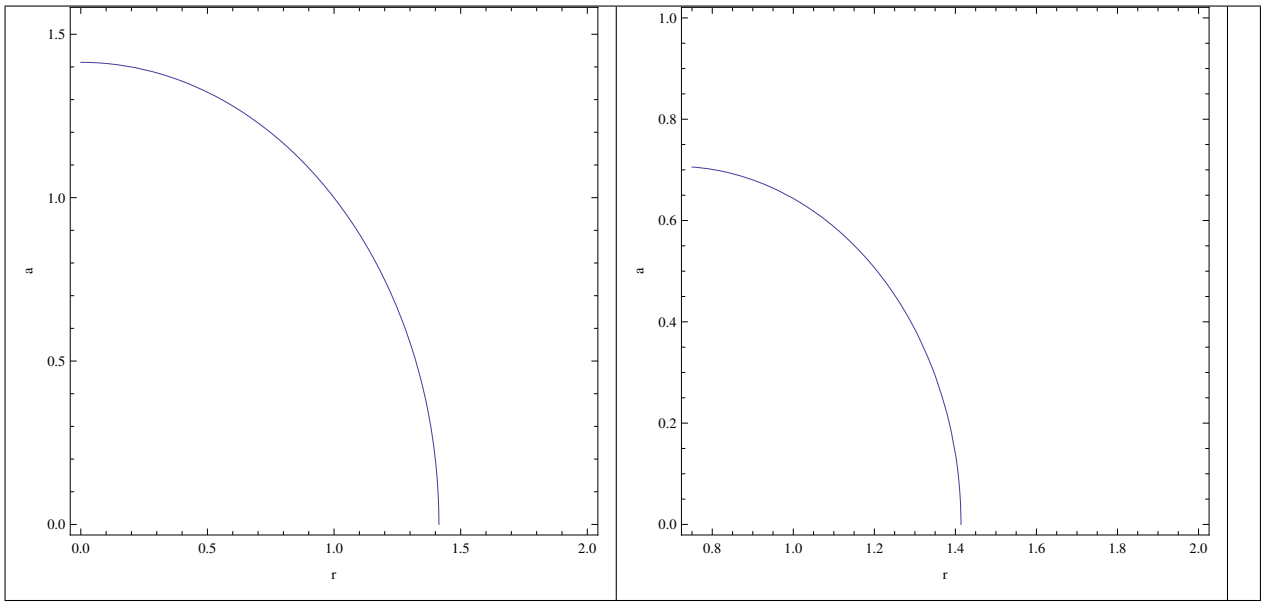

Figure 2.7: Plots showing the radial dependence of spin parameter a and b for the horizon. i) For spin parameter $a \neq b$. ii) For $a = b$.

may be noted that the event horizon r_+ is smaller for the larger value of rotation parameter a.

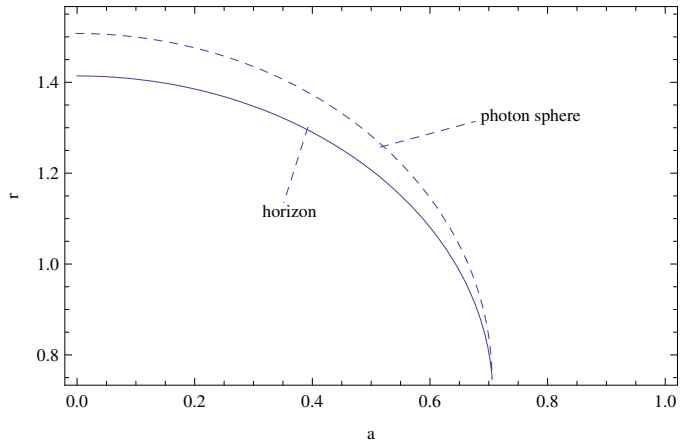

Figure 2.8: Plots showing the radial dependence of spin parameter for the horizon and light rays sphere for $a = b$.

The metric (2.12) is invariant on taking the following transformation:

$$a \leftrightarrow b, \quad \theta \leftrightarrow \left(\frac{\pi}{2} - \theta\right), \quad \phi \leftrightarrow \psi. \tag{2.14}$$

This metric possesses three killing vectors ∂_t, ∂_ϕ and ∂_ψ. For $a = b$ the metric has two additional Killing vectors [58].

In Fig. 3.2, we have shown the possible range of rotation parameters for the case $a \neq b$ and $a = b$. When $a \neq b$, range of rotation parameter is $0 < a < 1.4$, on the other hand for $a = b$ it is $0 < a < 1/\sqrt{2}$. In Fig. 2.8, we have shown the change in the behaviour of light rays sphere with horizon for $a = b$ case. It is interesting to note that with the increase in the value of rotation parameter light rays sphere is coming close to the central object, it is very important because light rays sphere around black hole will show the shape of the shadow.

To study the equation of motion of light ray in the field of a 5D rotating Myers-Perry black hole, we begin with the Lagrangian which reads

$$L = \frac{1}{2} g_{\mu\nu} \dot{x}^{\mu} \dot{x}^{\nu}, \tag{2.15}$$

where an overdot denotes the partial derivative with respect to an affine parameter. Therefore, the momenta calculated for the metric (2.12) are:

$$\begin{aligned}
p_t &= \left(-1 + \frac{r_0^2}{\rho^2}\right) \dot{t} + \frac{r_0^2}{\rho^2} \dot{\phi} + \frac{r_0^2 b \cos^2\theta}{\rho^2} \dot{\psi}, \\
p_\phi &= \frac{r_0^2 a \sin^2\theta}{\rho^2} \dot{t} + \left(x + a^2 + \frac{r_0^2 a^2 \sin^2\theta}{\rho^2}\right) \sin^2\theta \dot{\phi} + \frac{r_0^2 ab \sin^2\theta \cos^2\theta}{\rho^2} \dot{\psi}, \\
p_\psi &= \frac{r_0^2 b \cos^2\theta}{\rho^2} \dot{t} + \frac{r_0^2 ab \sin^2\theta \cos^2\theta}{\rho^2} \dot{\phi} + \left(x + b^2 + \frac{r_0^2 b^2 \cos^2\theta}{\rho^2}\right) \cos^2\theta \dot{\psi}, \\
p_x &= \frac{\rho^2}{4\Delta_{5D}} \dot{x}, \\
p_\theta &= \rho^2 \dot{\theta},
\end{aligned} \tag{2.16}$$

where $p_t = -E$, $p_\phi = L_\phi$ and $p_\psi = L_\psi$ correspond to energy and angular momentum with respect to the respective rotation axis respectively.

2.4 Energy emission from black hole

2.4.1 Energy emission from the Born-Infeld black hole

For completeness of our research here we investigate rate of the energy emission from the Einstein-Born-Infeld black hole with the help of

$$\frac{d^2E(\omega)}{d\omega dt} = \frac{2\pi^2\sigma_{lim}}{\exp\omega/T-1}\omega^3 \ , \tag{2.17}$$

where $T = \kappa/2\pi$ is the Hawking temperature, and κ is the surface gravity. At outer horizon the temperature T is equal to ([55])

$$\begin{aligned} T &= \frac{2Q^4\sqrt{1+\zeta^2(r_+)} - 2\beta^2Q^2r_+^4\left(1+2\sqrt{1+\zeta^2(r_+)}\right)}{12\beta^2\pi r_+^5(a^2+r_+^2)\sqrt{1+\zeta^2(r_+)}} \\ &+\frac{3r_+^4\beta^2D}{12\beta^2\pi r_+^5(a^2+r_+^2)\sqrt{1+\zeta^2(r_+)}} \ , \end{aligned} \tag{2.18}$$

where

$$\begin{aligned} D &= -a^2\sqrt{1+\zeta^2(r_+)}+ \\ &\quad r_+^2(\sqrt{1+\zeta^2(r_+)}+2\beta^2r_+^2(\sqrt{1+\zeta^2(r_+)}-1)) \end{aligned} \tag{2.19}$$

The limiting constant σ_{lim} defines the value of the absorption cross section vibration for a spherically symmetric black hole:

$$\sigma_{lim} \approx \pi R_s^2 \ .$$

Consequently according to [60] we have

$$\frac{d^2E(\omega)}{d\omega dt} = \frac{2\pi^3R_s^2}{e^{\omega/T}-1}\omega^3 \ .$$

The dependence of energy emission rate from frequency for the different values of electric charge Q and parameter β is shown in Fig. 2.9. One can see that with the increasing electric charge Q or parameter β the maximum value of energy emission rate decreases, caused by horizon area decrease.

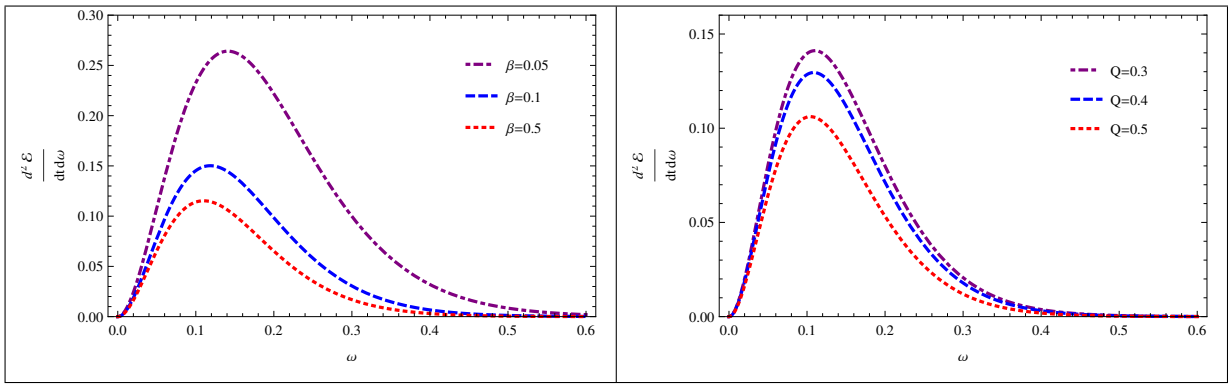

Figure 2.9: Energy emission of black hole in Einstein-Born-Infeld gravity. Left panel is for electric charge $Q = 0.5$ and right panel is for Born-Infeld parameter $\beta = 0.05$ ([55]).

2.4.2 Emission energy from Black hole in braneworld space-time

Now we consider the emission energy from the black hole in braneworld gravity using expression (2.4.1). Where $T = \frac{\sqrt{M^2-W^2}}{2\pi(M+\sqrt{M^2-W^2})}$ is Hawking temperatura in the Braneworld gravity.

The dependence of emission energy rate from frequency for the different values of brane paramtere W is shown in Fig. 2.10. It is clearly shown that with increasing brane parameter peak of the emission energy also increasing, because of horizon.

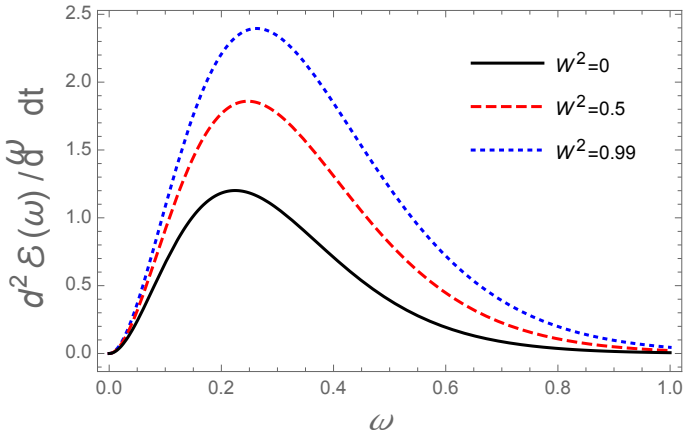

Figure 2.10: Emission energy of black hole in branewolrd space-time for different value of brane parameter W.

2.4.3 Energy emission from the 5D black hole

It is well known that, at high energy the absorption cross section of a black hole oscillates around a limiting constant value and the black hole shadow corresponds to its high energy absorption cross section for the observer located at infinity. The limiting constant value has been given in terms of geodesics, and is also analyzed for wave theories. For a black hole endowed with a light ray sphere, the limiting constant value is same as the geometrical cross section of this light ray sphere [61]. Here, we can use expression (2.4.1) for computing the energy emission rate.

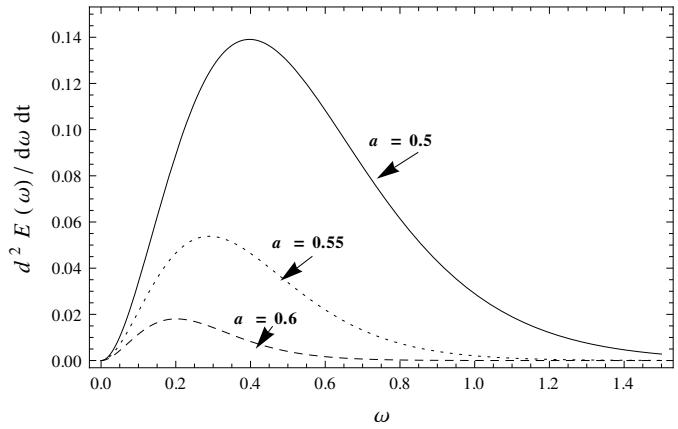

Figure 2.11: Plots showing the rate of energy emission varying with the frequency for different values of rotation parameter.

Hawking temperature is equal $T = (r_+^2 - a^2)r_+r_0^2/2\pi(r_+^2 + a^2)^3$(([57])) for the 5D rotating black hole.

In Fig. 2.12, we plot the energy emission rate versus frequency for different value of rotation parameter and it is seen that with the increase in the values of rotation parameter the peak of energy emission rate decreases.

2.4.4 Energy emission from the 6D black hole

As the next step we consider energy emission from rotating black hole in higher dimensional Gauss-Bonnet gravity using expresion 2.4.1. For calculation emission

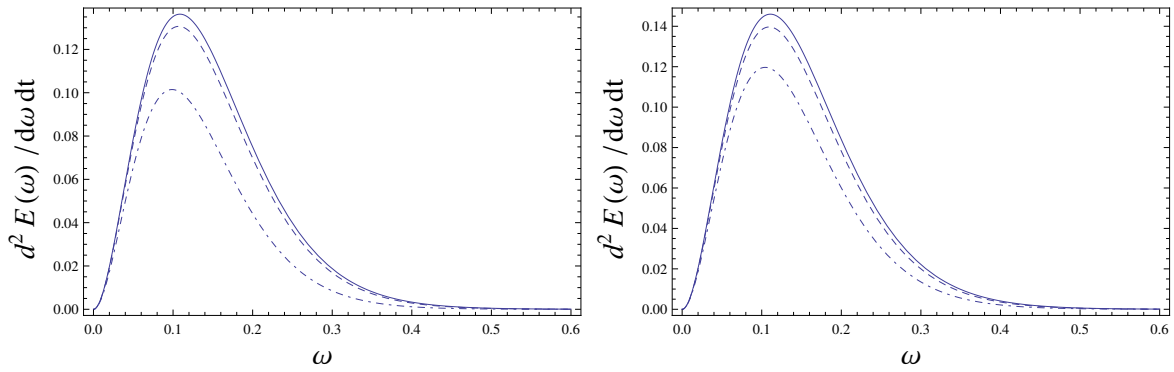

Figure 2.12: Dependence of the energy emission from the frequency for the different values of spin parameter a: $a/M = 0.1$ (solid line), $a/M = 0.3$ (dashed line), $a/M = a_{extr}/M = 3\sqrt{3}/16$ (dot-dashed line). Left panel is for black hole in the Gauss-Bonnet and right panel is for 4D black hole in the Kerr space-time.

energy from the black hole, we need Hawking temperature. And one can easily find Hawking temperature as following for the Gauss-Bonnet black hole: $T = \frac{r_+^2-3a^2}{8\pi r_+(r_+^2+a^2)}$(([31])), which can be computed from this expression $T = k/2\pi$, k is surface gravity. R_s is radius of shadow which is shown in Fig. 4.19 for the second order Lovelock space-time and ω.

Fig. 2.12 shows energy emission of rotating black hole in Gauss-Bonnet and Kerr space-time for the different values of spin parameters a: $a = 0.1$ (solid line), $a = 0.2$ (dashed line), $a = 0.3$ (dot-dashed line). The rate of energy emission decreases as the rotation parameter increases. The emission is more intense for the Kerr as compared to GB black hole.

2.5 Conclusion

In this chapter we have studied the event horizon structure around rotating Einstein-Born-Infeld black hole and Five dimensional Myers-Perry black hole. We also studied the energy emission from the black hole due to thermal radiation.

We have investigated the horizon structure of the charged rotating black hole

solution in Einstein-Born-Infeld theory, and explicitly discuss the effect of the Born-Infeld parameter β into event horizon and optical properties of black hole. Further, this rotating Einstein-Born-Infeld black hole solution generalizes both Reissner-Nordstrom ($\beta \to \infty$ and $a = 0$) and Kerr-Newman solutions ($\beta \to \infty$). Interestingly, it turns out that for given values of parameters $\{M;\ Q;\ \beta\}$, there exists $a = a_E$ for which the solution (2.8) can be an extremal black hole, which decreases with increase in the parameter. Further, we have also analyzed infinite red-shift surfaces, ergo-regions, energy emission and Hawking temperature of the rotating Einstein-Born-Infeld black hole. The Einstein-Born-Infeld black hole's horizon structure has been studied for the different values of electric charge Q and Born-Infeld parameter β, which explicitly demonstrates that outer (inner) horizon radius decreases (increases) with increase in the electric charge Q and Born-Infeld parameter β. The analysis of obtained numerical solutions shows, that the obtained results are different from the Kerr-Newman case due to non-zero Born-Infeld parameter. We have also analyzed energy emission and Hawking temperature of the rotating Einstein-Born-Infeld black hole, black holes in Braneworld and in higher dimension gravity models.

The analysis of the energy emission from the black hole due to thermal radiation shows that the increase the black hole brane tidal charge causes the increase the energy release process.

The study of the energy emission rate versus the frequency for the five dimensional rotating black hole for different values of the rotation parameter shows, that with the increase in the values of the rotation parameter the peak of the energy emission rate decreases.

Chapter III

Particle motion around axial-symmetric compact object

3.1 Introduction

Until now it is not found any observational proof of existence of gravitomagnetic monopole, i.e. so-called NUT [62] charge. Investigation of the massive and light ray motion in NUT spacetime may provide tool for studying new important general relativistic effects which are associated with nondiagonal components of the metric tensor and have no Newtonian analogues. [63, 64, 65] studied the solutions for electromagnetic waves and interferometry in spacetime with NUT parameter. [66] considered Kerr-Taub-NUT spacetime with Maxwell and dilation fields. The Penrose process in the spacetime of rotating black hole with nonvanishing gravitomagnetic charge has been considered by [67].

The geodesics of test charged (both electrically and magnetically charged) test particles in the Reissner-Nordström and Taub-NUT space-times fully analyzed by [68, 69]. [70, 68] considered higher-dimensional black hole spacetimes and null geodesics. In refs. [70] the parallel transport equations in the higher-dimensional Kerr-NUT-(A)dS spacetimes have been studied in detail. Magnetized black hole on the Taub-NUT instanton has been considered by [71]. [72] made detailed

analyse of few geometrical properties of Taub-NUT space-time metric.

3.2 Null geodesics in Kerr-Taub-NUT black hole

In this section we will study light ray trajectory around a rotating black hole with the total mass M in the presence of non vanishing gravitomagnetic charge. This black hole is described by the space-time metric [62]:

$$\begin{aligned} ds^2 &= -\frac{1}{\Sigma}\left(\Delta_l - a^2\sin^2\theta\right)dt^2 + \frac{1}{\Sigma}\left[(\Sigma + a\chi)^2\sin^2\theta - \chi^2\Delta_l\right]d\phi^2 \\ &\quad +\Sigma\left(\frac{dr^2}{\Delta_l} + d\theta^2\right) + \frac{2}{\Sigma}(\Delta_l\chi - a(\Sigma + a\chi)\sin^2\theta)dtd\phi. \end{aligned} \tag{3.1}$$

In above expression the following notations Δ, Σ, and χ are defined as

$$\Delta_l = r^2 + a^2 - l^2 - 2Mr, \quad \Sigma = r^2 + (l + a\cos\theta)^2, \quad \chi = a\sin^2\theta - 2l\cos\theta,$$

and a is the specific angular momentum of the black hole ($a = J/M$) and l is the gravitomagnetic charge. One can determine the event horizon by largest root of the equation $\Delta_l = 0$. The solution has the following form

$$r_+ = M + (M^2 - a^2 + l^2)^{1/2}. \tag{3.2}$$

It is obvious that light coming from the distant source will be deflected by the gravitational influence by the black hole originated between observer and the source of the light. The deflection is going to increase with the decreasing of impact parameter of the light ray and eventually the light ray emitted by the distant source can be captured by black hole. At the end this effect cause no-light zone or dark zone in the sky due to the existence of black hole between observer and light source. The above mentioned dark zone is called shadow of the black hole and the shape of it is totally defined geodesics of light rays trajectory. one can use the Hamilton-Jacobi equation to obtain the equation of motion of light

rays in the given space-time metric, in our case in space-time metric of rotating black hole with non vanishing gravitomagnetic charge:

$$\frac{\partial S}{\partial \tau} = -\frac{1}{2} g^{\alpha\beta} \frac{\partial S}{\partial x^\alpha} \frac{\partial S}{\partial x^\beta}, \tag{3.3}$$

here τ is an affine parameter along the null-geodesics. In order to separate variables (the separable problem of Hamilton-Jacobi equation in Kerr-Taub-NUT spacetime has been studied by [73]), one can choose the action for light ray in the following form:

$$S = \frac{1}{2} m^2 \tau - \mathcal{E} t + \mathcal{L}\phi + S_{\rm r}(r) + S_\theta(\theta) \ , \tag{3.4}$$

here m is the mass of a test particle. By $\mathcal{E}$ and $\mathcal{L}$ we designated the energy and the angular momentum of the particle, respectively. Putting the rest mass of light ray as zero $m = 0$ one may solve the Hamilton-Jacobi equation for null-geodesics

$$\Sigma \frac{dt}{d\tau} = \frac{r^2 + a^2 + l^2}{\Delta_l} \left[(r^2 + a^2 + l^2)\mathcal{E} - a\mathcal{L} \right] + \frac{\chi}{\sin^2\theta} (\mathcal{L} - \chi \mathcal{E}), \tag{3.5}$$

$$\Sigma \frac{d\phi}{d\tau} = \frac{a}{\Delta_l} \left[(r^2 + a^2 + l^2)\mathcal{E} - a\mathcal{L} \right] + \frac{1}{\sin^2\theta} (\mathcal{L} - \chi \mathcal{E}), \tag{3.6}$$

$$\Sigma \frac{dr}{d\tau} = \sqrt{\mathcal{R}}, \tag{3.7}$$

$$\Sigma \frac{d\theta}{d\tau} = \sqrt{\Theta}, \tag{3.8}$$

here $\mathcal{R}(r)$ and $\Theta(\theta)$ are introduced notations and they have the following form:

$$\mathcal{R} = \left[(r^2 + a^2 + l^2)\mathcal{E} - a\mathcal{L} \right]^2 - \Delta_l \left[\mathcal{K} + (\mathcal{L} - a\mathcal{E})^2 \right], \tag{3.9}$$

$$\Theta = \mathcal{K} + \left[\left(a^2 - \frac{4l^2}{\sin^2\theta} \right) \mathcal{E}^2 - \frac{\mathcal{L}^2}{\sin^2\theta} \right] \cos^2\theta + 4l\mathcal{E} \left(a\mathcal{E} - \frac{\mathcal{L}}{\sin^2\theta} \right) \cos\theta, \tag{3.10}$$

where $\mathcal{K}$ is Carter constant. Defining the effective potential for light ray as $(dr/d\tau)^2 = V_{\rm eff}$ one may study the radial motion of light ray in the presence of gravitomagnetic charge. In the Fig. 3.1 the radial dependence of the effective potential of radial light rays motion is shown. From the figure it is seen that with the increase of the gravitomagnetic charge the shape of the effective potential is

going to shift to the observer at infinity. This corresponds to increasing the event horizon of the Kerr-Taub-NUT black hole. Moreover, one may conclude from the Fig. 3.1 that with the increase of the gravitomagnetic charge the circular orbits of light rays become unstable.

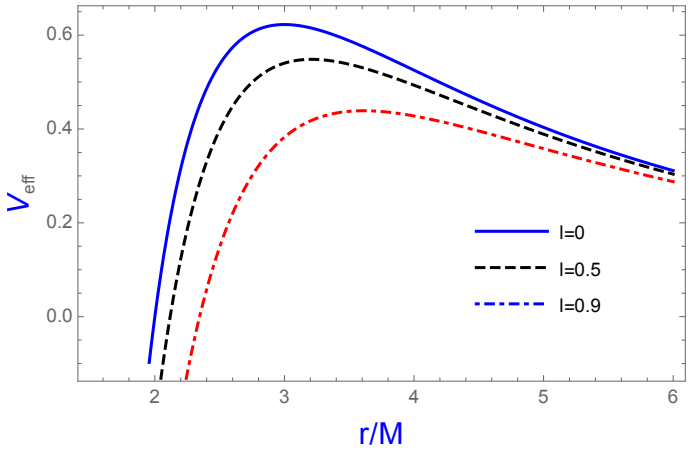

Figure 3.1: The radial dependence of the effective potential of radial motion of the light rays for the different values of the gravitomagnetic charge: solid line for $l/M = 0$, dashed line for $l/M = 0.5$, and dot-dashed line for $l = 0.9$.

Light rays trajectory around rotating black hole with non vanishing gravitomagnetic charge can be described using the expressions (3.5)–(3.8). One may easily introduce the following two impact parameters: $\xi = \mathcal{L}/\mathcal{E}$, $\eta = \mathcal{K}/\mathcal{E}^2$ in order to clarify the light rays trajectory in complete way. Now it useful to use the equation (3.7) for defining the shape of the dark zone created by rotating black hole with non vanishing gravitomagnetic charge. The condition of being boundary of shadow is the following: $\mathcal{R}(r) = 0 = d\mathcal{R}(r)/dr$. Using this condition one can obtain the following equations:

$$\xi(r) = \frac{a^2(1+r) + r^2(r-3) + l^2(1-3r)}{a(1-r)}, \tag{3.11}$$

$$\eta(r) = \frac{1}{a^2(r-1)}\Big\{r^3[4a^2 - r(r-3)^2] - l^2\big[4r^2a^2 + (1-3r)(l^2(1-3r) - 6r^2 + 4a^2r + 2r^3)\big]\Big\}. \tag{3.12}$$

3.3 Null geodesics in Einstein-Born-Infeld black hole space-time.

Next, we turn our attention to the study the geodesic of a light ray in Einstein-Born-Infeld black hole space-time. We need to study the separability of the Hamilton-Jacobi equation using the approach due to Carter [74]. First, for generality we consider a motion for a particle with mass m_0 falling in the background of a rotating Einstein-Born-Infeld black hole. The geodesic motion for this black hole is determined by the Hamilton-Jacobi equations (3.3). For this black hole background the Jacobi action S can be separated as expression 3.4 Like the Kerr space-time, rotating Born-Infeld black hole also has two Killing vector fields due to the assumption of stationarity and axisymmetry of the space-time, which in turn guarantees the existence of two conserved quantities for a geodesic motion, viz. the energy E and the axial component of the angular momentum L. Thus, the constants m_0, E, and L correspond to rest mass, conserved energy and rotation parameter related through $m_0^2 = -p_\mu p^\mu$, $E = -p_t$, and $L = p_\phi$. Obviously for a light ray null geodesic, we have $m_0 = 0$, and from (3.3) we obtain the null geodesics in the form of the first-order differential equations

$$\rho^2 \frac{dt}{d\tau} = \frac{r^2+a^2}{\Delta}\left[(r^2+a^2)E - aL\right] + a(L - aE\sin^2\theta), \tag{3.13}$$

$$\rho^2 \frac{d\phi}{d\tau} = \frac{a}{\Delta}\left[(r^2+a^2)E - aL\right] + \left(\frac{L}{\sin^2\theta} - aE\right), \tag{3.14}$$

$$\rho^2 \frac{dr}{d\tau} = \sqrt{\mathcal{R}}, \tag{3.15}$$

$$\rho^2 \frac{d\theta}{d\tau} = \sqrt{\Theta}, \tag{3.16}$$

where the functions $\mathcal{R}(r)$ and $\Theta(\theta)$ are defined as

$$\mathcal{R} = \left[(r^2+a^2)E - aL\right]^2 - \Delta\left(\mathcal{K} + (L-aE)^2\right), \tag{3.17}$$

$$\Theta = \mathcal{K} + \cos^2\theta\left(a^2E^2 - \frac{L^2}{\sin^2\theta}\right).$$

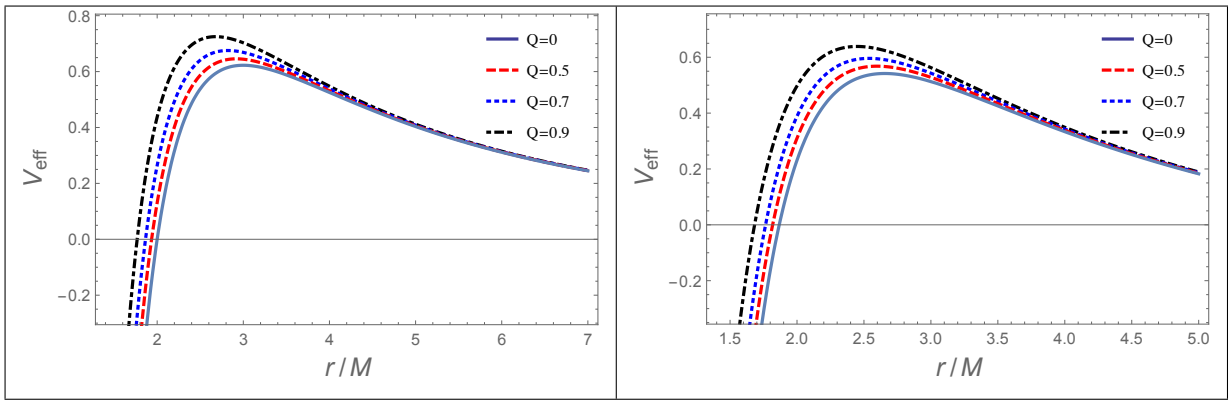

Figure 3.2: The radial dependence of effective potential V_{eff} for the light ray for the different values of electric charge Q. Left panel is for $\beta = 0.05$ and $a = 0.5$; right one is for $\beta = 0.5$ and $a = 0.5$.

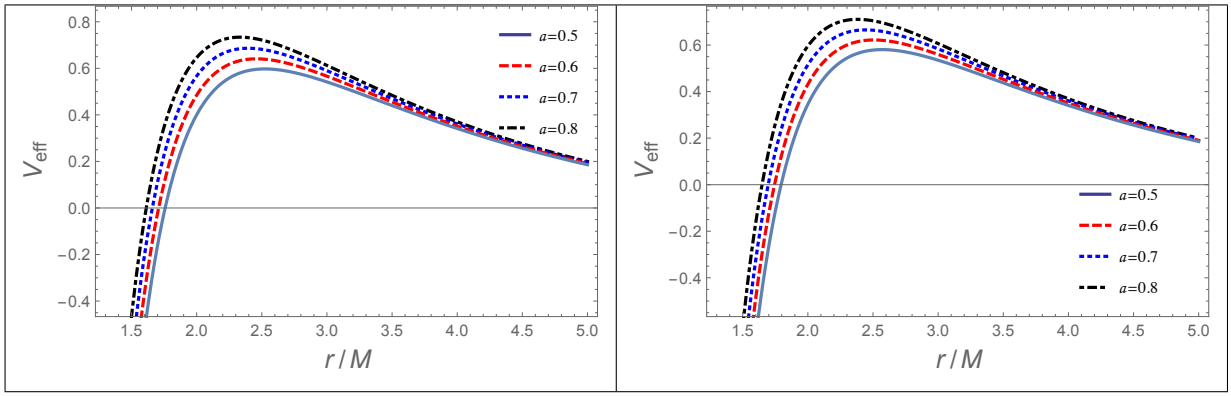

Figure 3.3: The radial dependence of effective potential V_{eff} for the light rays for the different values of rotation parameter a. Left panel is for $\beta = 0.05$ and $Q = 0.6$; right one is for $\beta = 0.5$ and $Q = 0.6$.

Thus, we find that Hamilton-Jacobi Eq. (3.3), using (3.4), is separable due existence of $\mathcal{K}$ namely Carter constant of separation. The above equations govern the light propagation in the Einstein-Born-Infeld black hole background. Obviously, for $Q = 0$, they are just the null geodesic equations for the Kerr black hole. The constant $K = 0$ is the necessary and sufficient condition for particles motion initially in the equatorial plane to remain there. Any particle which crosses the equatorial plane has $K > 0$. The discussion of effective potential is a useful tool for describing the motion of test particles. Further, we have to study radial motion of light ray around black hole for determining the black hole shadow boundary. The radial equation for timelike particles moving along geodesic in the equatorial

plane ($\theta = \pi/2$) is described by

$$\frac{1}{2}\dot{r}^2 + V_{eff} = 0, \tag{3.18}$$

with the effective potential

$$V_{eff} = -\frac{[E(r^2+a^2) - La]^2 - \Delta(L-aE)^2}{2r^4}\ . \tag{3.19}$$

From the last expression (3.19) one can easily get the plots presented in Figs. 3.2 and 3.3. There we have considered light rays trajectory around Einstein-Born-Infeld black hole for the different values of electric charge Q and parameter β. It is shown that with increasing electric charge Q or rotating parameter a particle is going to come closer to the central object.

3.4 The geodesic equations of rotating non-Kerr black holes

The deformed Kerr-like metric which describes a stationary axisymmetric, and asymptotically flat vacuum spacetime, in the standard Boyer-Lindquist coordinates, can be expressed as [34]

$$\begin{aligned} ds^2 &= -\left(1-\frac{2Mr}{\Sigma^2}\right)(1+h)dt^2 + \frac{\Sigma^2(1+h)}{\Delta_\epsilon + a^2 h\sin^2\theta}dr^2 + \\ &\quad \Sigma^2 d\theta^2 - \frac{4aMr\sin^2\theta}{\Sigma^2}(1+h)dtd\phi + \\ &\quad \sin^2\theta\left[\Sigma^2 + \frac{a^2(\Sigma^2+2Mr)\sin^2\theta}{\Sigma^2}(1+h)\right]d\phi^2, \end{aligned} \tag{3.20}$$

where

$$\Sigma^2 = r^2 + a^2\cos^2\theta, \quad \Delta_\epsilon = r^2 - 2Mr + a^2.$$

The metric (3.43) is a class of Kerr-like black-hole metrics which describes a stationary, axisymmetric, and asymptotically flat vacuum spacetime. Together with the mass and spin of the black hole, this spacetime metric contains parameters

that measure potential deviations from the Kerr metric and reduces to the Kerr metric in Boyer-Lindquist coordinates in the case when $h(r) = 0$. The function $h(r)$ can be chosen as

$$h(r) = \sum_{k=0}^{\infty} \epsilon_k \left(\frac{M}{r}\right)^k,$$

and the constraints on ϵ_k can be found from asymptotical properties of the metric (3.43). In the limit of large radii the stationary and asymptotically flat spacetimes are Schwarzschild-like [75]

$$\begin{aligned} ds^2 &= -\left(1 - \frac{2M}{r} + \mathcal{O}(r^{-2})\right) dt^2 \\ &\quad - \left(\frac{4a}{r}\sin^2\theta + \mathcal{O}(r^{-2})\right) dt d\phi \\ &\quad + \left(1 + \mathcal{O}(r^{-1})\right)\left(dr^2 + r^2 d\theta^2 + \sin^2\theta d\phi^2\right). \end{aligned} \tag{3.21}$$

In the $r \to \infty$ limit the metric (3.43) will take the following form:

$$\begin{aligned} ds^2 &= -\left(1 - \frac{2M}{r} + h(r)\right) dt^2 \\ &\quad - \frac{4a(1+h(r))}{r}\sin^2\theta dt d\phi \\ &\quad + \left(1 + \frac{2M}{r} + h(r)\right) dr^2 + r^2 d\theta^2 + \sin^2\theta d\phi^2. \end{aligned} \tag{3.22}$$

The requirement of the asymptotic flatness of the metric implies that $\epsilon_0 = \epsilon_1 = 0$. In the parameterized post-Newtonian (PPN) approach [76] the asymptotic spacetime expressed in the form

$$\begin{aligned} ds^2 &= -\left(1 - \frac{2M}{r} + 2(\beta - \gamma)\frac{M^2}{r^2}\right) dt^2 \\ &\quad + \left(1 + 2\gamma\frac{M}{r}\right) dr^2 + r^2 d\theta^2 + \sin^2\theta d\phi^2, \end{aligned} \tag{3.23}$$

where β and γ are the dimensionless PPN parameters. Comparision the constraint on β obtained from Lunar Laser Ranging experiment [77] as

$$|\beta - 1| \leq 2.3 \cdot 10^{-4},$$

and asymptotical expression of metric (3.43) given in (3.22) gives the value of $\epsilon_2 = 0$. Thus our choice of the function $h(r)$ to be third power of M/r as in Ref. [78] as

$$h(r,\theta) = \epsilon_3 \frac{M^3 r}{\Sigma^4}.$$

Further in the text we drop the index 3 and use the ϵ as deformation parameter. The quantity $\epsilon > 0$ or $\epsilon < 0$ corresponds to the cases in which the event horizon of compact object is more prolate or oblate than that of the Kerr black hole, respectively. As $\epsilon = 0$, the black hole is reduced to the typical Kerr black hole well known in general relativity.

Note that the spacetime metric (3.43) is stationary and axisymmetric and chosen $h(r,\theta)$ ensures the preservation of the properties of the Kerr metric. In general relativity, the Einstein tensor of metric (3.43) is nonzero for nonvanishing $h(r,\theta)$. One should regard the metric (3.43) as a vacuum spacetime of modified set of field equations which are unknown but different from the Einstein equations for nonzero $h(r,\theta)$.

From the Hamilton-Jacobi equation (3.3) for light ray, the following equations of motion are obtained:

$$\begin{aligned}
\Sigma^2 \frac{dt}{d\lambda} &= \frac{r^2+a^2}{\Delta_\epsilon + a^2 h \sin^2\theta}\left[(r^2+a^2)\mathcal{E} - a\mathcal{L}\right] + \\
&\quad \frac{\Delta_\epsilon a}{\Delta_\epsilon + a^2 h \sin^2\theta}[\mathcal{L} - a\mathcal{E}\sin^2\theta], && (3.24)\\
\Sigma^2 \frac{d\phi}{d\lambda} &= \frac{a}{\Delta_\epsilon + a^2 h \sin^2\theta}\left[(r^2+a^2)\mathcal{E} - a\mathcal{L}\right] + \\
&\quad \frac{\Delta_\epsilon}{\Delta_\epsilon + a^2 h \sin^2\theta}[\frac{\mathcal{L}}{\sin^2\theta} - a\mathcal{E}], && (3.25)\\
\frac{\Sigma^2}{1+h}\frac{dr}{d\lambda} &= \sqrt{\mathcal{R}}, && (3.26)\\
\Sigma^2 \frac{d\theta}{d\lambda} &= \sqrt{\Theta}, && (3.27)
\end{aligned}$$

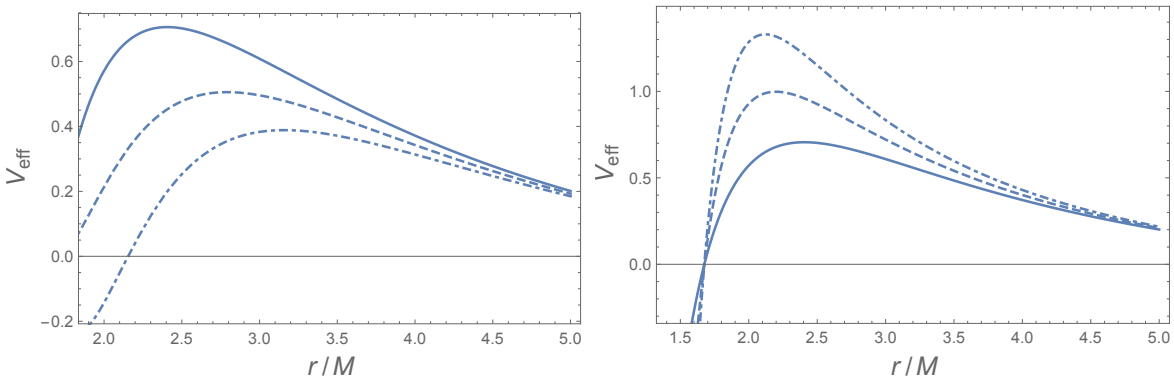

Figure 3.4: The radial dependence of the effective potential of radial motion of the light rays around black hole for the different values of the ϵ parameter: solid line for $\epsilon = 0$, dashed line for $\epsilon = -5$, dot-dashed line for $\epsilon = -10$ (left panel), and solid line for $\epsilon = 0$, dashed line for $\epsilon = 5$, dot-dashed line for $\epsilon = 10$ (right panel)

where the functions $\mathcal{R}(r)$ and $\Theta(\theta)$ are defined as

$$\mathcal{R} = \left[(r^2 + a^2)\mathcal{E} - a\mathcal{L}\right]^2 - \Delta_\epsilon[\mathcal{K} + (\mathcal{L} - a\mathcal{E})^2], \tag{3.28}$$

$$\Theta = \mathcal{K} - \frac{\Sigma^2}{\sin^2\theta}[a\mathcal{E}\sin^2\theta - \mathcal{L}]^2, \tag{3.29}$$

with $\mathcal{K}$ as Carter constant of separation.

In the Fig. 3.4 the radial dependence of effective potential of the light rays radial motion is shown. When $\epsilon < 0$ with decreasing the value of deformation parameter one may observe the increase of light rays sphere. The stability of circular orbits is decreasing with the increase the module of negative ϵ. From this dependence one can easily see that with the increase of ϵ parameter stable circular light ray orbits come closer to the central object. Then the stability of light ray orbits will also increase with the increasing the parameter ϵ. The similar effect for the particle motion around rotating non-Kerr black hole has been found in the paper [79] where it was shown that with the increase of the parameter ϵ the radius of the innermost stable circular orbits at the equatorial plane is decreasing.

The equations (3.24)-(3.27) determine the propagation of light in the non-

Kerr spacetime (3.43). The light ray is in general, characterized by two impact parameters which can be expressed in terms of the constants of motion $\mathcal{E}$, $\mathcal{L}$ and the Carter constant $\mathcal{K}$. Combining these quantities we define as usual $\xi = \mathcal{L}/\mathcal{E}$ and $\eta = \mathcal{K}/\mathcal{E}^2$ which are the impact parameters for general orbits around the black hole. We use Eq.(3.26) to derive the orbits with constant r in order to obtain the boundary of the shadow of the black hole. These orbits satisfy the conditions $\mathcal{R}(r) = 0 = d\mathcal{R}(r)/dr$ which are fulfilled by the values of the impact parameters that determine the contour of the shadow, namely

$$\xi(r) = \frac{a^2(1+r) + r^2(r-3)}{a(1-r)}, \tag{3.30}$$

$$\eta(r) = \frac{r^3[4a^2 - r(r-3)^2]}{a^2(1-r)^2}. \tag{3.31}$$

3.5 Null geodesics in 5D rotating black hole

In order to analyze the general orbit of light ray around a black hole, we study the separability of the Hamilton-Jacobi equation for which we adopt the approach originally suggested by Carter [74]. From (3.3) and (3.4) we can conclude:

$$\left(\frac{\partial S_\theta}{\partial \theta}\right)^2 - E^2(a^2\cos^2\theta + b^2\sin^2\theta) + \frac{L_\phi^2}{\sin^2\theta} + \frac{L_\psi^2}{\cos^2\theta} = \mathcal{K}, \tag{3.32}$$

and

$$4\Delta_{5D}\left(\frac{\partial S_x}{\partial x}\right)^2 - E^2 x - \frac{r_0^2(x+a^2)(x+b^2)}{\Delta_{5D}}\Sigma^2 - (a^2-b^2)\left(\frac{L_\phi^2}{(x+a^2)} - \frac{L_\psi^2}{(x+b^2)}\right) = -\mathcal{K}, \tag{3.33}$$

with $\mathcal{K}$ as a constant of separation and

$$\Sigma = E + \frac{aL_\phi}{x+a^2} + \frac{bL_\psi}{x+b^2}.$$

Equations (3.32) and (3.33) can be recast into the form:

$$\frac{\partial S_\theta}{\partial \theta} = \sqrt{\Theta}, \qquad \frac{\partial S_x}{\partial x} = \sqrt{X},$$

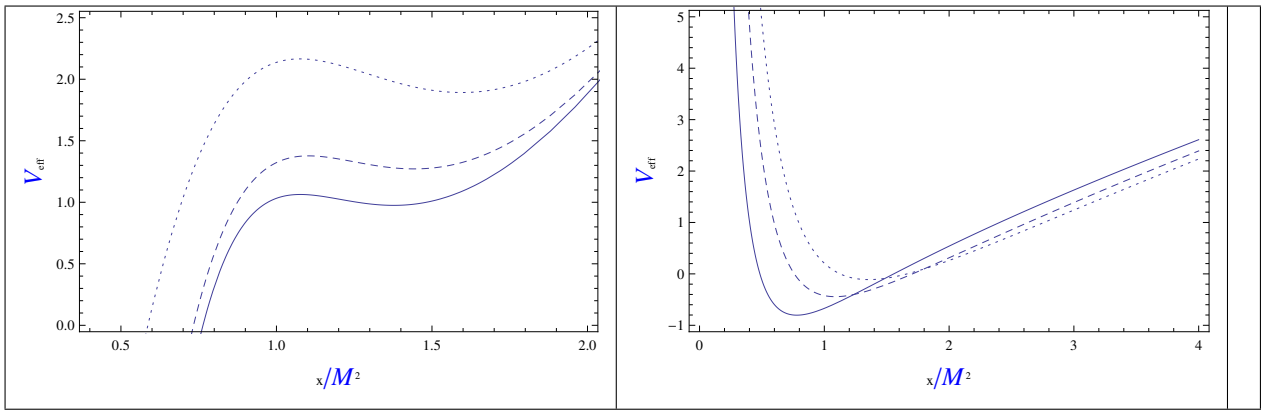

Figure 3.5: Plots showing the radial dependence of effective potential for rotation parameter a and b. (Left) For different values of a: $a = 1.2$ (solid line), $a = 1$ (dashed line), $a = 0.9$ (dot dashed line) and $b = 0$. (Right) For different values of $a = b$: $a = 0.4$ (solid line), $a = 0.3$ (dashed line), $a = 0.2$ (dot dashed line).

where X is given by

$$X = \frac{R}{4\Delta_{5D}^2}.$$

Here functions Θ and R are given by

$$\Theta = E^2(a^2\cos^2\theta + b^2\sin^2\theta) - \frac{\cos^2\theta}{\sin^2\theta}L_\phi^2 - \frac{\sin^2\theta}{\cos^2\theta}L_\psi^2 + \mathcal{K}, \tag{3.34}$$

$$R = \Delta_{5D}\left[xE^2 + (a^2 - b^2)\left(\frac{L_\phi^2}{(x+a^2)} - \frac{L_\psi^2}{(x+b^2)}\right) - \mathcal{K}\right] + r_0^2(x+a^2)(x+b^2)\Sigma^2. \tag{3.35}$$

We can write the Hamilton-Jacobi action in terms of these functions:

$$S = \frac{1}{2}m^2\lambda - Et + L_\phi\phi + L_\psi\psi + \int^\theta \sqrt{\Theta}d\theta + \int^x \sqrt{X}dx. \tag{3.36}$$

Hence from the Hamilton-Jacobi equation, the null geodesic equations are

$$\begin{aligned}
\rho^2\dot{\theta} &= \sqrt{\Theta}, \\
\rho^2\dot{x} &= 2\sqrt{R}, \\
\rho^2\dot{t} &= E\rho^2 + \frac{r_0^2(x+a^2)(x+b^2)}{\Delta_{5D}}\Sigma, \\
\rho^2\dot{\phi} &= \frac{L_\phi}{\sin^2\theta} - \frac{ar_0^2(x+b^2)}{\Delta_{5D}}\Sigma - \frac{(a^2-b^2)L_\phi}{(x+a^2)}, \\
\rho^2\dot{\psi} &= \frac{L_\psi}{\cos^2\theta} - \frac{br_0^2(x+a^2)}{\Delta_{5D}}\Sigma + \frac{(a^2-b^2)L_\psi}{(x+b^2)}.
\end{aligned} \tag{3.37}$$

These equations governs the propagation of light in the spacetime of 5D black hole. In order to obtain the boundary of the shadow of the black hole, we need to study the radial motion of light ray. First, we rewrite the radial equation as

$$\rho^2\dot{r} = \sqrt{R}. \tag{3.38}$$

The effective potential reads

$$\begin{aligned}
V_{eff} = \frac{1}{2}\frac{\Delta_{5D}}{\rho^2}\Bigg[xE^2 + (a^2-b^2)\left[\frac{L_\phi^2}{(x+a^2)} - \frac{L_\psi^2}{(x+b^2)}\right] \\
-\mathcal{K}\Bigg] + r_0^2(x+a^2)(x+b^2)\Sigma^2.
\end{aligned} \tag{3.39}$$

One can think of an effective potential for the light rays, which has a barrier with a maximum, goes to negative infinity below the horizon, and asymptotes to zero at $x \to \infty$. In the simplest case of Schwarzschild case, the effective potential for light ray has a maximum at $3M$, the location of the unstable orbit (there is no minimum of this potential). For rotating case, the picture is qualitatively the same, but a little more complex, because the spin breaks the spherical symmetry of the system. The general behavior of effective potential for the 5D Myers-Perry black as a function of x for different values of rotation parameter is shown in Fig. 3.5. For $b = 0$ and varying a, the effective potential shows one maximum and one minimum which corresponds to the unstable and stable circular orbits,

respectively. It is seen that with the increase in the value of rotation parameter peak of the graph shifts to left which signifies that the circular orbits are shifting towards the central object. For $a = b$, it is observed that there is only one minimum which shows the presence of stable circular orbits.

Now, we know that the equation of motion defined in Eq. (3.37) determines the propagation of light in the space time of 5D rotating black hole. The apparent shape of the black hole can be found by looking for the orbits around the black hole. Every orbit can be characterized by three impact parameters, which can be expressed in terms of constants of motion E, L_ϕ and L_ψ and the constant of separability $\mathcal{K}$. Combining these quantities, we define as usual $\xi_1 = L_\phi/E$, $\xi_2 = L_\psi/E$ and $\eta = \mathcal{K}/E^2$, which are impact parameters for general orbits around the black hole. Henceforth, for simplicity of analysis equal values of rotation parameters ($a = b$), we assume $a = b$, which gives

$$\begin{aligned} R &= \left[(x+a^2)^2 - r_0^2\right]\left(xE^2 - \mathcal{K}\right) + r_0^2(x+a^2)^2 \\ &\quad \times\left[E + \frac{a}{x+a^2}(L_\phi + L_\psi)\right]^2. \end{aligned} \tag{3.40}$$

The apparent shape of the black hole can be found by looking for the unstable orbits. We use Eq. (3.5) to derive the orbits with constant r in order to obtain the boundary of shadow of the black holes, which requires $V_{eff} = 0$, $\partial V_{eff}/\partial r = 0$ (or $R(r) = 0 = \partial R(r)/\partial r$), which are fulfilled by the values of the impact parameters that determine the contour of the shadow, namely

$$\eta(r) = \frac{a^6 - 5x^2 + 2x^3 + a^4(1+5x) + a^2x(7x-4) - 2(a^4 + 2a^2x + x(x-2))\sqrt{a^2+x}}{2(x+a^2-1)^2} \tag{3.41}$$

$$\xi_1(r) + \xi_2(r) = \frac{-a^4 + 2a^2(x-1) + x^2 + (a^4 + 2a^2x + x(x-2))\sqrt{a^2+x}}{2a(x+a^2-1)} \tag{3.42}$$

3.6 Particle motion around 6D rotating black hole

We wish to consider a pure Gauss-Bonnet rotating black hole in the critical 6 dimension (in odd $d = 5$ GB gravity is kinematic; i.e. GB flat and it becomes dynamic in even $d = 6$ [80]). There does not exist an exact solution of pure GB vacuum equation for an axially symmetric spacetime representing a rotating black hole. This is simply because the equations are very formidable to handle. However for Einstein gravity in 4 dimension there is the well known Newman-Janis algorithm for converting a static black hole into a rotating one without solving the equation. This may however not be applicable for GB gravity and in higher dimension [81]. Secondly one of us [82] has recently obtained the Kerr metric by appealing to the two simple physical considerations. One, it should incorporate Newton's law in the first approximation, and second, since one is free to choose affine parameter for a null curve and hence the radial coordinate is chosen as affine parameter for radially falling light ray. For this, one begins with an appropriate spatial geometry which has ellipsoidal symmetry and then implement these two common sense inspired physical considerations, and what results is the metric [83] considered here. This can describe a rotating black hole, though it is not an exact solution of pure GB vacuum equation, yet it has all the features of the usual Kerr metric. It however does satisfy the equation in the leading order. It has all the characteristics of a rotating black hole in existence of ergosphere, and the right limits; for $a = 0$ it reduces to pure GB static black hole while $M = 0$ leads to flat space. It is therefore perfectly appropriate metric for studying a rotating black hole in pure GB gravity. We shall thus employ this rotating black hole metric for studying its various physical properties.

The stationary axisymmetric metric for pure GB rotating black hole in the standard Boyer-Lindquist coordinates reads as [83]

$$
\begin{aligned}
ds^2 &= -\frac{\Delta_{6D}}{\Sigma}\Big[dt - a^2\sin^2\theta d\phi\Big]^2 + \frac{\Sigma}{\Delta_{6D}}dr^2 \\
&\quad + \Sigma d\theta^2 + \frac{\sin^2\theta}{\Sigma}\Big[(r^2+a^2)d\phi - a dt\Big]^2 \\
&\quad + r^2\cos^2\theta\big[d\psi^2 + \sin^2\psi d\chi^2\big] \ , \qquad (3.43)
\end{aligned}
$$

with

$$
\Delta_{6D} = r^2 + a^2 - M^{1/2}r^{3/2} \ , \quad \Sigma = r^2 + a^2\cos^2\theta \ , \qquad (3.44)
$$

where M and a have usual meaning of the total mass and specific angular momentum.

The spacetime (3.43) has horizon when $t = const$ becomes null; i.e. $\Delta_{6D} = 0$ which has the following four roots

$$
r_{+,-} = \frac{M}{4} + \frac{C}{4\sqrt{3}} \pm \sqrt{\frac{3M^2}{16} - a^2 - \frac{C^2}{192} + \sqrt{3}\frac{M^3 - 8a^2M}{8C}} \ , \qquad (3.45)
$$

$$
r_{3,4} = \frac{M}{4} - \frac{C}{4\sqrt{3}} \pm \sqrt{\frac{3M^2}{16} - a^2 - \frac{C^2}{192} - \sqrt{3}\frac{M^3 - 8a^2M}{8C}} \ , \qquad (3.46)
$$

with

$$
\begin{aligned}
C^2 &= 3M^2 - 16a^2 + \frac{64a^4}{A} + 4A \ , \\
A^3 &= \frac{27}{2}a^4M^2 - 64a^6 + 3\sqrt{3}a^4MD \ , \quad D = \sqrt{\frac{27}{4}M^2 - 64a^2} \ .
\end{aligned}
$$

The function under the square root in expression (3.46)

$$
F_1(a,M) = \frac{3M^2}{16} - a^2 - \frac{C^2}{192} - \sqrt{3}\frac{M^3 - 8a^2M}{8C}
$$

is always negative and consequently $r_{3,4}$ is not real, while the function under the square root in expression (3.45)

$$
F_2(a,M) = \frac{3M^2}{16} - a^2 - \frac{C^2}{192} + \sqrt{3}\frac{M^3 - 8a^2M}{8C}
$$

is non-negative for the range of rotation parameter $|a| \leq 3\sqrt{3}M/16$ (see Fig. 3.8), the equality indicates the extremal value of the rotation parameter. It is $r_{+,-}$ that mark outer and inner horizons of the hole. The static limit is defined where the time-translation Killing vector $\xi^{\alpha}_{(t)}$ becomes null (i.e. $g_{00} = \Delta_{6D} - a^2 \sin^2\theta = 0$). The region bounded by the outer horizon and the static limit defines the ergosphere (See Fig. 1), the extent of which increases with the rotation a of the hole.

3.6.1 Geodesics and circular orbits

In order to study particle motion around six dimensional pure GB black hole we first write the Hamilton-Jacobi equation (3.3) and (3.4), for Hamiltonian [84, 58, 57]:

$$S = \frac{1}{2}m^2\sigma - \mathcal{E}t + \mathcal{L}\phi + S_r(r) + S_\theta(\theta) + \mathcal{W}\chi + T_\Psi(\Psi) \ , \tag{3.47}$$

where m is mass, $\mathcal{E}$ and $\mathcal{L}$ are conserved energy and angular momentum of the particle.

The issue of the separability of the Hamilton-Jacobi equation in higher dimensional spacetime has been widely studied in the literature [84, 58, 57]. Particularly, the authors of the paper [84, 58] have shown that the spacetime metric (3.43) is Petrov type D.

For null geodesics (when m = 0), one can get the equations of motion from the

Hamilton-Jacobi equation (3.3) as

$$\Sigma\frac{dt}{d\sigma} = a(\mathcal{L}-a\mathcal{E}\sin^2\theta)+\frac{r^2+a^2}{\Delta_{6D}}\Big[(r^2+a^2)\mathcal{E}-a\mathcal{L}\Big]\ , \tag{3.48}$$

$$\Sigma\frac{d\phi}{d\sigma} = (\frac{\mathcal{L}}{\sin^2\theta}-a\mathcal{E})+\frac{a}{\Delta_{6D}}\Big[(r^2+a^2)\mathcal{E}-a\mathcal{L}\Big]\ , \tag{3.49}$$

$$\cos^2\theta\frac{d\chi}{d\sigma} = \frac{\csc^2\psi}{r^2}\mathcal{W}\ , \tag{3.50}$$

$$\Sigma\frac{dr}{d\sigma} = \sqrt{\mathcal{R}}\ , \tag{3.51}$$

$$\Sigma\frac{d\theta}{d\sigma} = \sqrt{\Theta}\ , \tag{3.52}$$

$$\cos^2\theta\frac{d\psi}{d\sigma} = \frac{\mathcal{W}}{r^2\sin\psi}\ , \tag{3.53}$$

where new functions $\mathcal{R}(r)$ and $\Theta(\theta)$

$$\mathcal{R} = \Big[(r^2+a^2)\mathcal{E}-a\mathcal{L}\Big]^2-\Delta_{6D}[\mathcal{K}+(\mathcal{L}-a\mathcal{E})^2]\ , \tag{3.54}$$

$$\Theta = \mathcal{K}-\frac{1}{\sin^2\theta}[a\mathcal{E}\sin^2\theta-\mathcal{L}]^2 \tag{3.55}$$

are introduced.

The conserved quantity $\mathcal{W}$ exists only when $\theta\neq\pi/2$ and is similar to angular momentum. So called Carter constant $\mathcal{K}$ characterizes together with the quantities $\mathcal{E}$, $\mathcal{W}$ and $\mathcal{L}$ the geodetic motion. The Carter constant is not related to any isometry of the space-time unlike the conserved quantities $\mathcal{E}$, $\mathcal{W}$ and $\mathcal{L}$.

By defining $\xi=\mathcal{L}/\mathcal{E}$, $\eta=\mathcal{K}/\mathcal{E}^2$ and $\zeta=\mathcal{W}/\mathcal{E}$ and using Eq. (3.51) we get for the circular orbits characterized by $\mathcal{R}(r)=0$ and $d\mathcal{R}(r)/dr=0$,

$$\xi(r,a) = \frac{a^2(2r+3r^{1/2})+r^2(2r-5r^{1/2})}{a(3r^{1/2}-2r)}\ , \tag{3.56}$$

$$\eta(r,a) = \frac{8a^2r^{7/2}-r^4(2r-5r^{1/2})^2}{a^2(2r-3r^{1/2})^2}\ . \tag{3.57}$$

3.6.2 Timelike circular orbits

Consider the equation of motion of test particle with nonzero rest mass at the equatorial plane ($\theta=\pi/2\ ,\ \dot{\theta}=0$). The equations of motion take the following

form

$$m\frac{dt}{d\sigma} = -\frac{\mathcal{E}r^2 - a\mathcal{L}\sqrt{M/r} + a^2E\left(\sqrt{M/r}+1\right)}{a^2 - M^{1/2}r^{3/2} + r^2} \ , \tag{3.58}$$

$$m\frac{d\phi}{d\sigma} = \frac{\mathcal{L} + (a\mathcal{E} - \mathcal{L})M^{1/2}r^{-1/2}}{a^2 - M^{1/2}r^{3/2} + r^2} \ , \tag{3.59}$$

$$m^2\left(\frac{dr}{d\sigma}\right)^2 = \mathcal{E}^2 - V_{\rm eff} \ , \tag{3.60}$$

where

$$V_{\rm eff} \ = \ m^2\left(1 - \sqrt{\frac{M}{r}}\right) - \frac{(\mathcal{L} - a\mathcal{E})^2M^{1/2}}{r^{5/2}} + \frac{\mathcal{L}^2 - a^2(\mathcal{E}^2 - m^2)}{r^2} \tag{3.61}$$

is the effective potential for radial motion. Note that for the orbits in the equatorial plane the new conserved quantity $\mathcal{W}$ does not appear in the equations of motion. In Fig. 3.6 the radial dependence of the effective potential of radial motion in equatorial plane has been shown for the fixed specific value of the rotation parameter $a = M$. The increase of the momentum of the particle leads to the increase of the peak of the potential: initially infalling test particles become bounded or escaped with the increase of the momenta.

The conditions of occurrence of circular orbits are

$$\frac{dr}{d\sigma} = 0 \, , \ V'_{\rm eff}(r) = 0 \ .$$

From these equations, it follows that energy $\mathcal{E}$ and angular momentum $\mathcal{L}$ of a circular orbit of radius r_c are given by

$$\begin{aligned}\mathcal{E}^2 \ = \ & \Big[a^2(12\sqrt{r} - 11)r^2 - 4(\sqrt{r} - 1)^2(4\sqrt{r} - 5)r^{7/2} \\ & \pm 4ar^{5/4}(a^2 - r^{3/2} + r^2)\Big] \times \Big[16a^2r^{5/2} - (5 - 4\sqrt{r})^2r^4\Big] \ , \end{aligned} \tag{3.62}$$

$$\begin{aligned}\mathcal{L}^2 \ = \ & \Big[5r^6 - a^4(11 + 4\sqrt{r})r^2 - 4r^{13/2} + 2a^2(10 - 11\sqrt{r} - 4r)r^{7/2} \\ & \pm (a^2 - r^{3/2} + r^2)(20r^2 + 4a^2)\Big] \times \Big[16a^2r^{5/2} - (5 - 4\sqrt{r})^2r^4\Big]^{-1} \end{aligned} \tag{3.63}$$

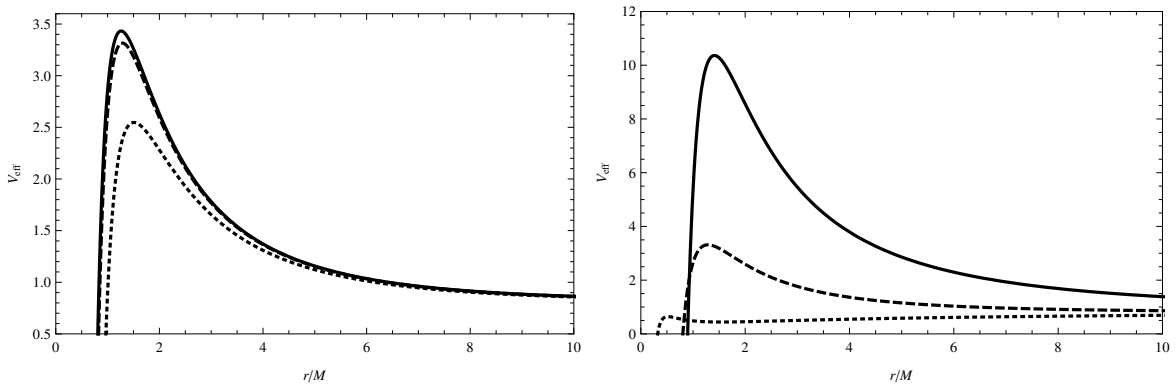

Figure 3.6: The radial dependence of effective potential for the different values of angular momentum and rotation parameter. The left plot corresponds to the case when a varies and the graphs are plotted for the different values of rotation parameter: $a/M = 0.1$ (dotted line), $a/M = 0.3$ (dashed line), and $a/M = a_{extr}/M = 3\sqrt{3}/16$ (solid line). The right plot corresponds the case to the case when L varies and the graphs are plotted for the different values of the angular momentum of the particle: $L/Mm = 1$ (dotted line), $L/Mm = 5$ (dashed line), and $L/Mm = 10$ (solid line)

where $+$ and $-$ signs correspond to the co-rotating and counter-rotating particles.

In the Fig. 3.7 we have shown energy and angular momentum of the co and counter rotating orbits in the equatorial plane for different values of rotation parameter a. One can easily see the shift in location of the minimal circular orbit (MC) marking the existence limit given by the light ray circular orbit and the innermost stable circular orbits (ISCO). The MC and ISCO come closer to the hole with increase in a for co-rotating orbits while opposite happens for counter rotating ones.

The vanishing of denominator in the expressions for $\mathcal{E}$ and $\mathcal{L}$ marks the location of light ray circular orbit or MC while for ISCO we have $dr/d\sigma = V'_{\rm eff}(r) = 0$ and $V''_{\rm eff}(r) \geq 0$. In Fig. 3.8 we have shown three regions as dark, light grey and white marking the boundaries of stable, unstable and no circular orbits. The inner boundary of light grey is defined by light ray circular orbit and the white region bounded between it and the horizon is the one where no circular orbits can

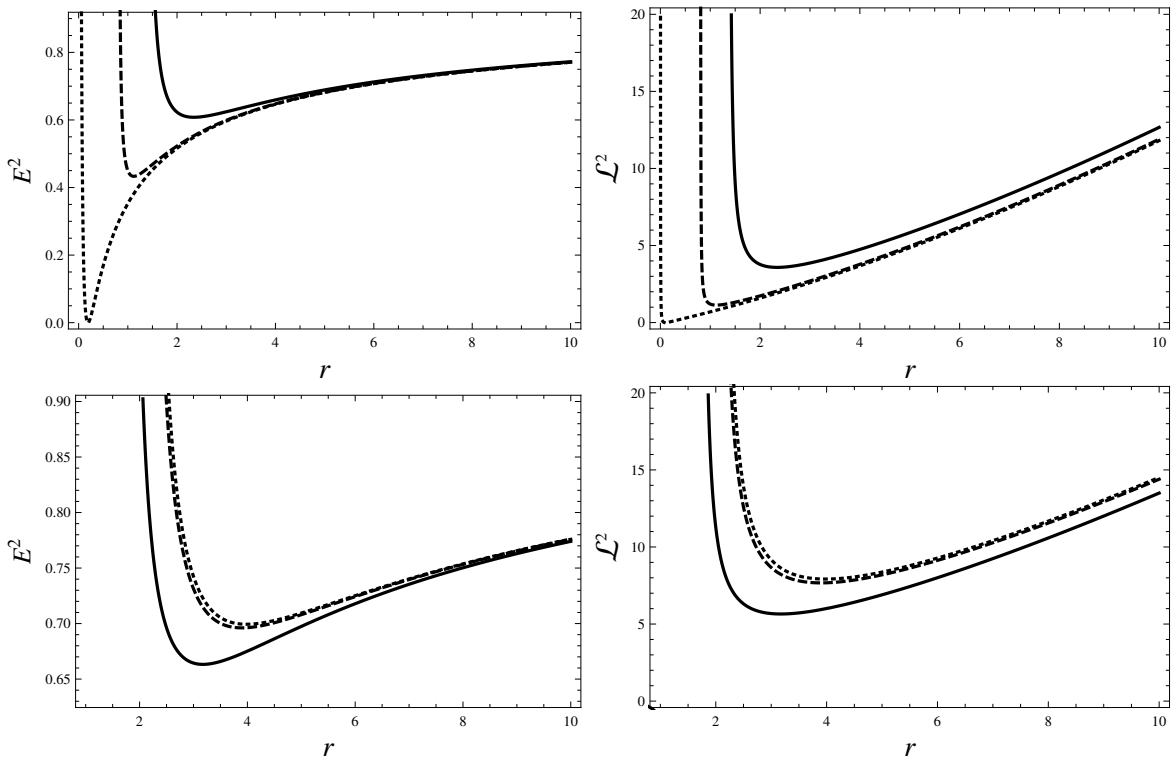

Figure 3.7: The radial dependence of energy (left) and angular momentum (right) squared of counter-rotating (upper plots) and co-rotating (lower plots) particle at circular orbits for the different values of parameter $a = 0.1$ (solid line), 0.3 (dashed line), and $3\sqrt{3}/16$ (dotted line).

exist. This is the region between 3M and 2M for the Schwarzschild black hole. As expected these regions are quite similar to that of the 4-dimensional Kerr black hole.

At this point it may be mentioned that bound orbits cannot exist for Einstein gravity in dimensions ≥ 4 [7] in general and in particular their non-existence is shown for 6-dimensional rotating black hole in Ref. [85]. For pure Lovelock gravity they do always exist in all even dimensions, $d = 2N + 2$ [7].

3.7 Conclusion

In this chapter we have considered the equation of motion of test particles around rotating black hole with nonzero gravitomagnetic charge, around rotating Einstein-Born-Infeld black hole, rotating deformed black hole and rotating black

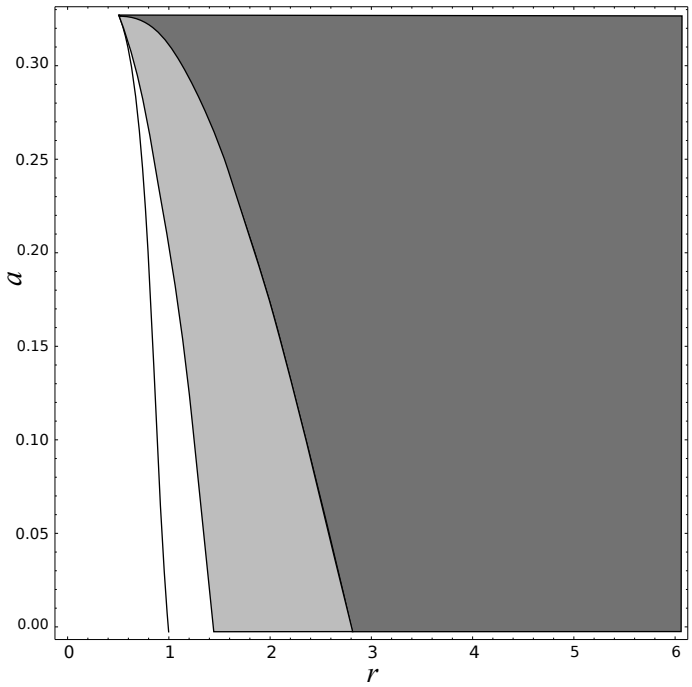

Figure 3.8: The regions of stable (dark grey) and unstable (light grey) circular orbits. The black curve indicates the border of event horizon of 6-D Gauss-Bonnet black hole.

hole in higher dimensional theories.

The analysis of the effective potential of radial motion of the light ray show, that with the increase of the gravitomagnetic charge the shape of the effective potential is going to shift to the observer at infinity. This corresponds to increasing the event horizon of the Kerr-Taub-NUT black hole.

The effective potential for geodesic motion of the light rays around rotating Einstein-Born-Infeld black hole has been studied for the different values of the electric charge and spin parameter of the black hole. With increasing either rotation parameter or electric charge of black hole particle is moving closer to the central object. Hence, circular orbit of the light ray becomes closer to the center of rotating Einstein-Born-Infeld black hole.

It was obtained that the decrease of the negative values of the deformation parameter of non-Kerr black holes causes the increase of light ray sphere. The stability of circular orbits is decreasing with the increase the module of negative

deformation parameter. It was shown that the increase of deformation parameter stable circular light rays orbits come closer to the central object.

The particle motion in higher dimensional gravity models have been also considered. Analysis of the energy and angular momentum of the co and counter rotating particle's orbits in the equatorial plane show that the shift in location of the minimal circular orbit marking the existence limit given by the light ray circular orbit and the innermost stable circular orbits. The circular orbits come closer to the hole with increase in a for co-rotating orbits while opposite happens for counter rotating ones.

Chapter IV

Optical properties and shadow of axial-symmetric compact objects

4.1 Introduction

For last fifteen years supermassive BH Sagittarius A* at the center of the Milky Way was observed by three orbiting X-ray telescopes. As a result we have much more clarity in the patterns of Sgr A*[86]. During the last year X-ray flares level of Sgr A* has increased. It coincides with the close passage of object named G2. For years of study astronomers thought that G2 is a cloud of gas and dust. But after passing close to Sgr A* at the end of 2013 G2 was almost not deformed by Sgr A* gravity, so the theories arise, stating that G2 is a star or a binary with dusty envelope. If the increase of X-ray flares is explained by G2, that will be the first sign of black hole absorbing excess material falling from the passing cloud. Sgr A* will have stripped some gas off G2. Hot material flowing towards the black hole will enhance the production of X-ray flares[86]. Still tho question is open, because thoere are other black holes with similar behaviour, so it's possible that the increased X-ray production is a common trait of supermassive black holes and have no relation to G2. It may be, for example, caused by a change of stellar wind from nearby massive stars. 150 Chandra and XMM-Newton observatories

pointed at the center of our Galaxy were used in the analysis that was performed over the last decade and a half, starting September 1999 up to November 2014. Last stages of observations have shown six bright flares within three days, while prognosis was only 0.8 bright flares on average[86].

It is strongly believed that there exist black holes in the centres of majority galaxies, for instance, a widely accepted opinion that radio-source Sgr A* in the galactic centre of Milky Way is likely to be a supermassive black hole [87, 88]. Since the galaxies are rotating, it is very likely that a black hole at the centre of a galaxy also possesses a spin. There is a great interest to investigate nature of the black holes, i.e., mass and spin of the black hole. Observation of black hole shadow is one of the possible methods to determine the mass and spin of a rotating black hole [89, 90, 28, 91]. Now, it is general belief that a black hole, if it is in front of a bright background produced by far radiating object, will cast a shadow. The apparent shape of a black hole silhouette is defined by the boundary of the black and it was first studied by Bardeen [92]. The ability of very long baseline interferometry (VLBI) observation has been improved significantly at short wavelength which led to strong expectation that within few years it may be possible to observe the direct image of the accretion flow around a black hole with a high resolution corresponding to black hole event horizon [93]. Nowadays resolution of the VLBI is about 55 μas, but for observing shadow of Sgr A* size is about 45 μas [93, 94, 95], near future the VLBI will reach better resolution size with including additional telescopes. The resolution of telescope is λ/D (where D is size of telescope) [95, 94]. Black hole at the center of the Galaxy Sgr A* and M87 are observed by EHT and Black hole Cam projects. If they observe image of black hole then one can explain properties of the black hole. Main purpose of this dissertation is to study properties of the black hole using shadow of the black hole,

which allows us to estimate parameters of the compact object with comparing theoretical and observational results. This may allow help us to test gravity in the strong field regime and investigate the properties of black hole candidates. The VLBI experiments is also looking for the shadow of a black hole, i.e. a dark area in front of a luminous background [92, 96]. The shadow of Schwarzschild black hole [97], rotating black hole with gravitomagnetic and electric charge [98] and other spherically symmetric black holes have been intensively studied. On the other hand, for rotating case, it has elongated shape in the direction of rotation [99, 100, 96]. Shadows of black holes possessing nontrivial NUT charge were obtained in [101], while the Kerr-Taub-NUT black hole was discussed in [101] and black hole solutions within Einstein-Maxwell-dilaton gravity and Chern-Simons gravity was considered in [102]. The apparent shape of the rotating braneworld black holes were investigated in [103]. Both Schwarzschild and rotating black hole with an accretion disc were investigated in [104]. Hence, their is a significant attention towards study of black hole shadow and it has become a quite active research field [103, 105, 28, 98, 55, 32, 101, 34, 33, 57, 106, 19]. For the Schwarzschild black hole the shadow of the black hole is a perfect circle [107], and that enlarges in the case of Reissner-Nordström black hole.

We also investigate the apparent shape of non-rotating Einstein-Born-Infeld black hole to visualize the shape of the shadow and compare the results with the images for the corresponding Reissner-Nordstrom black hole. In spite of the fact that a black hole is invisible, its shadow can be observed if it is in front of a bright background [104] as the result of the gravitational lensing effect, see, e.g., [21, 35]. The light ray that cross the event horizon, due to strong gravity, are removed from the observable universe which lead to a shadow (silhouette) imprinted by a black hole on the bright emission that exists in its vicinity. Furthermore new

general formalism to describe the shadow of black hole as an arbitrary polar curve expressed in terms of a Legendre expansion is developed in the recent paper [31]. In this dissertation, optical properties of the black hole using black hole's shadow are studied in classical method [87].

4.2 Silhouette of non-kerr black hole

Using the celestial coordinates one can easily describe the shadow (see for example [108]):

$$\alpha = \lim_{r_0 \to \infty} \left(-r_0^2 \sin\theta_0 \frac{d\phi}{dr} \right) , \tag{4.1}$$

and

$$\beta = \lim_{r_0 \to \infty} r_0^2 \frac{d\theta}{dr} , \tag{4.2}$$

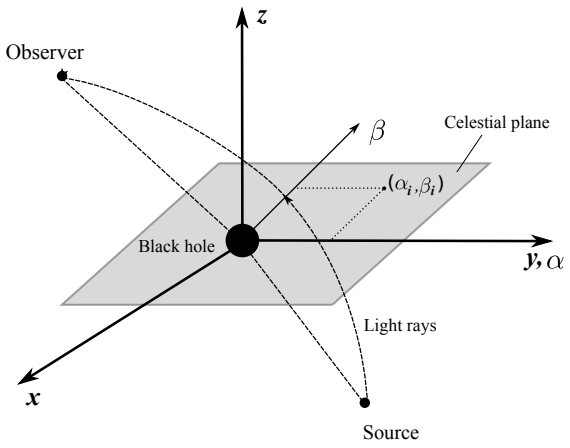

Figure 4.1: The scheme of the gravitational lens system. A reference coordinate system (x, y, z) with the black hole at the origin can be set up by an observer far away from the black hole. The straight continuation of observing light ray intersects the plane $\alpha - \beta$ at the position (α_i, β_i).

since here an observer far away from the black hole is considered at $r_0 \to \infty$, θ_0 is the angular coordinate of the observer, i.e. the inclination angle between the rotation axis of the black hole and the line of sight of the observer. The geometry of the introduced new coordinates is shown in Fig. 4.1. The coordinates α and

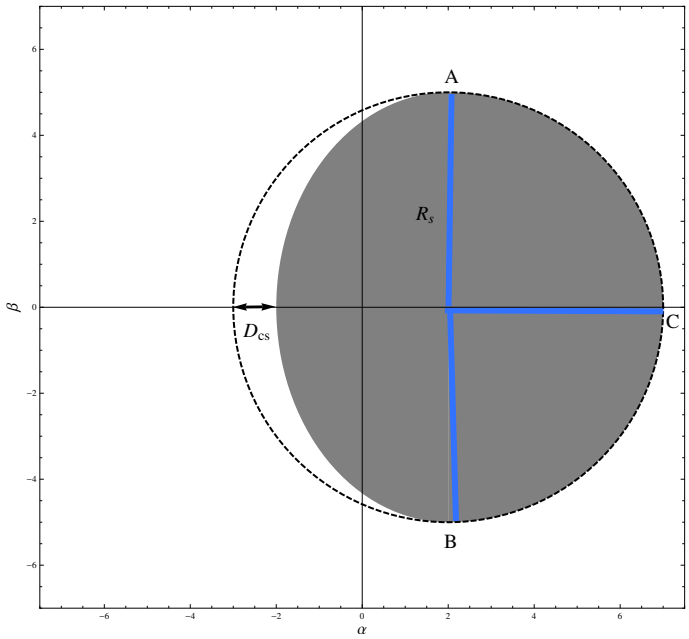

Figure 4.2: The observables for the apparent shape of a rotating black hole are the radius R_s and the distortion parameter $\delta_s = D_{cs}/R_s$. Here D_{cs} is the difference between the left endpoints of the circle and of the shadow.

β are the apparent perpendicular distances of the image as seen from the axis of symmetry and from its projection on the equatorial plane, respectively.

Calculating $d\phi/dr$ and $d\theta/dr$ using the spacetime metric given by expression (3.43) and taking the coordinate's limit of a far away observer one can obtain celestial coordinates functions of the constants of motion in the form

$$\alpha = -\frac{\Delta_\epsilon}{\Delta_\epsilon + a^2 h \sin^2\theta}\xi \csc\theta_0, \tag{4.3}$$

$$\beta = \pm\sqrt{\eta + a^2\cos^2\theta_0 - \xi\cot^2\theta_0}\ , \tag{4.4}$$

where Eqs. (3.25), (3.26) and (3.27) can be used to calculate $d\theta/dr$ and $d\phi/dr$. These equations have implicitly the same form as one for the Kerr spacetime metric with the new parameters ξ and η given by Eqs. (3.56) and (3.57) (a detailed calculation of the values of ξ and η and the expressions of the celestial coordinates α and β as a function of the constants of motion for the Kerr geometry

are given in [108]).

When the observer is situated in the equatorial plane of the black hole, the inclination angle is $\theta_0 = \pi/2$ and the gravitational effects on the shadow, which grow with θ_0, are larger. The inclination angle corresponding to the Galactic supermassive black hole is also expected to lie close to $\pi/2$. In this most simple case, we have

$$\alpha = -\frac{\Delta_\epsilon}{\Delta_\epsilon + a^2 h}\xi, \tag{4.5}$$

$$\beta = \pm\sqrt{\eta}. \tag{4.6}$$

For the visualization of the shape of the black hole shadow one needs to plot β vs α . In Fig. 4.3, we show the contour of the shadows of black holes with rotation parameters $a = 0.35$ (upper row, left), $a = 0.4$ (upper row, right), $a = 0.45$ (lower row, left), and $a = 0.5$ (lower row, right), for several values of the deformation parameter $\epsilon < 0$. In Fig. 4.4, we show the contour of the shadows of black holes with rotation parameters $a = 0.4$ (upper row, left), $a = 0.5$ (upper row, right), $a = 0.55$ (lower row, left), and $a = 0.6$ (lower row, right), for several values of the deformation parameter $\epsilon > 0$. From the Fig 4.3 and 4.4, one can see that with increasing deformation parameter($\epsilon > 0$), the shadow of the black hole decreases. This phenomena also related to the fact that the increase of deformation parameter forces light ray orbits to come closer which corresponds to the decrease of gravitational force acting on light ray. Light ray with smaller impact parameter could escape from absorbtion by black hole in the presence of positive parameter ϵ. In the case of negative ϵ the deflected light ray with particular value of impact parameter could be absorbed by central object while they could escape in pure Kerr black hole case with the same impact parameter. This of course corresponds to increasing the gravitational potential of deformed rotating black hole in the case of negative value of the deformation parameter.

In order to observe the shadow of a black hole, it is useful to introduce two observables which approximately characterise the apparent shape. First one should approximate the apparent shape by a circle passing through three points which are located at the top position, bottom and the most right end of the shadow as shown in Fig. 4.2. The radius R_s of the shadow is defined by the radius of this circle. One can also define the distortion parameter δ_s of the black hole shadow as $\delta_s = D_{cs}/R_s$. Two variables (R_s and δ_s) can be interpreted as observables in astronomical observation [87].

The observable R_s can be calculated from the equation

$$R_s = \frac{(\alpha_t - \alpha_r)^2 + \beta_t^2}{2|\alpha_t - \alpha_r|},$$

and the observable δ_s is given by

$$\delta_s = \frac{\tilde{\alpha}_p - \alpha_p}{R_s},$$

where $(\tilde{\alpha}_p, 0)$ and $(\alpha_p, 0)$ are the points where the reference circle and the contour of the shadow cut the horizontal axis at the opposite side of $(\alpha_r, 0)$, respectively. In Fig. 4.5, the observable R_s as functions of the ϵ deformation parameter are shown for the value of the spin parameter of the black hole $a = 0.5$. In Fig. 4.6, the observable δ_s as function of the deformation parameter ϵ is shown for the value of the spin parameter of the black hole $a = 0.5$. From these figures one may conclude that with the increase of deformation parameter the mean value of the shape of shadow is decreasing. The increase of δ_s with the increase of module of deformation parameter ϵ corresponds to deviation of the shape of shadows from pure circle. The deformed rotating black hole's shadow is also going to be deformed independently on sign of deformation parameter.

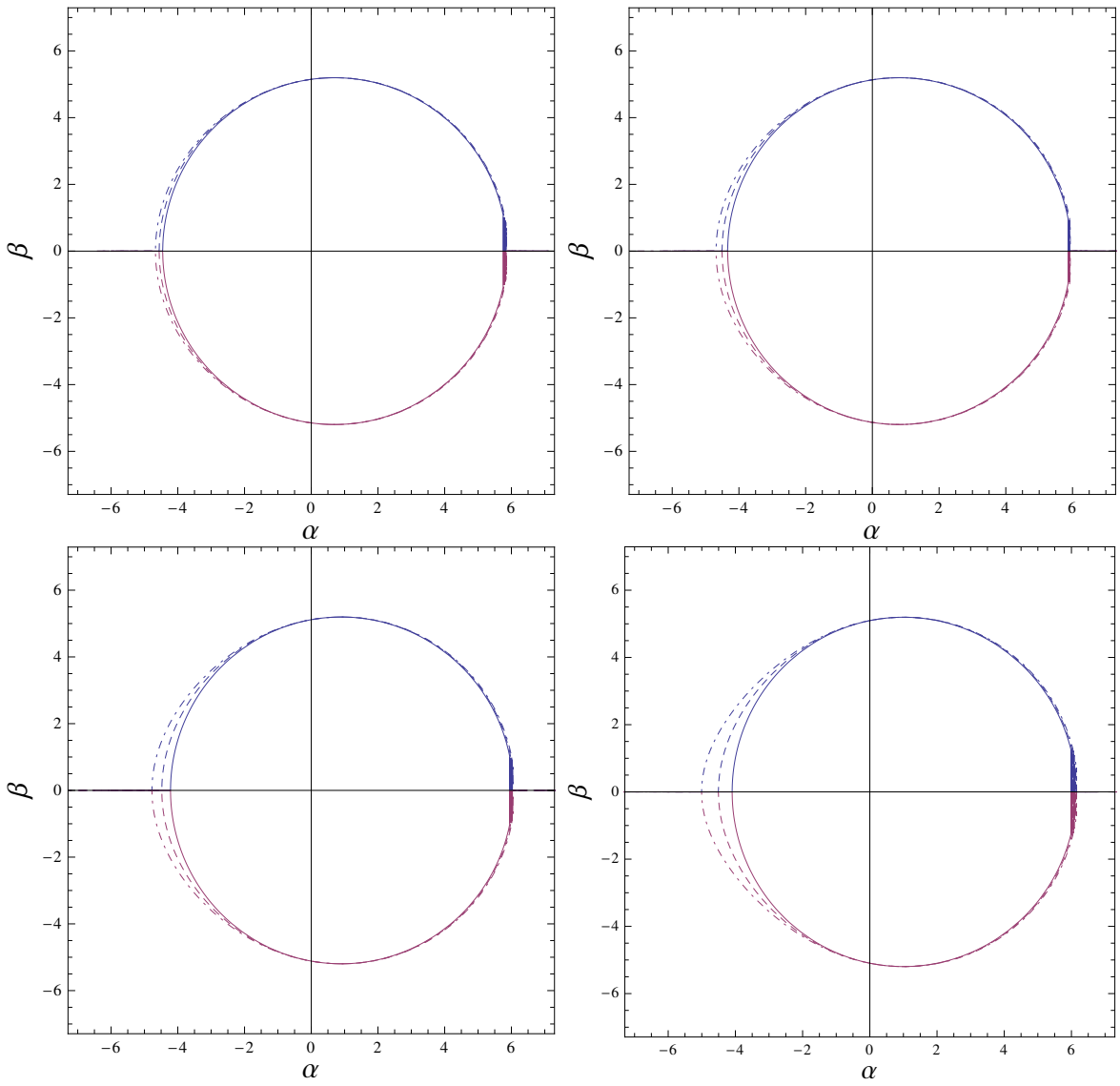

Figure 4.3: Silhouette of the shadow cast by a non-Kerr black hole situated at the origin of coordinates with inclination angle $\theta = \pi/2$, having a rotation parameter a and a deformation parameter ϵ. Upper row, left: $a/M = 0.35$, $\epsilon = 0$ (solid line), $\epsilon = -5$ (dashed line), and $\epsilon = -10$ (dashed-dotted line). Upper row, right: $a/M = 0.4$, $\epsilon = 0$ (solid line), $\epsilon = -5$ (dashed line), and $\epsilon = -10$ (dashed-dotted line). Lower row, left: $a/M = 0.45$, $\epsilon = 0$ (solid line), $\epsilon = -5$ (dashed line), and $\epsilon = -10$ (dashed-dotted line). Lower row, right: $a/M = 0.5$, $\epsilon = 0$ (solid line), $\epsilon = -5$ (dashed line), and $\epsilon = -10$ (dashed-dotted line). The shadow corresponds to each curve and the region inside it.

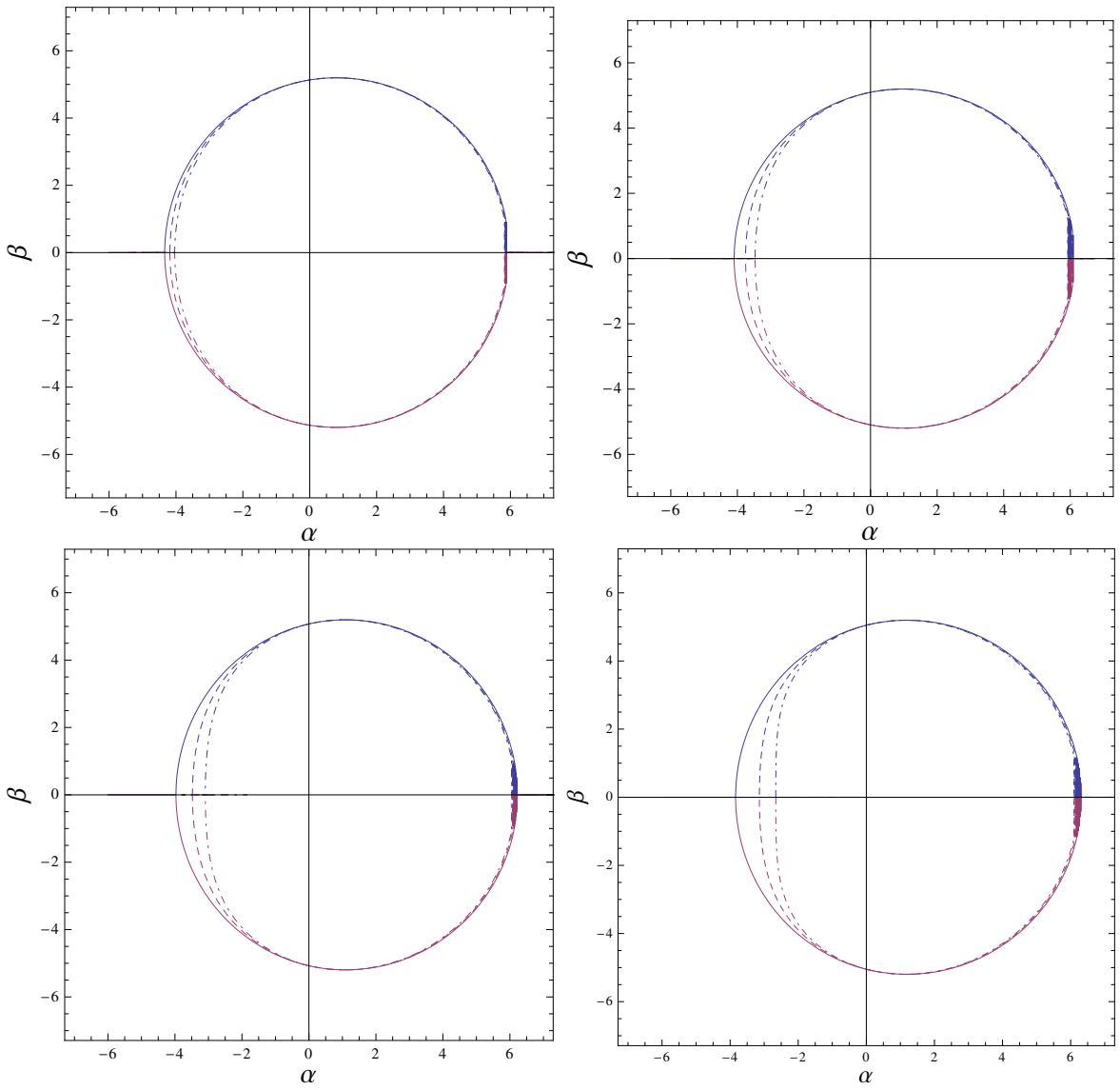

Figure 4.4: Silhouette of the shadow cast by a non-Kerr black hole situated at the origin of coordinates with inclination angle $\theta = \pi/2$, having a rotation parameter a and a deformation parameter ϵ. Upper row, left: $a/M = 0.4$, $\epsilon = 0$ (solid line), $\epsilon = 5$ (dashed line), and $\epsilon = 10$ (dashed-dotted line). Upper row, right: $a/M = 0.5$, $\epsilon = 0$ (solid line), $\epsilon = 5$ (dashed line), and $\epsilon = 10$ (dashed-dotted line). Lower row, left: $a/M = 0.55$, $\epsilon = 0$ (solid line), $\epsilon = 5$ (dashed line), and $\epsilon = 10$ (dashed-dotted line). Lower row, right: $a/M = 0.6$, $\epsilon = 0$ (solid line), $\epsilon = 5$ (dashed line), and $\epsilon = 10$ (dashed-dotted line). The shadow corresponds to each curve and the region inside it.

4.3 Shadow of Einstein-Born-Infeld black hole

Here, we plan to discuss the shadow of the Einstein-Born-Infeld black hole, and we shall confine to non-rotating ($a = 0$) case. It is possible to study equa-

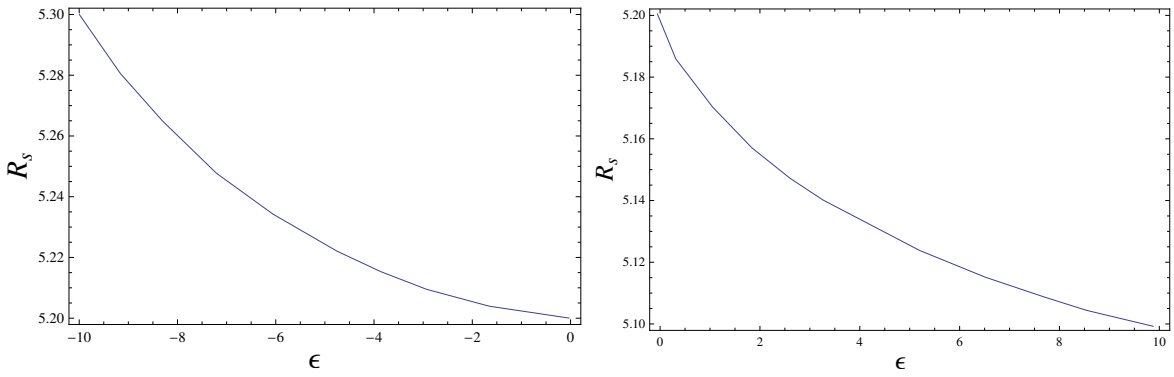

Figure 4.5: Observables R_s as functions of the $\epsilon < 0$ and $\epsilon > 0$ parameters, corresponding to the shadow of a black hole situated at the origin of coordinates with inclination angle $\theta = \pi/2$ and spin parameters $a = 0.5$.

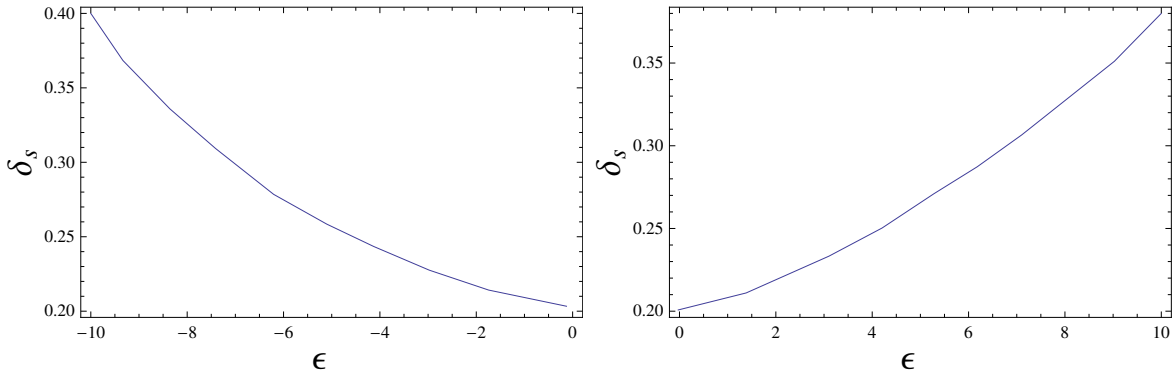

Figure 4.6: Observables δ_s as functions of the $\epsilon < 0$ and $\epsilon > 0$ parameters, corresponding to the shadow of a black hole situated at the origin of coordinates with inclination angle $\theta = \pi/2$ and spin parameters $a = 0.5$.

torial orbits of light ray around Einstein-Born-Infeld black holes via the effective potential. It is generally known, that the light ray orbits are of three types: scattering, falling and unstable [28]. *The falling orbits* are due to the light ray arriving from infinity that cross the horizon and fall down into the black hole, they have more energy than barrier of the effective potential. The light ray arriving from infinity move along *the scattering orbits* and come back to infinity, and with energy less than the barrier of the effective potential. Finally, the maximum value of the effective potential separates the captured and the scattering orbits

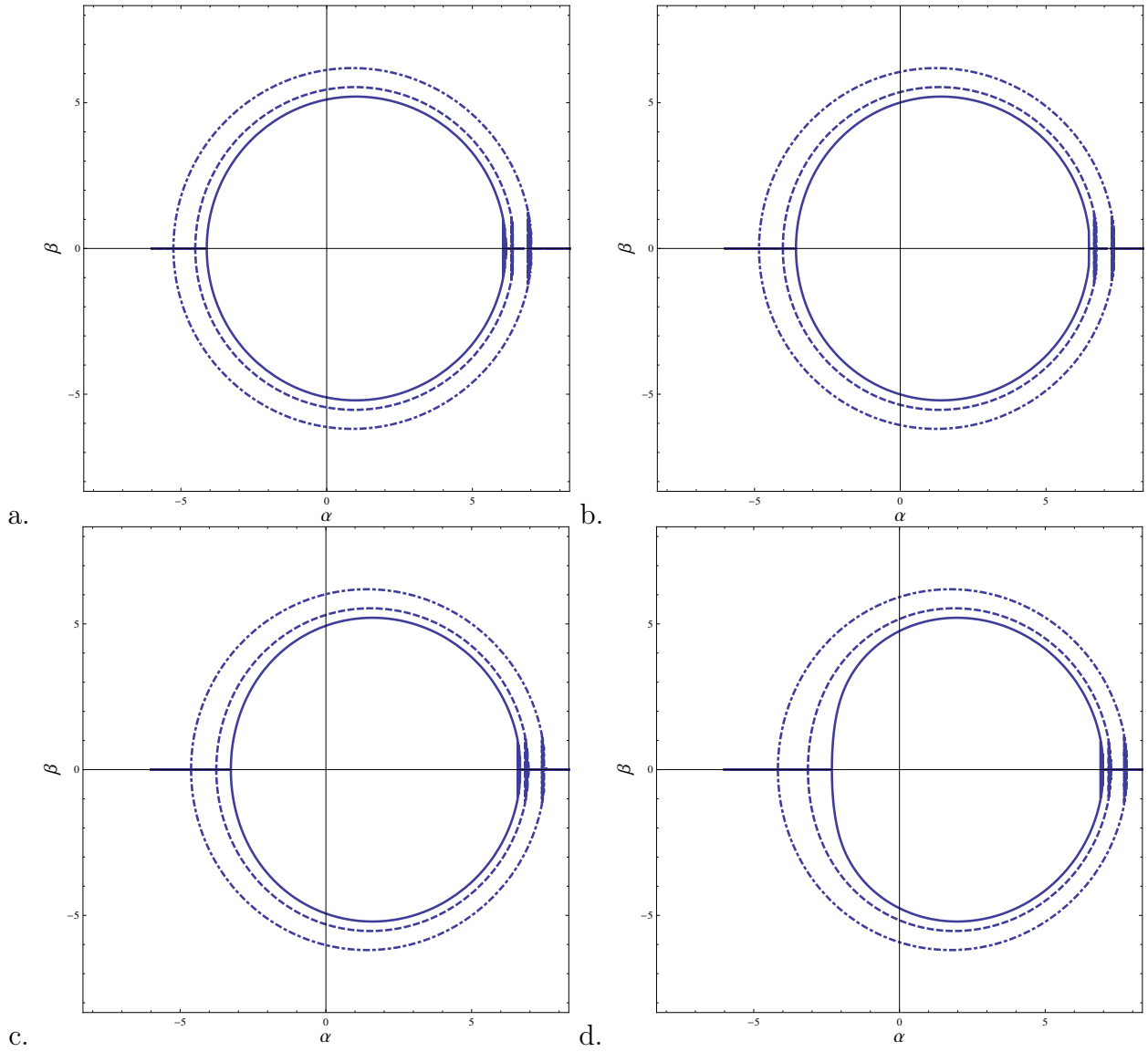

Figure 4.7: The shapes of the rotating black hole shadow with non vanishing NUT charge originated at centre of coordinates when $\theta = \pi/2$. (a): $a/M = 0.5$, (b): $a/M = 0.7$, (c): $a/M = 0.8$, and (d): $a/M = 0.99$. In all figures solid lines correspond to $l/M = 0.1$, dashed lines correspond to $l/M = 0.5$, and dashed-dotted lines correspond to $l/M = 0.9$. The region bounded by each curve corresponds to the balk hole shadow.

and defines unstable orbits of constant radius (it is circle located at $r = 3M$ for the Schwarzschild black hole) which is responsible for the apparent silhouette of a black hole. Distinct observer will be able to see only the light ray scattered away from the black hole, while those captured by the black hole will form a dark region. If the black hole appears between a light source and a distant observer, the light ray with small impact parameters fall into the black hole and form a dark zone in the sky which is usually termed as black hole shadow. We consider the following series expansion

$$\frac{4Q^2}{3}F\left(\frac{1}{4},\frac{1}{2},\frac{5}{4},-\zeta^2(r)\right) \approx \quad \frac{4Q^2}{3}\left(1-\frac{\zeta^2(r)}{10}\right)+\mathcal{O}(\frac{1}{\beta^4})\ . \tag{4.7}$$

Also, all the higher order terms from onwards have been dropped out from the series expansion of $F\left(\frac{1}{4},\frac{1}{2},\frac{5}{4},-\zeta^2(r)\right)$, which yields

$$Q^2(r) \quad \approx \frac{2\beta^2 r^4}{3}\left(1-\sqrt{1+\zeta^2(r)}\right)+\frac{4Q^2}{3}\left(1-\frac{\zeta^2(r)}{10}\right)+\mathcal{O}(\frac{1}{\beta^4})\ , \tag{4.8}$$

and accordingly Δ is also modified and we denote the new Δ as Δ', which reads

$$\Delta^{'} = -2+\frac{8Q^2\zeta^2(r)}{15r}+\frac{4Q^2}{3r\sqrt{1+\zeta^2(r)}}+2r-\frac{8\beta^2 r^3}{3}\left(-1+\sqrt{1+\zeta^2(r)}\right)\ . \tag{4.9}$$

Henceforth, all our calculations are valid up to $\mathcal{O}(\frac{1}{\beta^4})$ only. An effective potential for the light ray attains a maximum, goes to negative infinity beneath the horizon, asymptotically goes to zero at $r \to \infty$. In the standard Schwarzschild black hole, the maximum of the effective potential occurs at $r = 3M$, which is also the location of the unstable orbit and no minimum. The behavior of effective potential as a function of radial coordinate r for different values of parameter β, rotation parameter a and Q are depicted in Figs. 3.2 and 3.3. It is observed that the potential has a minimum which imply the presence of stable circular orbits. The apparent shape of the black hole is obtained by observing the closed orbits around the black hole governed by three impact parameters, which are functions

of E, L_ϕ and L_ψ and the constant of separability $\mathcal{K}$. The equations determining the unstable light ray orbits, in order to obtain the boundary of shadow of the black holes, are Eq.(3.18) or

$$R(r) = 0 = \partial R(r)/\partial r$$

which are fulfilled by the values of the impact parameters

$$\xi = \frac{(r^2+a^2)\Delta^{'} - 4r\Delta}{\Delta^{'}a}\ , \tag{4.10}$$

and

$$\eta = \frac{16\Delta r^2 a^2 - \left((r^2+a^2)\Delta^{'} - 4r\Delta - a\Delta^{'}\right)}{(\Delta^{'}a)^2}, \tag{4.11}$$

that determine the contour of the shadow. whereas the parameter ξ and η satisfy

$$\begin{aligned}\xi^2+\eta = &\frac{4A\left(\frac{8Q^2r_0\zeta^2(r_0)}{15} - \frac{8Q^2r_0}{3} + \frac{2Q^2r_0}{3\sqrt{1+\zeta^2(r_0)}} + 3r_0^2 - r_0^3\right)}{-1 + \frac{4Q^2\zeta^2(r_0)}{15r_0} + \frac{2Q^2}{3r_0\sqrt{1+\zeta^2(r_0)}} + r_0 - \frac{4}{3}\beta^2 r_0^3\left(-1+\sqrt{1+\zeta^2(r_0)}\right)} \\ &+\frac{60\beta^2 r_0^4 B}{C} + O(a^2)\end{aligned} \tag{4.12}$$

with

$$\begin{aligned}A &= -1 + \frac{4Q^2\zeta^2(r_0)}{15r_0} + \frac{2Q^2}{3r_0\sqrt{1+\zeta^2(r_0)}} \\ &\quad -r_0 - \frac{4}{3}\beta^2 r_0^3\left(-1+\sqrt{1+\zeta^2(r_0)}\right)\end{aligned} \tag{4.13}$$

$$\begin{aligned}B &= 6Q^6 - 14\beta^2Q^4r_0^4 + 15\beta^2Q^2r_0^5 - 10\beta^4Q^2r_0^8 + 15\beta^4r_0^9 \\ &\quad +10\beta^6r_0^{12} - 10\beta^6r_0^{12}\sqrt{1+\zeta^2(r_0)}\end{aligned} \tag{4.14}$$

$$\begin{aligned}C &= 4\beta Q^4\sqrt{1+\zeta^2(r_0)} + 20\beta^5 r_0^8\left(-1+\sqrt{1+\zeta^2(r_0)}\right) \\ &\quad -5\beta^3 r_0^4\left(2Q^2 - 3r_0(r_0-1)\sqrt{1+\zeta^2(r_0)}\right)^2\end{aligned} \tag{4.15}$$

The shadow of Einstein-Born-Infeld black holes may be determined through virtue of the above equation. In order to study the shadow of Einstein-Born-Infeld black hole, it is necessary to introduce the celestial coordinates according to [108]

$$\lambda = \lim_{r_0 \to \infty} \left(-r_0^2 \sin\theta_0 \frac{d\phi}{dr} \right) \ , \tag{4.16}$$

and

$$\mu = \lim_{r_0 \to \infty} r_0^2 \frac{d\theta}{dr} \ , \tag{4.17}$$

where λ and μ are celestial coordinates as (4.1) and (4.2)

The celestial coordinates can be rewritten as

$$\lambda = -\xi \csc\theta_0, \tag{4.18}$$

$$\mu = \pm\sqrt{\eta + a^2\cos^2\theta_0 - \xi\cot^2\theta_0}, \tag{4.19}$$

and formally coincide with that for the Kerr black hole. However in reality ξ and η are different for the Einstein-Born-Infeld black hole. The celestial coordinate in the equatorial plane ($\theta_0 = \pi/2$), where observer is placed, becomes

$$\lambda = -\xi, \tag{4.20}$$

and

$$\mu = \pm\sqrt{\eta} \ , \tag{4.21}$$

The apparent shape of the Einstein-Born-Infeld black hole shadow can be obtained by plotting λ vs μ as

$$\lambda^2 + \mu^2 = \xi^2 + \eta \ , \tag{4.22}$$

which suggests that the shadow of Einstein-Born-Infeld black holes in (λ, μ) space is a circle with radius of the quantity defined by the right hand side of equation (4.12). Thus, the shadow of the black hole depends on the electric charge Q and

Born-Infeld parameter β both. These are depicted in Figs. 4.8 and 4.9 for the different values of these parameters.

In the limit, $\beta \to \infty$, the above expression reduces to

$$\xi^2 + \eta \;=\; \lambda^2 + \mu^2 = \frac{2r_0^2(r_0^2-3)+4r_0Q^2}{(r_0-1)^2}. \tag{4.23}$$

which is same as that for Reissner-Nordstrom black hole. In addition, if we switch off electric charge $Q = 0$, one gets expression for Schwarzschild case, which reads as

$$\xi^2 + \eta \;=\; \lambda^2 + \mu^2 = \frac{2r_0^2(r_0^2-3)}{(r_0-1)^2}\ . \tag{4.24}$$

In order to extract more detailed information from the shadow of the Einstein-Born-Infeld black holes, we must create the observables. In general, there are two observable parameters as radius of shadow R_s and distortion parameter δ_s [87]. For non-rotating black hole there is only single parameter R_s which corresponds to radius of reference circle. From Figs. 4.8 and 4.9 one can get numerical value for the radius of black hole shadow which is clearly shown in Fig. 4.10. As is shown from the Fig. 4.11 and Fig. 4.12, the shadow of rotating Einstein-Born-Infeld black hole has been considered for various values of electric charge Q and Born-Infeld parameter β. The influence of rotating parameter a on the shadow of black hole is distorted, while with increasing electric charge of black hole the shadow starts becoming circle. One of the observable parameter is distortion parameter. Observable parameter is shown for different values of rotating parameter, electric charge and Born-Infeld parameter in Fig 4.13.

4.4 Observing shadow of Kerr-Taub-NUT black hole

To obtain the silhouette of the rotating black hole with non vanishing NUT charge it is very convenient to use the celestial coordinates. Calculating $d\phi/dr$

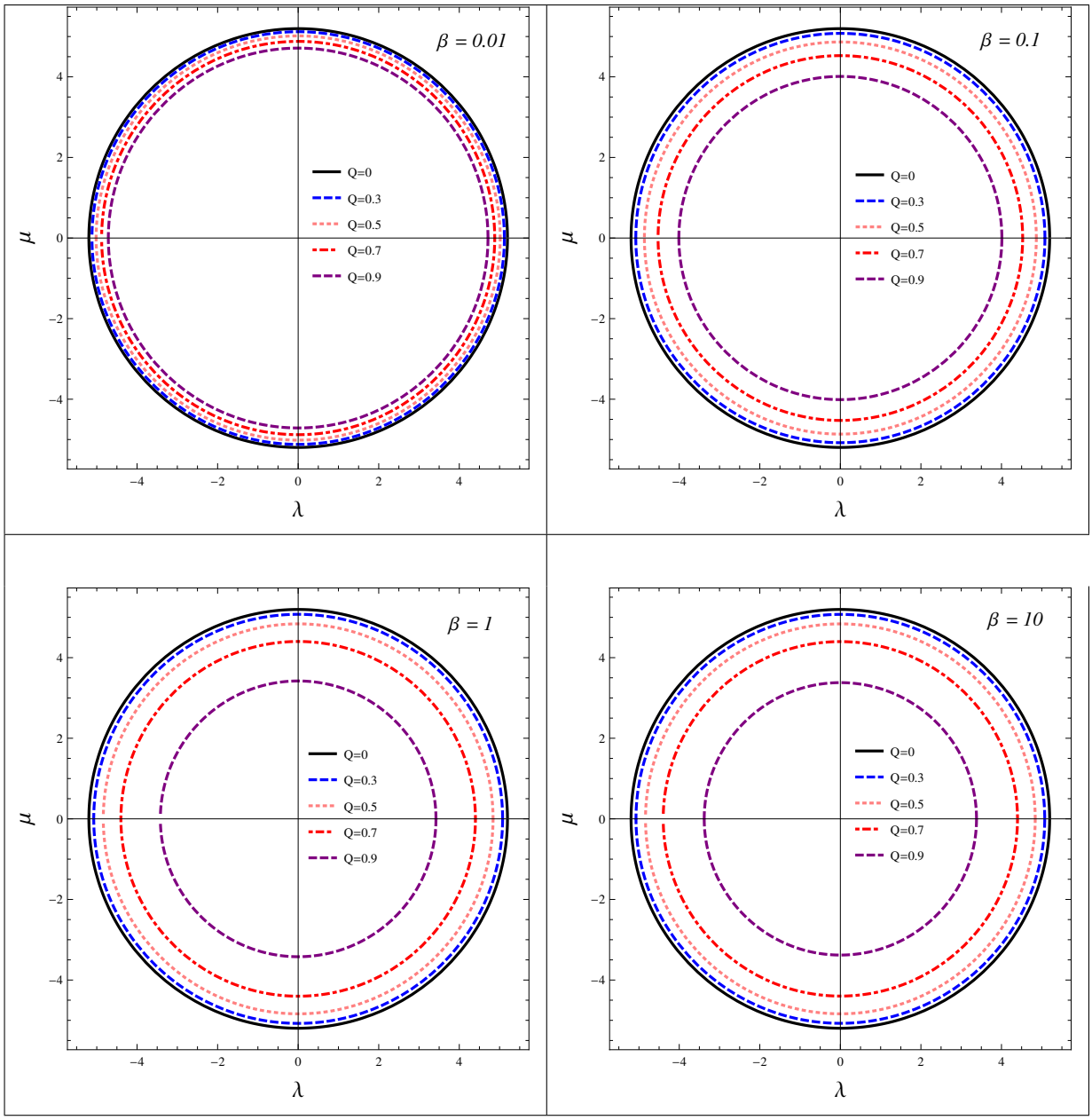

Figure 4.8: Shadow of the black hole for the different values of electric charge Q. Top, left panel is for Born-Infeld parameter $\beta = 0.01$. Top, right panel is for Born-Infeld parameter $\beta = 0.1$. Bottom, left panel is for Born-Infeld parameter $\beta = 1$. Bottom, right panel is for Born-Infeld parameter $\beta = 10$ (with $M = 1$ and $a = 0$).

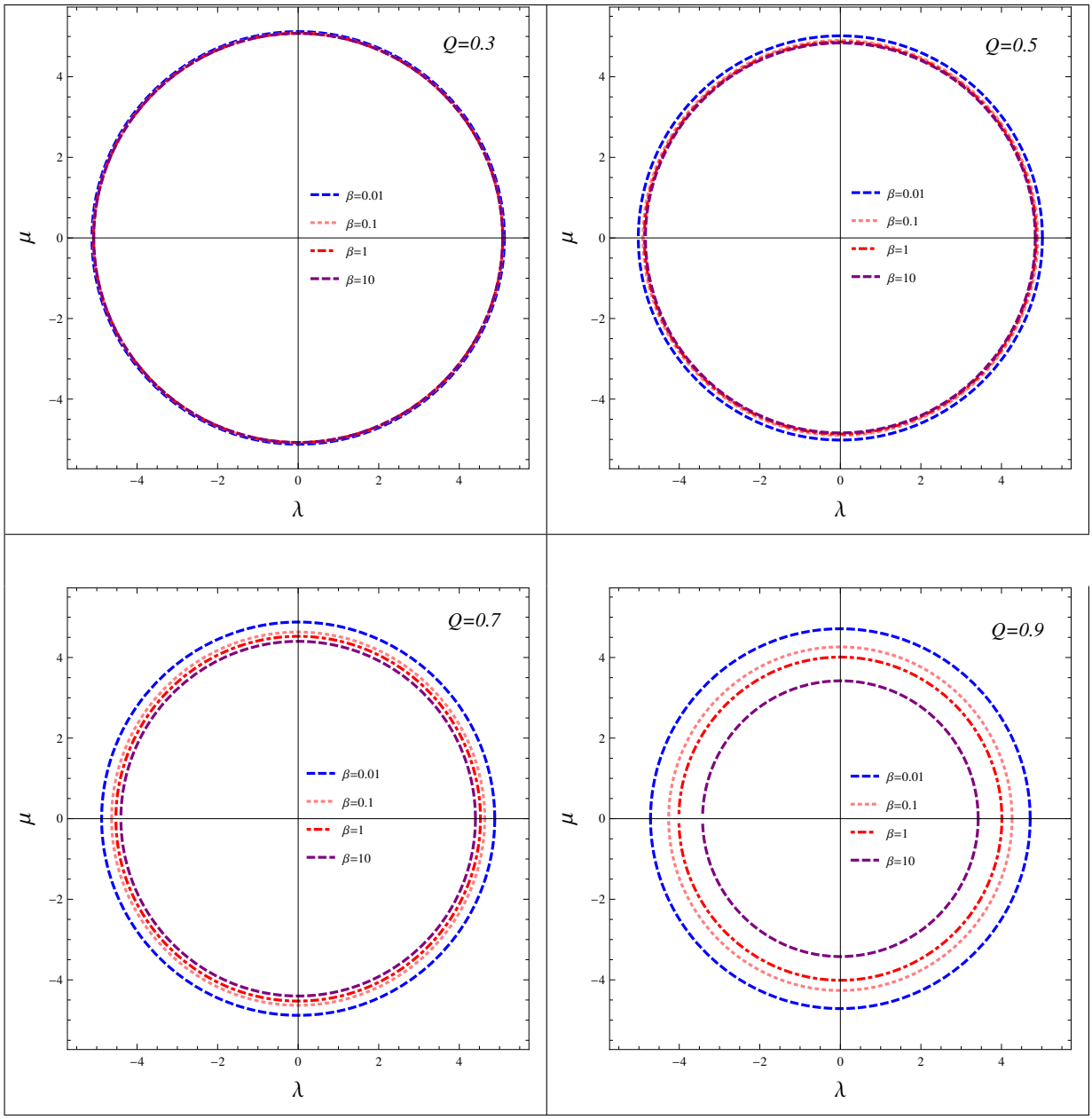

Figure 4.9: Shadow of the black hole for the different values of Born-Infeld parameter β. Top, left panel is for electric charge $Q = 0.3$. Top, right panel is for electric charge $Q = 0.5$. Bottom, left panel is for electric charge $Q = 0.7$. Bottom, right panel is for electric charge $Q = 0.9$ (with $M = 1$ and $a = 0$).

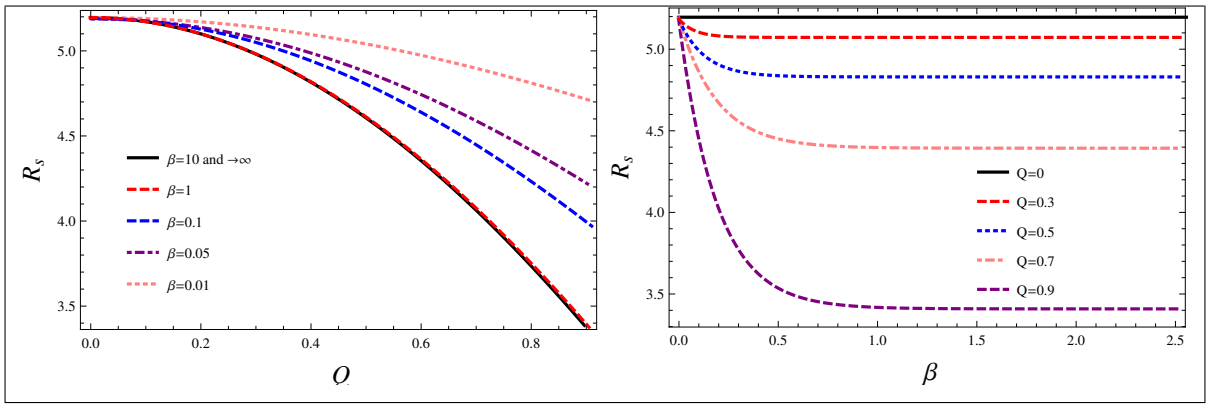

Figure 4.10: The dependence of observable radius of black hole shadow R_s from the electric charge Q and Born-Infeld parameter β. Left panel is showing graphs for the different values of Born-Infeld parameter β. The right panel is showing graphs for the different values of electric charge Q.

and $d\theta/dr$ using the spacetime metric (3.43) and putting the results into (4.1), (4.2), using (3.6), (3.7), and (3.8) we obtain equations for $(\alpha,\ \beta)$ coordinates in the following form:

$$\alpha = -\xi \csc\theta_0 \ , \tag{4.25}$$

and

$$\beta = \pm\Big[\eta + (a^2 - \frac{4l^2}{\sin^2\theta_0})\cos^2\theta_0 - \xi^2\cot^2\theta_0 + 4l\cos\theta_0(a - \frac{\xi}{\sin^2\theta_0})\Big]^{1/2} \ , \tag{4.26}$$

While considering the shape of the shadow of rotating black hole with non vanishing gravitomagnetic charge one may introduce the radius $R_{\rm sh}$ and the distortion parameter $\delta_{\rm sh}$ of the silhouette related by the expression $\delta_{\rm sh} = D_{\rm cs}/R_{\rm sh}$. The schematic explanation of these parameters are shown in Fig. 4.2 [87].

Consider the distant observer located in the equatorial plane of the rotating

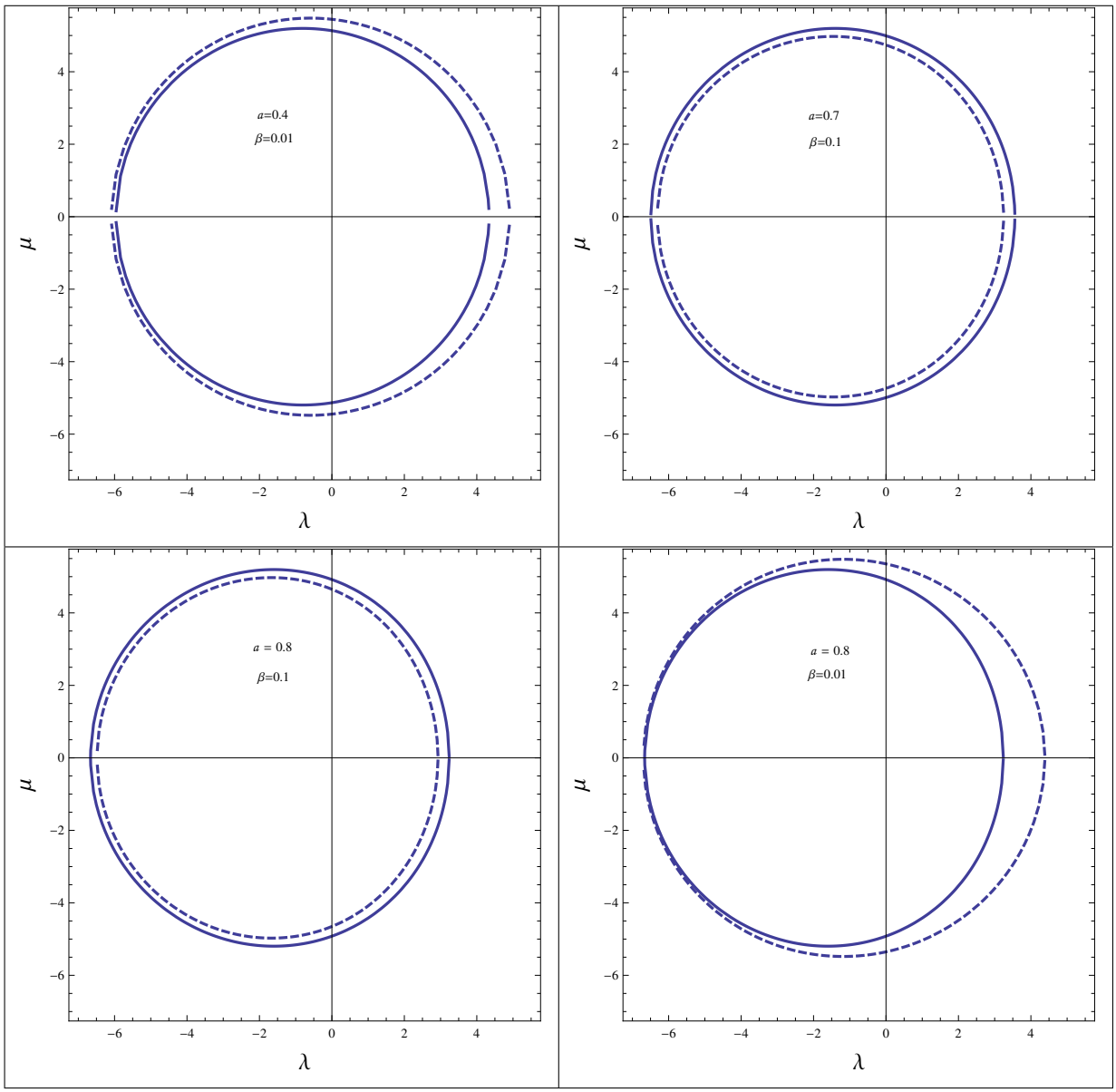

Figure 4.11: Shadow of rotating black hole for the different values of Born-Infeld parameter β, rotating parameters a and electric charge Q. Solid line is $Q = 0$ and dashed line is $Q = 0.5$ (with $M = 1$).

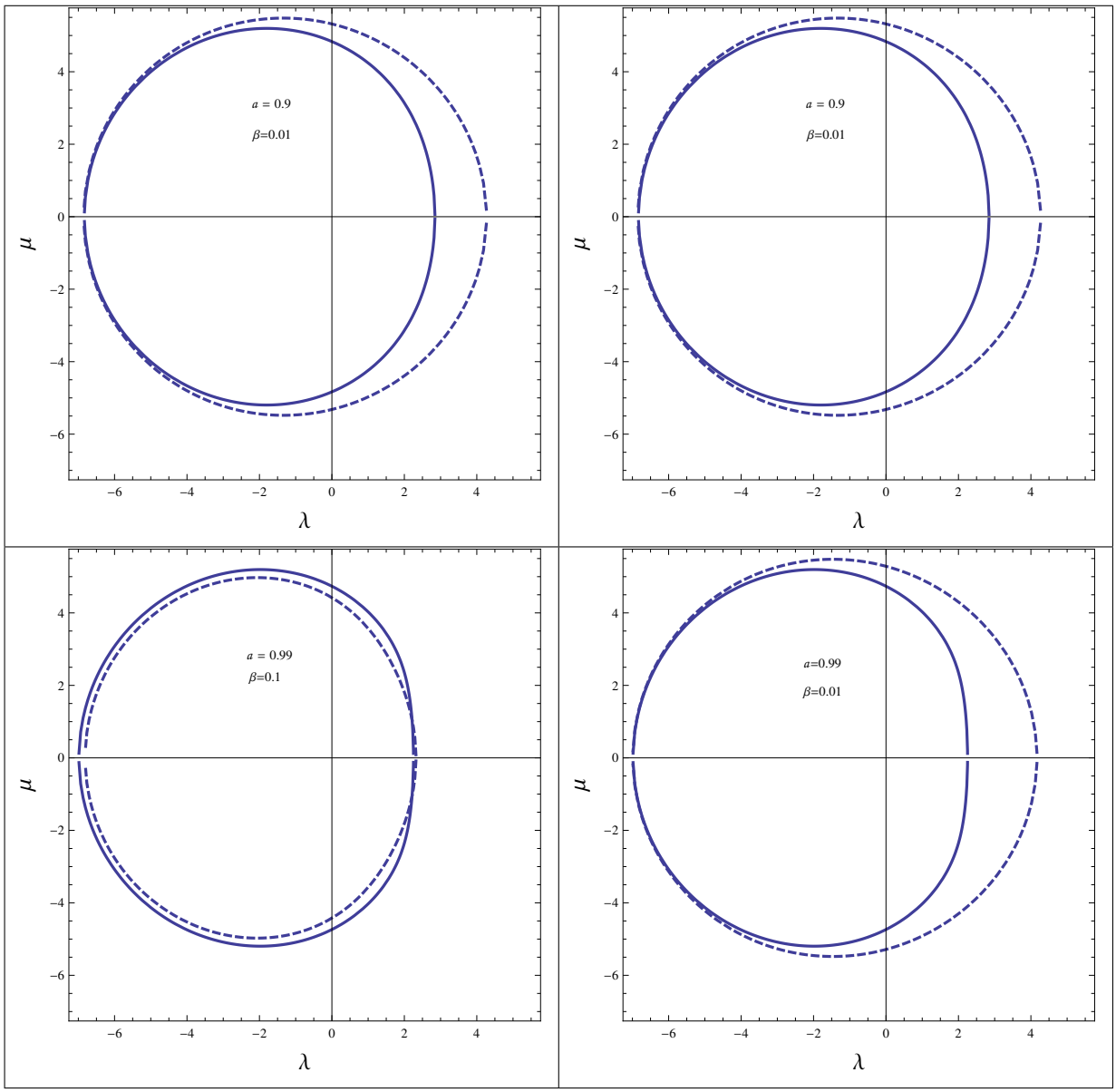

Figure 4.12: Shadow of rotating black hole for the different values of Born-Infeld parameter β, rotating parameters a and electric charge Q. Solid line is $Q = 0$ and dashed line is $Q = 0.5$ (with $M = 1$).

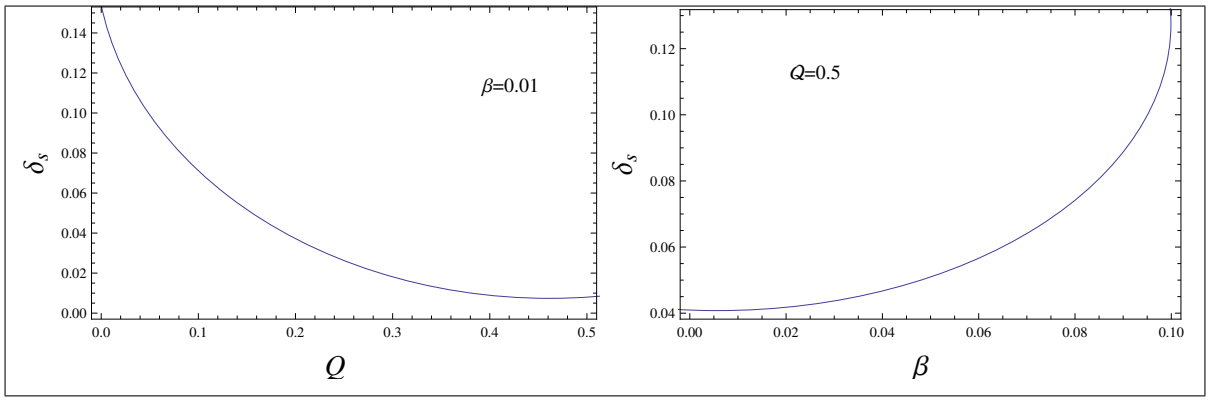

Figure 4.13: The dependence of observable distortion parameter of black hole shadow δ_s from the electric charge Q, Born-Infeld parameter β and rotation parameter $a = 0.9$. The right panel is showing graphs for the different values of Born-Infeld parameter β and the Left panel is showing graphs for the different values of electric charge Q.

black hole black hole with non vanishing gravitomagnetic charge. Then,

$$\alpha = -\xi \,, \tag{4.27}$$

and

$$\beta = \sqrt{\eta} \,. \tag{4.28}$$

Obtained numerical results are shown in Fig. 4.7 where the shape of the silhouettes of rotating Taub-NUT black hole for the different values of the rotation parameter and gtavitomagnetic charge are presented. From the plots one can see that the presence of the gravitomagnetic charge will increase the effective size of the shadow. In the figure the shapes of the silhouette of rotating black hole with the gravitomagnetic charge are given for the different values of black hole angular momentum a: $a/M = 0.5$, $a/M = 0.7$, $a/M = 0.8$, and $a/M = 0.99$. One can easily compare the effect of the NUT parameter and the black hole rotation parameter on modification of the shape of the shadow of black hole. It appears they have opposite effects on black hole shadow size. The gravitomagnetic charge increases the size of the shadow shape while black hole's angular momentum decreases its size. The parameters $R_{\rm sh}$ (radius) and $\delta_{\rm sh}$ (distortion) are shown as

functions of the gravitomagnetic charge l in Fig. 4.14. From the dependence of R_s from the NUT parameter one can again see that the gravitomagnetic charge forces to increase the size of the black hole shadow. The dependence of δ_s from NUT charge shows that gravitomagnetic charge forces to shadow to get the shape of circle than ellipse. In the case of rotation, with the increase of black hole's angular momentum the shape of black hole shadow takes form of ellipse rather than circle.

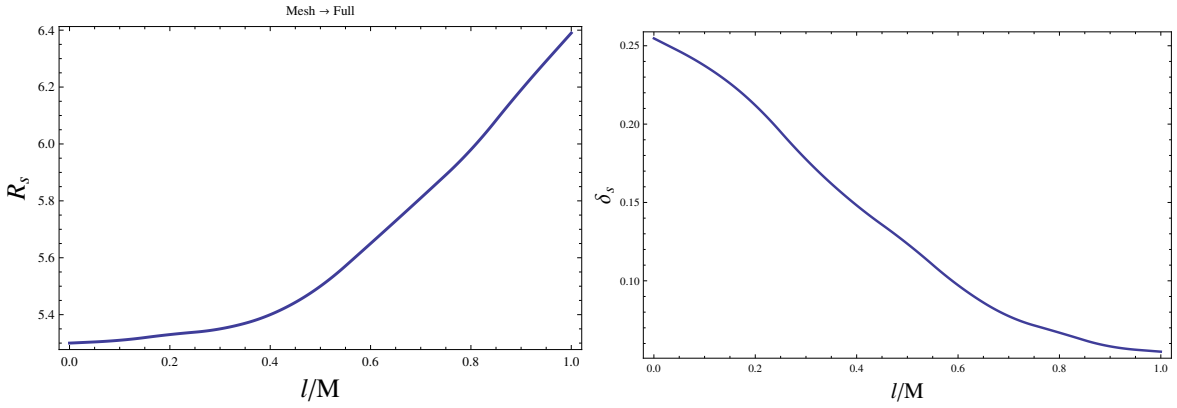

Figure 4.14: The dependence of the average radius of the silhouette $R_{\rm sh}$ and the distortion (deviation) parameter $\delta_{\rm sh}$ from the gravitomagnetic charge (NUT parameter).

4.5 Shadow of rotating five dimension black hole

For $\theta = 0$, $L_\phi = 0$ which implies $\xi_2(r) = 0$, therefore

$$\xi_1(r) = \frac{-a^4 + 2a^2(x-1) + x^2 + (a^4 + 2a^2x + x(x-2))\sqrt{a^2+x}}{2a(x + a^2 - 1)}, \qquad (4.29)$$

and for $\theta = \pi/2$, $L_\psi = 0$ which implies $\xi_1(r) = 0$, thus

$$\xi_2(r) = \frac{-a^4 + 2a^2(x-1) + x^2 + (a^4 + 2a^2x + x(x-2))\sqrt{a^2+x}}{2a(x + a^2 - 1)}. \qquad (4.30)$$

Here we investigate the shadow of a black hole and naked singularity. It is possible to obtain equatorial orbits of light ray around 5D black hole from the

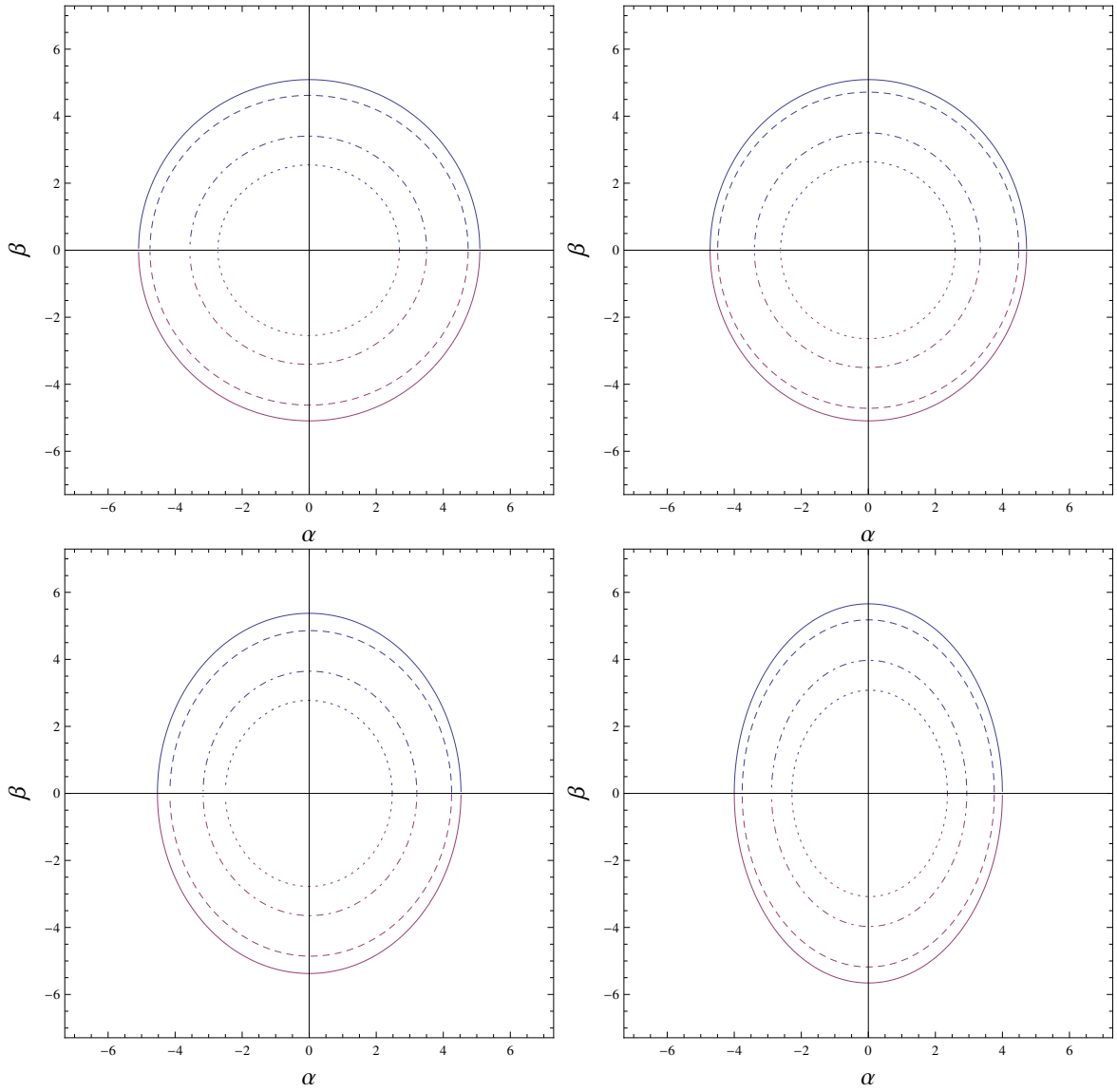

Figure 4.15: Shadow cast by 5D rotating black hole taking $a = b$. Top: For $\theta_0 = 0$ (left) for $\theta_0 = \pi/6$ (right). Bottom: For $\theta_0 = \pi/4$ (left) $\theta_0 = \pi/3$ (right). $\theta_0 = 0$ is same with $\theta_0 = \pi/2$ and a is as following: $a = 0$ (solid line), $a = 0.4$ (dashed line), $a = 0.5$ (dot-dashed line), $a = 0.6$ (dotted line).

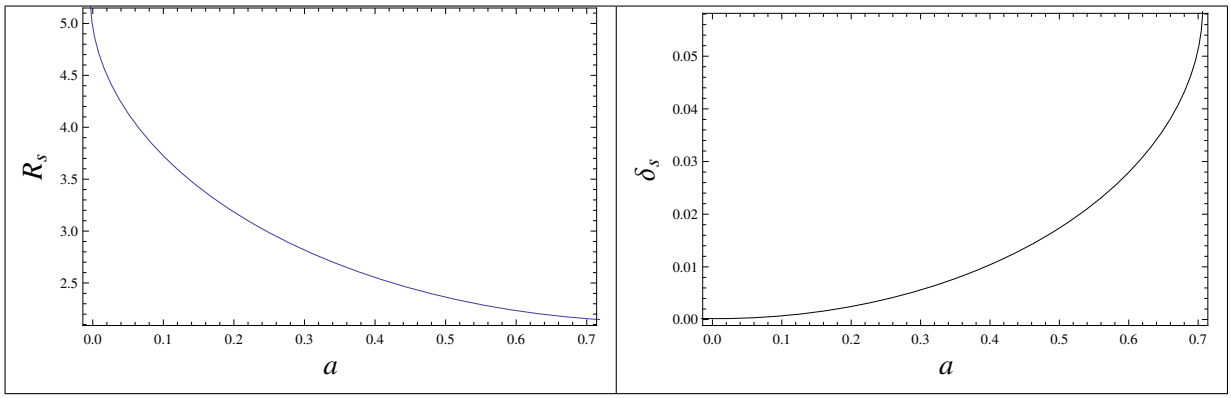

Figure 4.16: Plots showing the dependence of the observables, the radius of the shadow R_s (left) and distortion parameter δ_s (right) on the rotation parameter with inclination angle $\theta_0 = 0$.

effective potential. The light ray orbits are in general of three types: scattering, falling and unstable orbits. One can think of these there kinds of light ray orbits in terms of effective potential: (i) falling orbits, in which case the light ray arrives from infinity with energy larger than the barrier of the effective potential and then crosses into the horizon, (ii) scattering orbits, in which the light ray arrives from infinity with energy less than the barrier of the effective potential and then comes back to infinity, and (iii) unstable orbits of constant radius (at $r = 3M$ for Schwarzschild black hole, the location of the maximum of the effective potential) which separate the capture and the scattering orbits. The apparent shape of the black hole can be found by looking for the unstable orbits. An observer far away from the black hole will be able to see only the light ray scattered away from the black hole, while those captured by the black hole will form a dark region. When a black hole is placed between a source of light and an observer, part of the light coming from source behind the black hole reaches the observer after being deflected by the gravitational field of the black hole; but those light ray with small impact parameters fall into the black hole. As a consequence, there is a dark zone in the sky which we call is shadow. The apparent shape of a black hole is then given by the boundary of the shadow. For obtaining this apparent shape, we need to study the geodesic structure of the light ray in the black hole background.

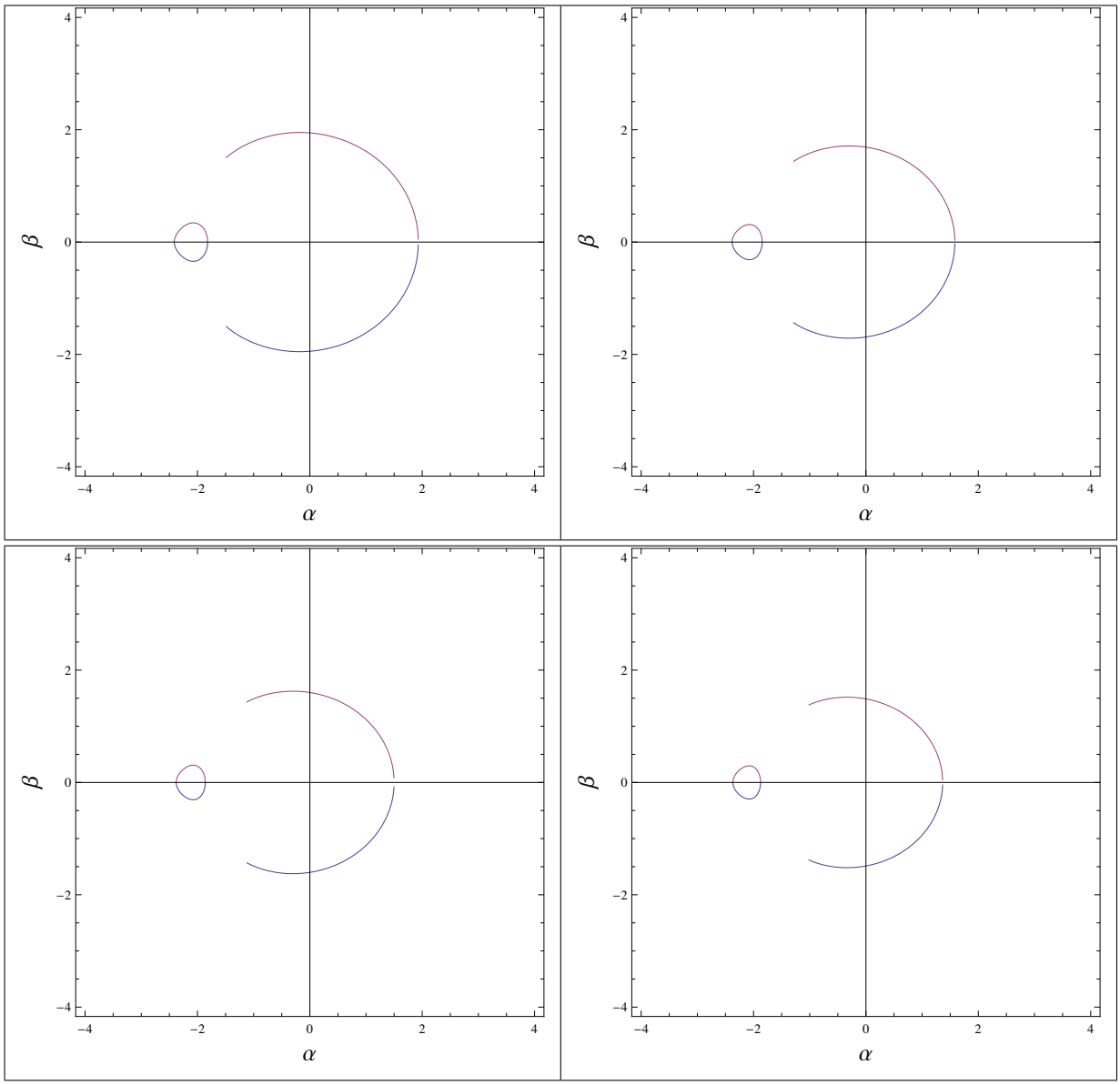

Figure 4.17: Shadow cast by naked singularity taking $a = b$ and for the different value of rotation parameter a: $a = 0.9$ (top panel, left), $a = 1$ (top panel, right), $a = 1.1$ (bottom, left) and $a = 1.2$ (bottom, right). Here inclination angle is $\theta = 0$ and it is same with $\theta = \pi/2$.

The shadow of a black hole is better described by the celestial coordinates α and β [108], which in 5D case are modified to [57]:

$$\alpha = \lim_{\tilde{r}_0 \to \infty} -\tilde{r}_0^2 \left(\sin\theta_0 \frac{d\varphi}{dr} + \cos\theta_0 \frac{d\psi}{dr} \right), \tag{4.31}$$

and

$$\beta = \lim_{\tilde{r}_0 \to \infty} \tilde{r}_0^2 \frac{d\theta_0}{dr}. \tag{4.32}$$

Here we have defined $\tilde{r}_0$ as observers distance to the black hole, the coordinate α is the apparent perpendicular distance of the image from the axis of symmetry, and the coordinate β is the apparent perpendicular distance of the image from its projection on the equatorial plane. For further details and a useful diagram, see Ref. [108].

Next we consider that the observer is far away from the black hole and hence, r_0 goes to infinity, and θ_0 is the angular coordinate of the observer, i.e., the inclination angle between the axis of rotation of the black hole and the line of sight of the observer. We define two coordinates (α, β) to discuss the shape of the shadow. Eqs.(4.31) and (4.32) are obtained by writing (α, β) in the Euclidean frame, changing to spherical coordinates, and using the geometrical description of the straight line connecting the far away observer with the apparent position of the image.

On using Eq. (3.37), in Eqs. (4.31) and (4.32), and taking the limit of a far away observer, we found the celestial coordinates, as a function of the constant of motion, take the form

$$\begin{aligned} \alpha &= -\left(\xi_1 \frac{1}{\sin\theta_0} + \xi_2 \frac{1}{\cos\theta_0} \right), \\ \beta &= \pm\sqrt{\eta - \xi_1^2 \cot^2\theta_0 - \xi_2^2 \tan^2\theta_0 + a^2}. \end{aligned} \tag{4.33}$$

In the equatorial plane $\theta_0 = \pi/2$, then the celestial coordinates can be written as

$$\begin{aligned} \alpha &= -\xi_1, \\ \beta &= \pm\sqrt{\eta + a^2}. \end{aligned} \tag{4.34}$$

For $\theta = 0$,

$$\begin{aligned} \alpha &= -\xi_2, \\ \beta &= \pm\sqrt{\eta + a^2}. \end{aligned} \tag{4.35}$$

Now we show the shadows of 5D rotating black hole using Eq. (4.33). In Fig. 4.15, we plot α Vs β to show the contour of the shadow of the black holes for different values of rotation parameter at different inclination angles. It can be seen from the figure that with increasing the value of rotation parameter the effective size of the shadow is decreasing.

In Fig. 4.16, the observables R_s and δ_s are plotted as a function of the rotation parameter a. The observable R_s gives information about the size of the shadow. From Fig. 4.16, we observe that the observable R_s monotonically decrease with the increase in the value of rotation parameter . Whereas the observable δ_s gives distortion of the shadow with respect to the circumference of reference, which increases with a.

In Fig. 4.15, the shadows are plotted for different values of the rotation parameter a and the angle of inclination θ_0, for the $5D$ Myers-Perry black hole. In all the cases, we take values for the angular momentum that go from 0 to 0.6, and it can be seen clearly that the shape of the shadow is decreasing with the increase in the value of rotation parameter. Also, the shape is more distorted with the increase in the value of rotation parameter. It is interesting to note that the rate of distortion also depends on the angle of inclination, it is seen that rate of distortion is more for $\theta_0 = \pi/4$ than in the case of $\theta_0 = 0$.

In the case of Schwarzschild black hole, the apparent image of the black hole is a perfect circle of radius $\approx 5.20M$ [109]. The main feature of the shape of Kerr black holes is the asymmetry along the spin axis, because of the different effective potential for light ray orbiting around the black hole in one or the other direction. The radius of the unstable circular orbit is smaller for light ray with angular momentum parallel to the black hole spin and that slightly flattens the black hole shadow on one side.

Whereas, in the Brane-world case [110], in addition to the angular momentum, the tidal charge term also deforms the shape of the shadow. For a given value of the rotation parameter, the presence of a negative tidal charge enlarges the shadow and reduces its deformation with respect to Kerr spacetime, while for a positive charge, the opposite effect is obtained. However, in the Brane world, for fixed tidal charge, there is a very small variation in the size of the shadow as a function of a. In a similar study in for the Kaluza-Klein black holes in Einstein gravity coupled to a Maxwell field and a dilaton, the size and the shape of the shadow depend on the mass, the charge, and the angular momentum and, for fixed values of these parameters, the shadow is slightly larger and less deformed than for its Kerr-Newman counterpart. On the contrary, our results demonstrate that the size of the the $5D$ Myers-Perry black hole shadow is smaller than for Kerr black hole shadow. In general, the size of the shadow decreases with rotation parameter in 5D Myers-Perry black hole compared to the four-dimensional Kerr black hole

4.5.1 Naked Singularity Shadow

A naked singularity is defined as a spacetime singularity without an event horizon which can be seen by some observer. According to the cosmic censor-

ship conjecture, the singularities that appear in gravitational collapse are always surrounded by an event horizon. Moreover, according to the strong version of the conjecture, such singularities are not even locally naked, i.e., no nonspacelike curve can emerge from such singularities. The cosmic censorship conjecture has as yet no precise mathematical formulation or proof for either version. Hence the cosmic censorship conjecture remains one of the most important unsolved problems in general relativity and gravitation theory today. But as we are still far from having a general proof of this hypothesis so it is interesting to study about the shadow of a naked singularity. Consequently, such a study is an important tool to get insight to this unresolved issue.

When, $r_0^2 < 4a^2$ or $a > 1/\sqrt{2}$, from Eq. (2.13) one see that horizons do not exist and singularity is exposed to an external observer, i.e., there exists a naked singularity violating cosmic censorship conjecture. For non-rotating case ($a = 0$), one obtains a point naked singularity whilst the rotating case ($a \neq 0$) corresponds to a ring type naked singularity. For the visualization of naked singularities shadow, we show a contour of them for different values of rotation parameters. In the case of a Kerr naked singularity, the shadow consists of two parts: the arc and the dark spot or the straight line. Next we show the shadows of a 5D Myers-Perry naked singularity in Fig. 4.17. In the case of a naked singularity, the event horizon does not exist and then the apparent shapes drastically different from those of a black hole. The unstable spherical light rays orbit with a positive radius constructs an arc rather than a closed curve. This is because the light ray near the arc may come back to the observer due to the nonexistence of horizon. In Fig. 4.17, we have plotted α vs β to show the shadow of naked singularities of $5D$ rotating Myers-Perry spacetime. Indeed, the shadow consists of two parts an arc and a dark spots. Fig. 4.17, we observe that arc of shadow tends to

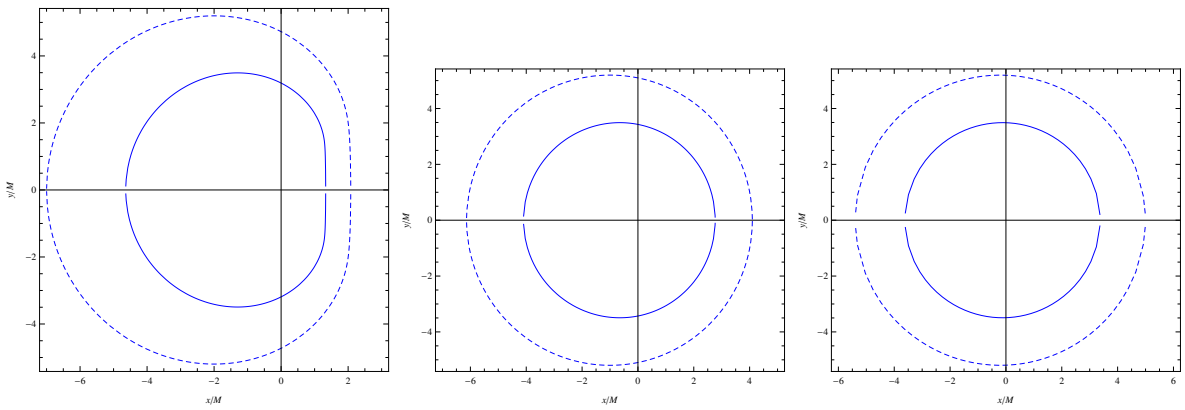

Figure 4.18: Shadow of the rotating GB black holes when the inclination angle $\theta = \pi/2$. For the comparison we present the shadow of rotating Kerr black hole (dashed lines). From left to right, the rotation parameter scans as $a = 0$, $a_{\rm ext}/2$, and $a_{\rm ext}$. Note that for the pure GB 6-D black hole $a_{\rm ext} = 3\sqrt{3}/16$ as against $a_{\rm ext} = 1$ for the Kerr black hole.

open with increase rotation parameter a. Whereas the size of shadow decreases with increasing black hole's spin a. Thus, we observed that the shadow of a 5D rotating naked singularity, which consists of a dark arc and a dark spot, is very different from a 5D rotating black hole one. So, the two observables, viz. R_s and δ_s defined above are no longer valid for a naked singularity. However, another two new observables [87, 60] can be defined to describe the shadow of a naked singularity.

4.6 Shadow of the rotating 6D black hole

In this section we study the optical properties of black hole in Gauss-Bonnet gravity. If the bright source is located behind black hole then a distant observer is able to detect only light ray scattered away from the black hole, and those captured by the event horizon form a dark spot. This dark region which could be detected and extracted from the luminous background is traditionally called the black hole shadow or silhouette. In practice, the distant observer at infin-

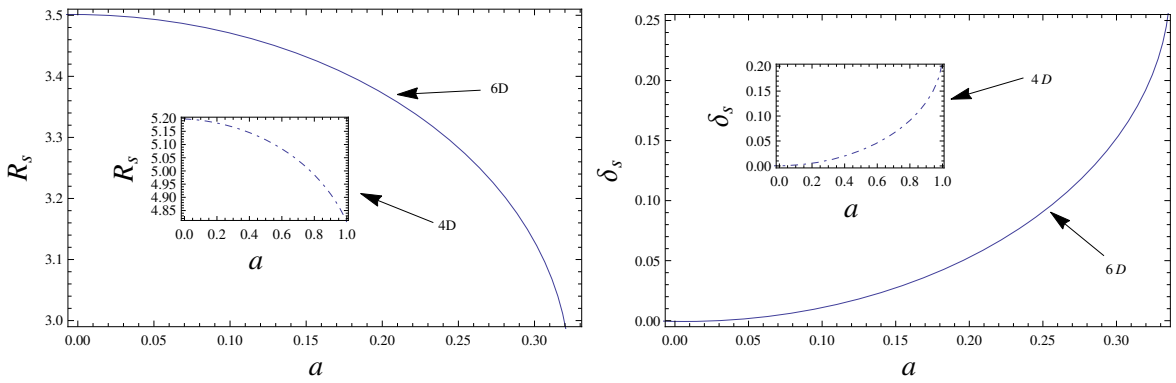

Figure 4.19: Observables R_s and δ_s as functions of the rotation parameter, corresponding to the shadow of black hole situated at the origin of coordinates with inclination angle $\theta = \pi/2$ and dimensions d: $D = 6$ (solid line) and $d = 4$ (dot-dashed line) [87, 100].

ity could see a projection of it at the flat plane passing through the black hole and normal to the line connecting it with the observer (the line of sight). The Cartesian coordinates at this plane, which are usually denoted by α and β and called celestial coordinates, give the apparent position of the shadow image. The celestial coordinates are connected with the geodesic equations of light ray around black hole as [108].

Note here that a silhouette of the black hole is observed in 3-D space and here we would like to check the influence of the extra dimensions to the shape of the black hole shadow.

Using expressions for the impact parameters derived in the Sec. 3.6.1 and the equations of motion obtained from the Hamilton-Jacobi equation (3.21), one can get $d\phi/dr$ and $d\theta/dr$, and insert them into the equations (4.1) and (4.2) in order to get the explicit expressions for the celestial coordinates as

$$\alpha = -\xi \csc\theta_0 \,, \tag{4.36}$$

$$\beta = \pm\sqrt{\eta + a^2\cos^2\theta_0 - \xi\cot^2\theta_0} \,. \tag{4.37}$$

We will concentrate here on the special case when the inclination angle $\theta_0 = \pi/2$ is similar to that for four dimensional Kerr space-time (see e.g. [111, 102, 110,

87]). Then for the pure GB 6-D rotating black hole we have

$$\alpha = -\xi \,, \tag{4.38}$$

$$\beta = \pm\sqrt{\eta} \,. \tag{4.39}$$

For describing the black hole shadow one can plot dependence of β from α, see e.g. [34]. In Fig. 4.18, we compare shadow of six dimensional black hole in Gauss-Bonnet gravity with one of four dimensional Kerr black hole, which are shown for the different values of the rotation parameter a. The contours of the shadows of the Gauss-Bonnet black hole for the spin parameters $a = 0$, $a = a_{ext}/2$, and $a = a_{ext}$ are shown in Fig. 4.18. One can easily see, light rays sphere is decreased with the increase of spin of the black hole in Gauss-Bonnet gravity. This behavior is exactly the same as in the Kerr space-time.

The observable parameters as distortion parameter δ_s and radius of the shadow R_s can be computed numerically using either the expressions (4.38) and (4.39) or Fig. 4.18. Distortion parameter $\delta_s = \Delta x/R_s$ [34, 87], where Δx is deviation parameter which is distance between edge point of full circle and edge point of shadow [34]. Consequently if rotation parameter is equal to zero $a = 0$ then Δx must vanish. On the other hand, if we consider rotating black hole, Δx is nonzero and consequently δ_s depends on spin of black hole. In Fig. 4.19, the observables R_s and δ_s as functions of the rotation parameter of the black hole are shown when the inclination angle $\theta_0 = \pi/2$. From these plots one may conclude that with the increase of spin parameter a of the black hole in Gauss-Bonnet gravity shape of shadow is decreasing which is similar to the Kerr black hole case. The increase of δ_s with the increase of rotation parameter a corresponds to deviation of the shape of shadow from circle.

4.7 Conclusion

In this chapter we have considered the shadow of the black hole casted by the strong gravitational field of latter. We have analyzed the shape and sizes of the black hole shadow for different gravity models.

It was shown that with increasing deformation parameter of non-Kerr black hole the shadow of the latter decreases. This phenomena also related to the fact that the increase of deformation parameter forces light ray orbits to come closer which corresponds to the decrease of gravitational force acting on light ray. Light ray with smaller impact parameter could escape from absorbtion by black hole in the presence of positive deformation parameter. The increase of distortion parameter of the shadow with the increase of module of deformation parameter corresponds to deviation of the shape of shadows from pure circle. It was obtained that the deformed rotating black hole's shadow is also going to be deformed independently on sign of deformation parameter. Using the theoretical results for the black hole's shadow comparing with EHT observational results[94, 93, 95] one can obtain deformation parameter as $|\epsilon| < 80$.

We have studied the shadow cast by the non-rotating ($a = 0$) and rotating ($a \neq 0$) Einstein-Born-Infeld black hole and demonstrated that the null geodesic equations can be integrated that allows us investigate the shadow cast by a black hole. It was shown that the shadow is slightly smaller and less deformed than that for its Reissner-Nordstrom counterpart. In addition, the presence of Born-Infeld parameter causes appearance additional asymmetries in the shape of the black hole's shadow. For the non-rotating black the radius of the shadow have been obtained by numerical calculation. In the presence of the rotating parameter a the shape of black hole shadow is distorted, while with increasing electric charge of black hole the distortion decreases and shadow starts becoming a circle.

Observable parameter δ is most important point for comparing with observation. The results shows that the increase of Born-Infeld parameter causes the shape of the black hole shadow to be more distorted.

The analysis of the effect of the NUT parameter and the black hole rotation parameter on modification of the shape of the shadow of black hole show that they have opposite effects on black hole shadow size. The gravitomagnetic charge increases the size of the shadow shape while black hole's angular momentum decreases its size. A comparison of the obtained theoretical results on the shadow of black hole size with the observational data(for $R_s = 6M$ [95, 94, 93]) in the EHT project provides the upper limit for the dimensionless gravitomagnetic charge $l/M < 0.85$.

The shadow cast by a black hole in five dimensional Myers-Perry spacetime in the case of two equal rotation parameters have been studied. There is intriguing dissimilarity of this problem with the case of four-dimensional Kerr black hole, e.g., while in the four-dimensional Kerr case there exists stable circular orbit around the black hole, they are absent for 5D Myers-Perry black hole. In this chapter we analyzed the unstable spherical light ray orbits 5D Myers-Perry black hole. We have investigated how the size and apparent shape of the black hole is distorted due to the extra dimension by analyzing unstable circular orbits, i.e., we have studied the effect of rotation parameter on the shape of the shadow of a 5D black hole. Adopting two observables, the radius and the distortion parameter, characterizing the apparent shape, we found that the shape of the shadow is affected by the value of rotation parameter. It was shown that the size of the shadow decreases with rotation parameter in 5D Myers-Perry black hole resulting in a smaller shadow than in the four dimensional Kerr black hole. Thus the larger value of rotation parameter leads to decrease in the size of shadow. This

may be understood by the fact that as the black hole starts spinning rapidly, it forces light ray orbits to come closer resulting in the decrease in gravitational force acting on light ray. The deformation of the shadow is characterized by the distortion parameter which increases monotonically with rotation parameter and takes maximal value when black hole approaches extremal. Thus, the distortion also increases with the increase in rotation parameter. It corresponds to the deviation of the shape of the shadow from circular orbit and it is also seen that the rate of change of distortion with rotation parameter also depends on the angle of inclination. We have also found that, on the contrary to the Braneworld where the size of shadow does not changes much for fixed tidal charged as a function of rotation parameter, the size of 5D Myers Perry black hole shadow decreases significantly.

We extended our analysis to study the shadow of 5D Myers-Perry naked singularity, which have two parts the dark arc and distorted circular shape. It has been observed that the deviation of the peak of effective potential towards the central object.

Main results and conclusions

We have studied optical and energetic processes in vicinity of relativistic compact objects. The obtained results can be summarised as follows:

1. The exact expressions for the deflection angle of the light ray have been obtained due to the effect of weak gravitational lensing around black hole in braneworld. It was shown, that the increase of the module of brane tidal charge of the black hole causes the increase the magnification of the size image. It was also shown that the presence of the negative brane charge sufficiently increases the image source magnification and deflection angle. A comparison of the obtained theoretical results on the deflection angle with the observational data for the Sun provides the upper limit for the dimensionless brane parameter as $W^2/R^2 < 0.96 \cdot 10^{-7}$.

2. The analysis of the Einstein-Born-Infeld black hole's event horizon structure demonstrated that outer (inner) horizon radius decreases (increases) with the increase in the electric charge and Born-Infeld parameter. It was shown that the increase the black hole brane tidal charge causes the increase the energy release process. It was shown that with the increase of the rotation parameter the efficiency of the energy emission decreases in five dimensional black hole.

3. The analysis of the effective potential of radial motion of the light ray show, that with the increase of the gravitomagnetic charge the shape of the effective

potential is going to shift to the observer at infinity which corresponds to increasing the event horizon of the Kerr-Taub-NUT black hole. It was obtained that with increasing either rotation parameter or electric charge of black hole particle is moving closer to the central object in Einstein-Born-Infeld model.

4. It was obtained that the decrease of the negative values of the deformation parameter of non-Kerr black holes causes the increase of light ray sphere. The stability of circular orbits is decreasing with the increase the module of negative deformation parameter. It was shown that the increase of deformation parameter stable circular light ray orbits come closer to the central object.

5. It was shown that with increasing deformation parameter of non-Kerr black hole the shadow of the latter decreases. This phenomena also related to the fact that the increase of deformation parameter forces light ray orbits to come closer which corresponds to the decrease of gravitational force acting on light ray. It was obtained that the deformed rotating black hole's shadow is also going to be deformed independently on sign of deformation parameter. A comparison of the obtained theoretical results on the shadow of black hole size with the observational data(for $R_s = 6M$) in the EHT project provides the upper limit for the dimensionless deformation parameter as $|\epsilon| < 80$ and gravitomagnetic charge $l/M < 0.85$.

6. It was shown that the shadow of Einstein-Born-Infeld is slightly smaller and less deformed than that for its Reissner-Nordstrom counterpart. It was obtained that the presence of Born-Infeld parameter causes appearance additional asymmetries in the shape of the black hole's shadow. It was also shown that the increase of Born-Infeld parameter causes the shape of the black hole shadow to be more distorted. It was shown that the gravitomagnetic charge

increases the size of the shadow shape while black hole's angular momentum decreases its size.

7. It was shown that the size of the shadow decreases with rotation parameter in 5D Myers-Perry black hole resulting in a smaller shadow than in the four dimensional Kerr black hole. It was found that, on the contrary to the Braneworld where the size of shadow does not changes much for fixed tidal charged as a function of rotation parameter, the size of 5D Myers Perry black hole shadow decreases significantly.

Bibliography

[1] W. W. Campbell and R. Trumpler, "Observations on the Deflection of Light in Passing Through the Sun's Gravitational Field, Made During the Total Solar Eclipse of September 21, 1923," *Publications of the Astronomical Society of the Pacific*, vol. 35, pp. 158–163, June 1923.

[2] N. Tsukamoto and Y. Gong, "Retrolensing by a charged black hole," *Phys. Rev. D*, vol. 95, p. 064034, Mar. 2017.

[3] N. Tsukamoto, "Retrolensing by a wormhole at deflection angles π and 3 π," *Phys. Rev. D*, vol. 95, p. 084021, Apr. 2017.

[4] O. Y. Tsupko and G. S. Bisnovatyi-Kogan, "Gravitational lensing in plasma: Relativistic images at homogeneous plasma," *Phys. Rev. D*, vol. 87, p. 124009, June 2013.

[5] G. S. Bisnovatyi-Kogan and O. Y. Tsupko, "Gravitational lensing in a non-uniform plasma," *Mon. Not. R. Astron. Soc*, vol. 404, pp. 1790–1800, June 2010.

[6] V. S. Morozova, B. J. Ahmedov, and A. A. Tursunov, "Gravitational lensing by a rotating massive object in a plasma," *Astrophys Space Sci*, vol. 346, pp. 513–520, Aug. 2013.

[7] O. Y. Tsupko and G. S. Bisnovatyi-Kogan, "Gravitational lensing in the presence of plasmas and strong gravitational fields," *Gravitation and Cosmology*, vol. 20, pp. 220–225, July 2014.

[8] G. S. Bisnovatyi-Kogan and O. Y. Tsupko, "Gravitational lensing in a non-uniform plasma," *Monthly Notices of the Royal Astronomical Society*, vol. 404, pp. 1790–1800, June 2010.

[9] O. Y. Tsupko and G. S. Bisnovatyi-Kogan, "Relativistic Rings due to Schwarzschild Gravitational Lensing," *Gravitation and Cosmology*, vol. 15, pp. 184–187, June 2009.

[10] V. Perlick, "Gravitational Lensing from a Spacetime Perspective," *Living Reviews in Relativity*, vol. 7, p. 9, Sept. 2004.

[11] B. Paczynski, "Gravitational microlensing by the galactic halo," *Astrophys J.*, vol. 304, pp. 1–5, May 1986.

[12] C. Alcock, C. W. Akerlof, R. A. Allsman, T. S. Axelrod, D. P. Bennett, S. Chan, K. H. Cook, K. C. Freeman, K. Griest, S. L. Marshall, H.-S. Park, S. Perlmutter, B. A. Peterson, M. R. Pratt, P. J. Quinn, A. W. Rodgers, C. W. Stubbs, and W. Sutherland, "Possible gravitational microlensing of a star in the Large Magellanic Cloud," *Nature*, vol. 365, pp. 621–623, Oct. 1993.

[13] B. Paczynski, "Gravitational Microlensing in the Local Group," *Annual Review of Astronomy and Astrophysics*, vol. 34, pp. 419–460, 1996.

[14] V. Perlick, O. Y. Tsupko, and G. S. Bisnovatyi-Kogan, "Influence of a plasma on the shadow of a spherically symmetric black hole," *Phys. Rev. D*, vol. 92, p. 104031, Nov. 2015.

[15] J. Bicak and P. Hadrava, "General-relativistic radiative transfer theory in refractive and dispersive media," *Astronomy and Astrophysics*, vol. 44, pp. 389–399, Nov. 1975.

[16] A. Abdujabbarov, B. Toshmatov, J. Schee, Z. Stuchlík, and B. Ahmedov, "Gravitational lensing by regular black holes surrounded by plasma," *International Journal of Modern Physics D*, vol. 26, pp. 1741011–187, 2017.

[17] J. Schee and Z. Stuchlík, "Gravitational lensing and ghost images in the regular Bardeen no-horizon spacetimes," *JCAP*, vol. 6, p. 48, June 2015.

[18] P. Bakala, P. Čermák, S. Hledík, Z. Stuchlík, and K. Truparová, "Extreme gravitational lensing in vicinity of Schwarzschild-de Sitter black holes," *Central European Journal of Physics*, vol. 5, pp. 599–610, Dec. 2007.

[19] A. Abdujabbarov, F. Atamurotov, N. Dadhich, B. Ahmedov, and Z. Stuchlík, "Energetics and optical properties of 6-dimensional rotating black hole in pure Gauss-Bonnet gravity," *European Physical Journal C*, vol. 75, p. 399, Aug. 2015.

[20] Z. Stuchlík and J. Schee, "Optical effects related to Keplerian discs orbiting Kehagias-Sfetsos naked singularities," *Classical and Quantum Gravity*, vol. 31, p. 195013, Oct. 2014.

[21] J. Schee and Z. Stuchlík, "Optical Phenomena in the Field of Braneworld Kerr Black Holes," *International Journal of Modern Physics D*, vol. 18, pp. 983–1024, 2009.

[22] J. Kovář and Z. Stuchlík, "Optical reference geometry and inertial forces in Kerr de Sitter spacetimes," *Classical and Quantum Gravity*, vol. 24, pp. 565–594, Feb. 2007.

[23] M. Ghasemi-Nodehi, Z. Li, and C. Bambi, "Shadows of CPR black holes and tests of the Kerr metric," *European Physical Journal C*, vol. 75, p. 315, July 2015.

[24] C. Bambi, "Testing the Kerr Paradigm with the Black Hole Shadow," *ArXiv e-prints*, July 2015.

[25] N. Tsukamoto, Z. Li, and C. Bambi, "Constraining the spin and the deformation parameters from the black hole shadow," *Journal of Cosmology and Astroparticles*, vol. 6, p. 43, June 2014.

[26] Z. Li, L. Kong, and C. Bambi, "Testing the Nature of the Supermassive Black Hole Candidate in SgrA* with Light Curves and Images of Hot Spots," *Astrophys J.*, vol. 787, p. 152, June 2014.

[27] Z. Li and C. Bambi, "Measuring the Kerr spin parameter of regular black holes from their shadow," *JCAP*, vol. 1, p. 041, Jan. 2014.

[28] C. Bambi and N. Yoshida, "Shape and position of the shadow in the $\delta = 2$ Tomimatsu-Sato spacetime," *Classical and Quantum Gravity*, vol. 27, p. 205006, Oct. 2010.

[29] A. Abdujabbarov, B. Juraev, B. Ahmedov, and Z. Stuchlík, "Shadow of rotating wormhole in plasma environment," *Astrophys Space Sci*, vol. 361, p. 226, 2016.

[30] A. Abdujabbarov, M. Amir, B. Ahmedov, and S. G. Ghosh, "Shadow of rotating regular black holes," *Phys. Rev. D*, vol. 93, p. 104004, May 2016.

[31] A. A. Abdujabbarov, L. Rezzolla, and B. J. Ahmedov, "A coordinate-independent characterization of a black hole shadow," *Mon. Not. R. Astron. Soc.*, vol. 454, pp. 2423–2435, Dec. 2015.

[32] F. Atamurotov, B. Ahmedov, and A. Abdujabbarov, "Optical properties of black holes in the presence of a plasma: The shadow," *Phys. Rev. D*, vol. 92, p. 084005, 2015.

[33] F. Atamurotov, A. Abdujabbarov, and B. Ahmedov, "Shadow of rotating Hořava-Lifshitz black hole," *Astrophys Space Sci*, vol. 348, pp. 179–188, Nov. 2013.

[34] F. Atamurotov, A. Abdujabbarov, and B. Ahmedov, "Shadow of rotating non-Kerr black hole," *Phys. Rev. D*, vol. 88, p. 064004, Sept. 2013.

[35] Z. Stuchlík and J. Schee, "Circular geodesic of Bardeen and Ayon-Beato-Garcia regular black-hole and no-horizon spacetimes," *International Journal of Modern Physics D*, vol. 24, p. 50020, Dec. 2015.

[36] A. Abdujabbarov and B. Ahmedov, "Test particle motion around a black hole in a braneworld," *Phys. Rev. D*, vol. 81, p. 044022, Feb. 2010.

[37] J. Schee and Z. Stuchlík, "Profiles of emission lines generated by rings orbiting braneworld Kerr black holes," *General Relativity and Gravitation*, vol. 41, pp. 1795–1818, Aug. 2009.

[38] J. L. Synge, *Relativity: The General Theory.* North-Holland, Amsterdam, 1960.

[39] A. F. Zakharov and Y. V. Baryshev, "Gravitational Lens Amplification of Gravitational Radiation," *International Journal of Modern Physics D*, vol. 11, pp. 1067–1074, 2002.

[40] A. Abdujabbarov, B. Ahmedov, N. Dadhich, and F. Atamurotov, "Optical properties of a braneworld black hole: Gravitational lensing and retrolensing," *Phys. Rev. D*, vol. 96, p. 084017, Oct. 2017.

[41] M. Born and L. Infeld, "Foundations of the New Field Theory," *Proceedings of the Royal Society of London Series A*, vol. 144, pp. 425–451, Mar. 1934.

[42] B. Hoffmann, "Gravitational and Electromagnetic Mass in the Born-Infeld Electrodynamics," *Physical Review*, vol. 47, pp. 877–880, June 1935.

[43] E. S. Fradkin and A. A. Tseytlin, "Non-linear electrodynamics from quantized strings," *Physics Letters B*, vol. 163, pp. 123–130, Nov. 1985.

[44] M. N. R. Wohlfarth, "CORRIGENDUM: Gravity à la Born–Infeld," *Classical and Quantum Gravity*, vol. 21, pp. 5297–5298, Nov. 2004.

[45] S. Fernando and D. Krug, "Letter: Charged Black Hole Solutions in Einstein-Born-Infeld Gravity with a Cosmological Constant," *General Relativity and Gravitation*, vol. 35, pp. 129–137, Jan. 2003.

[46] R. Linares, M. Maceda, and D. Martínez-Carbajal, "Test particle motion in the Born-Infeld black hole," *Phys. Rev. D*, vol. 92, p. 024052, July 2015.

[47] R. P. Kerr, "Gravitational field of a spinning mass as an example of algebraically special metrics," *Phys. Rev. Lett.*, vol. 11, pp. 237–238, 1963.

[48] E. T. Newman and A. I. Janis, "Note on the Kerr Spinning-Particle Metric," *Journal of Mathematical Physics*, vol. 6, pp. 915–917, June 1965.

[49] D. Julio Cirilo Lombardo, "The Newman Janis algorithm, rotating solutions and Einstein Born Infeld black holes," *Classical and Quantum Gravity*, vol. 21, pp. 1407–1417, Mar. 2004.

[50] E. T. Newman, E. Couch, K. Chinnapared, A. Exton, A. Prakash, and R. Torrence, "Metric of a rotating charged mass," *J. Math. Phys.*, vol. 6, no. 6, pp. 918–919, 1965.

[51] A. A. Shoom, "Geometric properties of stationary and axisymmetric Killing horizons," *Phys. Rev. D*, vol. 91, p. 024019, Jan. 2015.

[52] G. T. Horowitz, *Black Holes in Higher Dimensions.* Apr. 2012.

[53] R. Emparan and H. S. Reall, "A Rotating Black Ring Solution in Five Dimensions," *Physical Review Letters*, vol. 88, p. 101101, Mar. 2002.

[54] R. C. Myers and M. J. Perry, "Black holes in higher dimensional space-times," *Annals of Physics*, vol. 172, pp. 304–347, Dec. 1986.

[55] F. Atamurotov, S. G. Ghosh, and B. Ahmedov, "Horizon structure of rotating Einstein-Born-Infeld black holes and shadow," *European Physical Journal C*, vol. 76, May 2016.

[56] M. Abramowitz and I. A. Stegun, *Handbook of Mathematical Functions.* 1972.

[57] U. Papnoi, F. Atamurotov, S. G. Ghosh, and B. Ahmedov, "Shadow of five-dimensional rotating Myers-Perry black hole," *Phys. Rev. D*, vol. 90, p. 024073, July 2014.

[58] V. Frolov and D. Stojković, "Particle and light motion in a space-time of a five-dimensional rotating black hole," *Phys. Rev. D*, vol. 68, p. 064011, Sept. 2003.

[59] F. R. Tangherlini, "Schwarzschild field inn dimensions and the dimensionality of space problem," *Il Nuovo Cimento*, vol. 27, pp. 636–651, Feb. 1963.

[60] S.-W. Wei and Y.-X. Liu, "Observing the shadow of Einstein-Maxwell-Dilaton-Axion black hole," *Journal of Cosmology and Astroparticles*, vol. 11, p. 063, Nov. 2013.

[61] C. W. Misner, K. S. Thorne, and J. A. Wheeler, *Gravitation*. San Francisco: W. H. Freeman, 1973.

[62] E. Newman, L. Tamburino, and T. Unti, "Empty-Space Generalization of the Schwarzschild Metric," *Journal of Mathematical Physics*, vol. 4, pp. 915–923, July 1963.

[63] M. Nouri-Zonoz, "Electromagnetic waves in NUT space: solutions to the Maxwell equations," *Classical and Quantum Gravity*, vol. 21, pp. 471–482, Jan. 2004.

[64] V. Kagramanova, J. Kunz, and C. Lämmerzahl, "Charged particle interferometry in Plebański Demiański black hole spacetimes," *Classical and Quantum Gravity*, vol. 25, p. 105023, May 2008.

[65] V. S. Morozova, B. J. Ahmedov, and V. G. Kagramanova, "General Relativistic Effects of Gravitomagnetic Charge on Pulsar Magnetospheres and Particle Acceleration in the Polar Cap," *Astrophys. J.*, vol. 684, pp. 1359–1365, Sept. 2008.

[66] A. N. Aliev, H. Cebeci, and T. Dereli, "Kerr-Taub-NUT spacetime with Maxwell and dilaton fields," *Phys. Rev. D*, vol. 77, p. 124022, June 2008.

[67] A. A. Abdujabbarov, B. J. Ahmedov, S. R. Shaymatov, and A. S. Rakhmatov, "Penrose process in Kerr-Taub-NUT spacetime," *Astrophys Space Sci*, vol. 334, pp. 237–241, Aug. 2011.

[68] S. Grunau and V. Kagramanova, "Geodesics of electrically and magnetically charged test particles in the Reissner-Nordström space-time: Analytical solutions," *Phys. Rev. D*, vol. 83, p. 044009, Feb. 2011.

[69] V. Kagramanova, J. Kunz, E. Hackmann, and C. Lämmerzahl, "Analytic treatment of complete and incomplete geodesics in Taub-NUT space-times," *Phys. Rev. D.*, vol. 81, p. 124044, June 2010.

[70] P. Connell, V. P. Frolov, and D. Kubizňák, "Solving parallel transport equations in the higher-dimensional Kerr-NUT-(A)dS spacetimes," *Phys. Rev. D*, vol. 78, p. 024042, July 2008.

[71] P. G. Nedkova and S. S. Yazadjiev, "Magnetized black hole on the Taub-NUT instanton," *Phys. Rev. D*, vol. 85, p. 064021, Mar. 2012.

[72] A. Virmani, "Asymptotic flatness, Taub-NUT metric, and variational principle," *Phys. Rev. D*, vol. 84, p. 064034, Sept. 2011.

[73] N. Dadhich and Z. Y. Turakulov, "The most general axially symmetric electrovac spacetime admitting separable equations of motion," *Classical and Quantum Gravity*, vol. 19, pp. 2765–2775, June 2002.

[74] B. Carter, "Global Structure of the Kerr Family of Gravitational Fields," *Physical Review*, vol. 174, pp. 1559–1571, Oct. 1968.

[75] R. Beig, "The static gravitational field near spatial infinity I," *General Relativity and Gravitation*, vol. 12, pp. 439–451, June 1980.

[76] C. M. Will, "The Confrontation between General Relativity and Experiment," *Living Reviews in Relativity*, vol. 9, p. 3, Mar. 2006.

[77] J. G. Williams, S. G. Turyshev, and D. H. Boggs, "Progress in Lunar Laser Ranging Tests of Relativistic Gravity," *Physical Review Letters*, vol. 93, p. 261101, Dec. 2004.

[78] F. Atamurotov, B. Ahmedov, and S. Shaymatov, "Formation of black holes through BSW effect and black hole-black hole collisions," *Astrophys. Space Sci.*, vol. 347, pp. 277–281, Oct. 2013.

[79] A. A. Abdujabbarov, B. J. Ahmedov, and N. B. Jurayeva, "Charged-particle motion around a rotating non-Kerr black hole immersed in a uniform magnetic field," *Phys. Rev. D.*, vol. 87, p. 064042, Mar. 2013.

[80] N. Dadhich, S. G. Ghosh, and S. Jhingan, "The Lovelock gravity in the critical spacetime dimension," *Physics Letters B*, vol. 711, pp. 196–198, May 2012.

[81] D. Hansen and N. Yunes, "Applicability of the Newman-Janis algorithm to black hole solutions of modified gravity theories," *Phys. Rev. D*, vol. 88, p. 104020, Nov. 2013.

[82] N. Dadhich, "A novel derivation of the rotating black hole metric," *General Relativity and Gravitation*, vol. 45, pp. 2383–2388, Nov. 2013.

[83] N. Dadhich and S. G. Ghosh, "Rotating black hole in Einstein and pure Lovelock gravity," *ArXiv e-prints*, July 2013.

[84] V. P. Frolov and D. Kubizňák, "Higher-dimensional black holes: hidden symmetries and separation of variables," *Classical and Quantum Gravity*, vol. 25, p. 154005, Aug. 2008.

[85] E. Hackmann, V. Kagramanova, J. Kunz, and C. Lämmerzahl, "Analytic solutions of the geodesic equation in higher dimensional static spherically symmetric spacetimes," *Phys. Rev. D*, vol. 78, p. 124018, Dec. 2008.

[86] G. Ponti, B. De Marco, M. R. Morris, A. Merloni, T. Muñoz-Darias, M. Clavel, D. Haggard, S. Zhang, K. Nandra, S. Gillessen, K. Mori,

J. Neilsen, N. Rea, N. Degenaar, R. Terrier, and A. Goldwurm, "Fifteen years of XMM-Newton and Chandra monitoring of Sgr A: evidence for a recent increase in the bright flaring rate," *Mon. Not. R. Astron. Soc.*, vol. 454, pp. 1525–1544, Dec. 2015.

[87] K. Hioki and K.-I. Maeda, "Measurement of the Kerr spin parameter by observation of a compact object's shadow," *Phys. Rev. D*, vol. 80, p. 024042, July 2009.

[88] B. C. Bromley, F. Melia, and S. Liu, "Polarimetric Imaging of the Massive Black Hole at the Galactic Center," *Astrophys. J.*, vol. 555, pp. L83–L86, July 2001.

[89] A. de Vries, "The apparent shape of a rotating charged black hole, closed photon orbits and the bifurcation set A_4," *Classical and Quantum Gravity*, vol. 17, pp. 123–144, Jan. 2000.

[90] R. Takahashi, "Shapes and Positions of Black Hole Shadows in Accretion Disks and Spin Parameters of Black Holes," *Astrophys. J*, vol. 611, pp. 996–1004, Aug. 2004.

[91] G. V. Kraniotis, "Precise analytic treatment of Kerr and Kerr-(anti) de Sitter black holes as gravitational lenses," *Classical and Quantum Gravity*, vol. 28, p. 085021, Apr. 2011.

[92] J. M. Bardeen, "Timelike and null geodesics in the Kerr metric.," in *Black Holes (Les Astres Occlus)* (C. Dewitt and B. S. Dewitt, eds.), pp. 215–239, 1973.

[93] S. S. Doeleman, J. Weintroub, A. E. E. Rogers, R. Plambeck, R. Freund, R. P. J. Tilanus, P. Friberg, L. M. Ziurys, J. M. Moran, B. Corey, K. H.

Young, D. L. Smythe, M. Titus, D. P. Marrone, R. J. Cappallo, D. C.-J. Bock, G. C. Bower, R. Chamberlin, G. R. Davis, T. P. Krichbaum, J. Lamb, H. Maness, A. E. Niell, A. Roy, P. Strittmatter, D. Werthimer, A. R. Whitney, and D. Woody, "Event-horizon-scale structure in the supermassive black hole candidate at the Galactic Centre," *Nature*, vol. 455, pp. 78–80, Sept. 2008.

[94] M. D. Johnson, V. L. Fish, S. S. Doeleman, D. P. Marrone, R. L. Plambeck, J. F. C. Wardle, K. Akiyama, K. Asada, C. Beaudoin, L. Blackburn, R. Blundell, G. C. Bower, C. Brinkerink, A. E. Broderick, R. Cappallo, A. A. Chael, G. B. Crew, J. Dexter, M. Dexter, R. Freund, P. Friberg, R. Gold, M. A. Gurwell, P. T. P. Ho, M. Honma, M. Inoue, M. Kosowsky, T. P. Krichbaum, J. Lamb, A. Loeb, R.-S. Lu, D. MacMahon, J. C. McKinney, J. M. Moran, R. Narayan, R. A. Primiani, D. Psaltis, A. E. E. Rogers, K. Rosenfeld, J. SooHoo, R. P. J. Tilanus, M. Titus, L. Vertatschitsch, J. Weintroub, M. Wright, K. H. Young, J. A. Zensus, and L. M. Ziurys, "Resolved magnetic-field structure and variability near the event horizon of Sagittarius A*," *Science*, vol. 350, pp. 1242–1245, Dec. 2015.

[95] D. Castelvecchi, "How to hunt for a black hole with a telescope the size of Earth," *Nature*, vol. 543, pp. 478–480, Mar. 2017.

[96] H. Falcke, F. Melia, and E. Agol, "Viewing the Shadow of the Black Hole at the Galactic Center," *Astrophys. J. Lett.*, vol. 528, pp. L13–L16, Jan. 2000.

[97] H. C. Ohanian, *Gravitation and spacetime.* Gravitation and spacetime., by Ohanian, H. C.. New York, NY (USA): Norton, 14 + 461 p., 1976.

[98] A. Grenzebach, V. Perlick, and C. Lämmerzahl, "Photon regions and shadows of Kerr-Newman-NUT black holes with a cosmological constant," *Phys. Rev. D*, vol. 89, p. 124004, June 2014.

[99] V. Bozza and G. Scarpetta, "Strong deflection limit of black hole gravitational lensing with arbitrary source distances," *Phys. Rev. D*, vol. 76, p. 083008, Oct. 2007.

[100] A. F. Zakharov, A. A. Nucita, F. De Paolis, and G. Ingrosso, "Measuring the black hole parameters in the galactic center with RADIOASTRON," *New Astron. Rev.*, vol. 10, pp. 479–489, June 2005.

[101] A. Abdujabbarov, F. Atamurotov, Y. Kucukakca, B. Ahmedov, and U. Camci, "Shadow of Kerr-Taub-NUT black hole," *Astrophys. Space Sci.*, vol. 344, pp. 429–435, Apr. 2013.

[102] L. Amarilla, E. F. Eiroa, and G. Giribet, "Null geodesics and shadow of a rotating black hole in extended Chern-Simons modified gravity," *Phys. Rev. D*, vol. 81, p. 124045, June 2010.

[103] L. Amarilla and E. F. Eiroa, "Shadow of a rotating braneworld black hole," *Phys. Rev. D*, vol. 85, p. 064019, Mar. 2012.

[104] J.-P. Luminet, "Image of a spherical black hole with thin accretion disk," *Astronomy and Astrophysics*, vol. 75, pp. 228–235, May 1979.

[105] H. Falcke and S. B. Markoff, "Toward the event horizon - the supermassive black hole in the Galactic Center," *Class. Quantum Grav*, vol. 30, p. 244003, Dec. 2013.

[106] A. F. Zakharov, A. A. Nucita, F. De Paolis, and G. Ingrosso, "Measuring the black hole parameters in the galactic center with RADIOASTRON," *New Astronomy*, vol. 10, pp. 479–489, June 2005.

[107] V. Bozza, "Gravitational lensing by black holes," *General Relativity and Gravitation*, vol. 42, pp. 2269–2300, Sept. 2010.

[108] S. E. Vázquez and E. P. Esteban, "Strong-field gravitational lensing by a Kerr black hole," *Nuovo Cim. B*, vol. 119, p. 489, May 2004.

[109] C. Bambi and K. Freese, "Apparent shape of super-spinning black holes," *Phys. Rev. D*, vol. 79, p. 043002, Feb. 2009.

[110] L. Amarilla and E. F. Eiroa, "Shadow of a Kaluza-Klein rotating dilaton black hole," *Phys. Rev. D*, vol. 87, p. 044057, Feb. 2013.

[111] Z. Stuchlík and J. Schee, "Observational phenomena related to primordial Kerr superspinars," *Classical and Quantum Gravity*, vol. 29, p. 065002, Mar. 2012.